

IMMUNOASSAY DESIGN OF A FIBER OPTIC BIOSENSOR FOR MEDICAL AND AGRO-FOOD APPLICATIONS

Jiadi Lu

Supervisors:

Prof. J. Lammertyn
Dr. D. Spasic

Dissertation presented in partial
fulfilment of the requirements
for the degree of Doctor of
Bioscience Engineering

Examination Committee:

Prof. W. Keulemans, chair
Prof. J. Lammertyn, promotor
Dr. D. Spasic, co-promotor
Prof. A. Gils
Prof. B. Cammue
Dr. F. Delpont
Prof. C. Caucheteur
(University of Mons)

October 2018

Doctoraatsproefschrift nr. 1532 aan de faculteit Bio-
ingenieurswetenschappen van de KU Leuven

© 2018 KU Leuven, Science, Engineering & Technology

Uitgegeven in eigen beheer, Jiadi Lu, Willem de Croylaan 42 box 2428, B-3000,
Leuven , Belgium

Alle rechten voorbehouden. Niets uit deze uitgave mag worden vermenigvuldigd
en/of openbaar gemaakt worden door middel van druk, fotokopie, microfilm,
elektronisch of op welke andere wijze ook zonder voorafgaandelijke schriftelijke
toestemming van de uitgever.

All rights reserved. No part of the publication may be reproduced in any form by print,
photoprint, microfilm, electronic or any other means without written permission from
the publisher.

Acknowledgements

I would like to express my gratitude to many people who have been greatly supportive during the journey of this PhD project. I am particularly grateful to my promotor, Prof. Jeroen Lammertyn, who provided me the opportunity to work on this interesting and exciting project in a dynamic group. Thank you for sharing your expertise and all the constructive advice and guidance, for encouragement and support over the past five years, and for proofreading this thesis. I would like to extend my gratitude to my co-promotor, Dr. Dragana Spasic, who was always available for discussions on results and papers. Thank you for both scientific and non-scientific inputs. I would also like to express my gratitude to my daily supervisor, Dr. Filip Delport, for introducing me the new knowledge from the beginning of the PhD, and for countless helpful discussions and new ideas whenever I needed them.

I would like to thank the members of my examination committee for all their critical comments during my PhD. These were very valuable to improve the quality of my work. Being part of NANODIAG project, I have learned both academic and industrial knowledge during the project meetings. Special thanks to Prof. Ann Gils, for providing not only the expertise, but also antibody and patient samples. Prof. Bruno Cammue, thank you for the critical questions. Thomas, Tanne, Sumin, it was a pleasure to work together with you on this project.

I would like to say thank you to all the current and former members from Biosensors group. Iulia, thank you for showing me in the lab from my first day and being a dear friend throughout this journey. Karen, Iene and Lisa, your warm and kind personality shed me some light towards the end of my PhD. Karen, thank you so much for translating the abstract and doing all the chores regarding to the thesis printing! Special thanks to my office buddies: Bram, Wouter and Makdim. Thank you for all the academic discussions, personal advice, encouragements and the fun time during lunch, it was a

pleasure to share an office with you. Wouter, thank you for all your help with my last set of experiments. Thanks to all the members in the FO-SPR group: Devin, Bernd, Suresh and Elfie, for sharing the experience and frustrations together and for all the heated discussions. Devin, thanks for your valuable input on the progesterone chapter in this thesis. Deborah, Elena and Karen L., thank you for bringing the nice atmosphere to the group. I would also like to thank former group members Phalguni, Nathalie, Tadge, Pelin, Frederica, Bram L., Karel, Kris, Bert, Dan, as well as more recent members Jaraslov, Saba and Henry, and anyone else whose name I may have unintentionally neglected to mention. Francesco, Valérie, Bert J., Matthias and Victor, thank you for the light conversations during lunch. I have learned so many things about science and much else besides from each and every one of you. Thank you for all the countless occasions when you were there for a friendly chat or discussion in the office, the lab, the lunch room, or the pub. I will treasure the memories of my experiences with all of you. All the administrative work could not have been done without Inge and Bert, thank you for all the help.

There were thousands of experiments have been carried out, but some of them never got published. These experiments cannot be done without the help of many scientists and researchers within KU Leuven. Thanks to Els in VCBT for lending me the spectrometer. Thanks to Ben Aernouts for helping me setting up the spectrometer. I would like to thank Prof. Abram Aertsen and Ines in the Department of Microbial and Molecular Systems for providing me with the *Salmonella* culture.

Finally, I would like to further extend my gratitude towards my family both in China and Ireland. To my dearest grandparents and parents: 姥姥姥爷，很遗憾你们看不到我的毕业论文了，谢谢你们从小到大对我的教诲，让我有勇气追求自己的理想。妈妈爸爸，谢谢你们对我人生选择的支持。每当我遇到困境时，你们的一通电话总能给予我力量继续前进。Thanks to my parents-in-law, Lena and Sean for always showing great interest in my research. Thank you to all of my extended families, for all your love and supports. Above all, I would like to thank my husband Ciaran for hundreds of times of travelling back and forth between Ireland and Belgium, for staying late in the office with me, for correcting my English, for giving me strength to come to the end of the thesis, and for your unconditional love, support and encouragement.

Abstract

Over the last decades, biosensors have emerged as innovative tools at the interface between advanced biotechnology and sensor technology. They have been used in multiple applications, ranging from agricultural industry and food safety to medical diagnosis and environmental monitoring, and they have drawn increasing commercial attention from the market. The ever increasing cost in the healthcare sector has driven the research towards biosensors that allow fast, sensitive, accurate and robust on-site detection. However, a single biosensor that fulfills all of these requirements is not yet available on the market.

Surface plasmon resonance (SPR) based optical biosensors show a huge potential for multiple biosensing applications. These sensors exploit surface plasmon waves to measure local refractive index changes due to interactions between target molecules of interest and biomolecules immobilized on the sensor surface. The most commonly used SPR biosensor, commercialized by Biacore, employs a prism for SPR excitation and provides both sensitive and reliable results. However, the device is bulky and expensive, and is therefore not suited for on-site detection. An alternative approach for SPR excitation is to exploit optical fibers, which have the advantages of being affordable and small. In this thesis, a fiber-optic SPR (FO-SPR) biosensor is explored for a variety of biosensing applications. The FO-SPR biosensor is fully automated, easy to miniaturize, affordable, and reliable. Although it has been employed in antibody-based and DNA-based bioassays, it has never been fully deployed in real biological samples.

The aim of this work is to investigate the capability of the FO-SPR biosensor for sensitive and rapid detection of a variety of target analytes in real matrices using immunoassays. To achieve this, two target molecules were selected based on their sizes and applications, namely progesterone (small

molecule relevant to the agriculture industry) and infliximab (antibody relevant to the healthcare sector).

In the agriculture industry, maximum yields are crucial to allow farmers to remain competitive. For milk production, it is critically important to detect heat in cows so that herd owners can conduct artificial insemination to attain an optimal successful pregnancy rate. Monitoring the level of progesterone is frequently employed for detection of heat. ELISA is the conventional technique for this situation, but this requires tests to be performed in a central laboratory and takes several hours to obtain results. Recently, a lateral flow immunoassay (LFIA) has been commercialized to perform on-farm tests and obtain results in 15 min. However, the sensitivity is worse than ELISA. To solve this problem a competitive immunoassay was developed using the FO-SPR biosensor for determining progesterone levels in milk. A limit of detection (LOD) of 0.5 ng/mL (1.6 nM) was achieved in standard milk. Moreover, validation of the assay was conducted with 6 bovine milk samples and benchmarked to the commercially available ELISA (cELISA) reference technology. A high correlation was obtained (Pearson correlation of 0.98 and ICC of 0.97) between both technologies. This work demonstrates that the FO-SPR biosensor is capable of detecting small molecules in the nanomolar range in a complex milk matrix within 20 minutes.

In the healthcare sector, patients can benefit from techniques that enable continuous monitoring of chronic diseases and early diagnosis of diseases. Infliximab (IFX) is a therapeutic antibody used for patients with inflammatory bowel disease. This biologic agent requires therapeutic drug monitoring to allow dosage adjustment and therefore improve therapeutic outcomes. The traditional methods for detection of IFX such as ELISA, radioimmunoassay, and homogeneous mobility shift assay, require the tests to be performed in a central laboratory. Therefore, immediate dosage adjustment is not feasible. For this application, a sandwich immunoassay was developed. An LOD of 2.2 ng/ml (15 pM) was achieved in 100-fold diluted serum. The total time from sample to result was 40 min. The evaluation of the established immunoassay was tested with 5 serum samples from IFX treated inflammatory bowel disease (IBD) patients. The results show excellent agreement between the FO-SPR and the clinically validated ELISA (Pearson correlation of 0.998 and ICC of 0.983 with inter-CV being less than 10%).

Since detection of IFX concentrations is usually done in patients' serum/plasma samples, this requires sample preparation from blood, which hampers the turnaround time. Thus, by establishing direct IFX detection in whole blood, sample preparation can be avoided. Furthermore, dried blood spot (DBS) sampling allows patients to collect blood sample at home and avoid visits to hospital. An advanced immunoassay was developed with a total detection time of 10 min. This short immunoassay was tested in matrices including serum, plasma, whole blood and DBS. An LOD of 0.9 ng/mL (5 pM) was achieved in 10-fold diluted whole blood and a LOD below 2 ng/mL (10 pM) was obtained in 100-fold diluted matrices listed above. The calibration curves for 100-fold diluted matrices indicated that the matrix effect is insignificant for this dilution factor. More importantly, all of the calibration curves were performed on two independent days with two batches of independently prepared FO-SPR sensor and gold nanoparticles (AuNPs) in a random manner. The statistical results indicate insignificant difference between the results generated on the two days, meaning that a new calibration is unnecessary for each batch of FO-SPR sensors and AuNPs. Finally, an immunoassay validation was carried out on 10 clinical samples from IFX-treated IBD patients and benchmarked with the clinically validated ELISA. Excellent agreement was obtained between the two systems.

This thesis demonstrates the potential of the FO-SPR biosensor for a variety of applications that require specific, sensitive, rapid and robust detection with an affordable and portable device for POC diagnostics or on-site measurements.

Samenvatting

Biosensoren hebben een breed toepassingsgebied variërend van de landbouwindustrie en voedselveiligheid tot medische diagnose en milieumonitoring, en krijgen steeds meer commerciële aandacht. De steeds toenemende kosten in de gezondheidszorg stimuleren bovendien het onderzoek naar biosensoren die snelle, gevoelige, nauwkeurige en robuuste detectie ter plaatse mogelijk maken. Eén enkele biosensor die aan al deze vereisten voldoet, is echter nog niet op de markt verkrijgbaar.

Surface plasmon resonance (SPR) gebaseerde optische biosensoren vormen een veelbelovende technologie voor meerdere biosensor-gerelateerde toepassingen. Deze sensoren maken gebruik van plasmonische oppervlaktegolven om lokale veranderingen in brekingsindex te meten als gevolg van interacties tussen doelmoleculen en biomoleculen die op het sensoroppervlak zijn geïmmobiliseerd. De meest gebruikte SPR biosensor, gecommmercialiseerd door Biacore, maakt gebruik van een prisma voor SPR-excitatie en verschaft zowel gevoelige als betrouwbare resultaten. Het apparaat is echter omvangrijk en duur en daarom niet geschikt voor detectie ter plaatse. Een beloftevol alternatief voor SPR-excitatie is het gebruik van optische vezels, met als voordeel dat deze betaalbaar en klein zijn. In dit proefschrift wordt een optische vezel SPR (FO-SPR) biosensor onderzocht voor een verscheidenheid aan toepassingen. De FO-SPR-biosensor is volledig geautomatiseerd, eenvoudig te miniaturiseren, betaalbaar en betrouwbaar. Hoewel dit principe reeds aangetoond werd voor antilichaam- en DNA-gebaseerde bioassays, werd het tot nu toe nooit in echte biologische stalen geïmplementeerd.

Dit werk heeft tot doel om het potentieel van de FO-SPR biosensor te onderzoeken voor gevoelige en snelle detectie van doelmoleculen in reële matrices met behulp van immunoassays. Om dit te bereiken werden twee doelmoleculen geselecteerd op basis van hun grootte en toepassingen,

namelijk progesteron (een klein molecuul dat relevant is voor de landbouwindustrie) en infliximab (een antilichaam dat relevant is voor de gezondheidszorgsector).

In de landbouwsector zijn maximale opbrengsten cruciaal om boeren in staat te stellen competitief te blijven. Voor melkproductie is het meer bepaald van cruciaal belang om tochtigheid bij koeien te detecteren, zodat kunstmatige inseminatie toegepast kan worden om zo het percentage aan geslaagde zwangerschappen te optimaliseren. Tochtigheid wordt vaak gedetecteerd door het progesteron-niveau in de melk te monitoren. Conventioneel wordt hiervoor ELISA gebruikt, maar dit vereist analyse van de stalen in een centraal laboratorium en het duurt bovendien enkele uren om de resultaten te verkrijgen. Onlangs werd een laterale flow-immunoassay (LFIA) op de markt gebracht, waarmee analyse op het bedrijf mogelijk wordt gemaakt in 15 minuten. Dit assay is echter minder gevoelig dan de commercieel beschikbare ELISA (cELISA). Om dit probleem op te lossen, werd een competitief immunoassay ontwikkeld met behulp van de FO-SPR-biosensor voor het bepalen van het progesteronniveau in melk. Een detectielimiet (LOD) van 0,5 ng/ml (1,6 nM) werd bereikt in melk-standaarden. Bovendien werd validatie van de test uitgevoerd in 6 stalen koemelk en vergeleken met de referentie cELISA, waarbij een goede correlatie werd verkregen (Pearson correlatie = 0,98, ICC = 0,97). Dit werk toont aan dat de FO-SPR-biosensor in staat is om binnen 20 minuten kleine moleculen in nanomolaire concentraties te detecteren in een complexe melkmatrix.

In de zorgsector kunnen patiënten baat hebben bij technieken voor continue opvolging van chronische aandoeningen en vroegtijdige diagnose van ziekten. Infliximab (IFX) is een therapeutisch antilichaam dat wordt toegediend aan patiënten met inflammatoire darmaandoeningen. Dit biologische middel vereist therapeutische monitoring om aanpassingen van de dosering mogelijk te maken en derhalve de uitkomst van de behandeling te optimaliseren. De traditionele methoden voor detectie van IFX, zoals ELISA en radio-immunoassay worden echter in een centraal laboratorium uitgevoerd, wat onmiddellijke aanpassingen van de toegediende dosis onmogelijk maakt. Voor deze toepassing werd een sandwich-immunoassay ontwikkeld. Een LOD van 2,2 ng/ml (15 pM) werd bereikt in 100-voudig verdund serum, in een totale tijd van 40 minuten. Het immunoassay werd gevalideerd met 5 serum-stalen van patiënten met inflammatoire darmziekte (IBD) die met IFX

behandeld werden. Deze resultaten toonden een uitstekende overeenkomst tussen de FO-SPR en de klinisch gevalideerde ELISA (Pearson-correlatie van 0,998 en ICC van 0,983 met een inter-CV van minder dan 10%).

Aangezien detectie van IFX meestal uitgevoerd wordt in serum- of plasmastalen, moet hiervoor het bloedstaal van de patiënt bewerkt worden, hetgeen de doorlooptijd verlengt. Deze staalvoorbereiding kan echter vermeden worden door de directe detectie van IFX in volbloed. Bovendien kunnen patiënten via de gedroogde bloedspot (DBS) methode thuis bloed verzamelen en dus bezoeken aan het ziekenhuis vermijden. Een geavanceerd immunoassay werd ontwikkeld met een totale detectietijd van 10 minuten. Dit snelle immunoassay werd getest in matrices waaronder serum, plasma, volbloed en DBS. Een LOD van 0,9 ng/ml (5 pM) werd bereikt in 10-voudig verdund volbloed en een LOD van minder dan 2 ng/ml (10 pM) werd verkregen in 100-voudig verdunde matrices die hierboven werden vermeld. De kalibratiecurven voor deze 100-voudige verdunning gaven bovendien aan dat het matrixeffect voor deze verdunningsfactor niet significant was. Bovendien werden alle kalibratiecurven op een willekeurige manier en op twee onafhankelijke dagen uitgevoerd, met twee batches onafhankelijk voorbereide FO-SPR-sensoren en gouden nanopartikels (AuNP's). De statistische resultaten toonden aan dat er geen significant verschil was tussen de resultaten die op de twee verschillende dagen werden gegenereerd, wat een nieuwe kalibratie voor elke nieuwe batch FO-SPR-sensoren en AuNP's overbodig maakt. Ten slotte werd een validatie van het immunoassay uitgevoerd met behulp van 10 klinische stalen van IFX-behandelde IBD-patiënten. Vergelijking van de resultaten van de FO-SPR sensor met de klinisch gevalideerde ELISA gaf een uitstekende overeenstemming tussen de twee systemen aan.

Dit proefschrift demonstreert het potentieel van de FO-SPR biosensor voor een verscheidenheid aan toepassingen die specifieke, gevoelige, snelle en robuuste detectie vereisen met een betaalbaar en draagbaar apparaat, zowel voor POC-diagnostiek als metingen ter plaatse.

Abbreviations and symbols

| | |
|--------------|---|
| β hCG | β human chorionic gonadotropin |
| ϵ_d | permittivity of the dielectric |
| ϵ_m | permittivity of the metal |
| λ_0 | wavelength of incident light in free space |
| ω | angular frequency of the incident light in free space |
| A | grating period |
| ADM | Adalimumab |
| Al | Aluminum |
| Au | Gold |
| AuNP | gold nanoparticle |
| BSA | bovine serum albumin |
| c | speed of light in vacuum |
| cELISA | commercially available ELISA |
| CFU | colony forming units |
| cSPR | conventional surface plasmon resonance |
| CV | coefficient of variation |
| DBS | dried blood spot |
| E_0 | amplitude of the electric field |

| | |
|----------------|--|
| <i>E. coli</i> | <i>Escherichia coli</i> |
| EDC | 1-ethyl-3-(3-dimethylaminopropyl) carbodiimide hydrochloride |
| ELISA | enzyme linked immunosorbent assay |
| Fab | fragment antigen-binding |
| Fc | fragment crystallizable |
| FO | fibre optics (optical fiber) |
| FO-SPR | fiber optic surface plasmon resonance |
| FBG | fiber Bragg grating |
| FWHM | full width at half maximum |
| GAM | goat anti mouse antibody |
| GC-SPR | grating-coupled SPR |
| HMSA | homogeneous mobility shift assay |
| HRP | horseradish peroxidase |
| IBD | inflammatory bowel disease |
| ICC | intraclass coefficient |
| IFX | infliximab |
| $k_{in,x}$ | wave vector of the incident light along the x axis |
| $k_{in,z}$ | wave vector of the incident light along the z axis |
| $k_{SP,x}$ | wave vector of SPs along the x axis |
| $k_{SP,z1}$ | electric field of the SP waves decaying along the z direction in the dielectric region |
| $k_{SP,z2}$ | electric field of the SP waves decaying along the z direction in the metal region |
| LFIA | lateral flow immunoassay |
| LOD | limit of detection |

| | |
|------------------|--------------------------------------|
| LPFG | long period fiber grating |
| LRSPR | long-range surface plasmon resonance |
| m | order of diffraction |
| MES | 2-(N-Morpholino)ethanesulfonic acid |
| MgF ₂ | magnesium fluoride |
| MMF | multi-mode fiber |
| MNP | magnetic nanoparticle |
| MOF | microstructured optical fiber |
| MZI | Mach-Zehnder interferometer |
| NA | numerical aperture |
| n_d | refractive index of the dielectric |
| NHS | N-hydroxysuccinimide |
| n_m | refractive index of the metal |
| n_s | refractive index of the sample |
| OD | optical density |
| P4 | progesterone |
| PBG | photonic bandgap |
| PBS | phosphate-buffered saline |
| PC-SPR | prism-coupled SPR |
| PCF | photonic crystal fiber |
| POCT | point-of-care testing |
| RI | refractive index |
| RIA | radioimmunoassay |
| RIU | refractive index units |
| RU | response unit |

| | |
|---------------|-----------------------------------|
| SAM | self-assembling monolayer |
| <i>S. epi</i> | <i>Staphylococcus epidermidis</i> |
| SMF | single mode fiber |
| SP | surface plasmon |
| SPP | surface plasmon polariton |
| SPR | surface plasmon resonance |
| SPRi | surface plasmon resonance imaging |
| TDM | therapeutic drug monitoring |
| Teflon-AF | Teflon amorphous fluoropolymer |
| TFBG | tilted fiber Bragg grating |
| TIR | total internal reflection |
| TNF- α | tumor necrosis factor alpha |
| UTI | urinary tract infection |
| WHO | World Health Organization |

Table of Contents

| | |
|--|------------|
| Abstract | iii |
| Samenvatting | vii |
| Abbreviations and symbols | xi |
| Table of Contents..... | xv |

1. General introduction..... 1

| | | |
|-------|---|----|
| 1.1 | Biosensors | 2 |
| 1.2 | Portable biosensors and point-of-care testing | 4 |
| 1.3 | Diagnostic targets..... | 6 |
| 1.3.1 | Progesterone detection in the agriculture industry..... | 7 |
| 1.3.2 | Infliximab detection in the healthcare sector | 8 |
| 1.4 | Outline and objectives..... | 9 |
| 1.5 | References..... | 13 |

2. Surface plasmon resonance: state-of-the-art..... 17

| | | |
|-----|--------------------------------------|----|
| 2.1 | Plasma oscillations and SPs | 18 |
| 2.2 | Characteristics of SPR sensors..... | 21 |
| 2.3 | Classifications of SPR sensors | 22 |

| | | |
|-------|--|----|
| 2.3.1 | Diffraction grating-coupled SPR | 23 |
| 2.3.2 | Prism-coupled SPR..... | 24 |
| 2.3.3 | FO-SPR sensors..... | 27 |
| 2.4 | Miniaturized SPR biosensors | 34 |
| 2.5 | Surface modification of the sensor surface | 39 |
| 2.6 | Conclusions..... | 42 |
| 2.7 | References..... | 45 |

3. Competitive inhibition assay for the detection of progesterone in dairy milk using a fiber optic SPR biosensor 51

| | | |
|-------|--|----|
| 3.1 | Introduction..... | 53 |
| 3.2 | Materials and methods | 55 |
| 3.2.1 | Reagents..... | 55 |
| 3.2.2 | FO-SPR setup | 56 |
| 3.2.3 | Immobilization of goat anti-mouse antibody on gold nanoparticles | 57 |
| 3.2.4 | Competitive inhibition assay on the FO-SPR | 57 |
| 3.2.5 | ELISA procedure | 58 |
| 3.2.6 | Data processing..... | 58 |
| 3.3 | Results and discussion | 60 |
| 3.3.1 | FO-SPR competitive inhibition assay development | 60 |
| 3.3.2 | Progesterone detection in buffer and milk standards with ciFO-SPR assay..... | 62 |
| 3.3.3 | Screening of biological samples | 65 |
| 3.4 | Conclusions..... | 66 |
| 3.5 | Supplementary information..... | 67 |

| | | |
|---------|---|----|
| 3.5.1 | Detection protocol | 67 |
| 3.5.2 | Results and discussion | 68 |
| 3.5.2.1 | FO-SPR competitive inhibition assay development | 68 |
| 3.5.2.2 | Screening of biological samples | 71 |
| 3.6 | References | 72 |

4. Fiber optic-SPR platform for fast and sensitive infliximab detection in serum of inflammatory bowel disease patients 75

| | | |
|---------|---|----|
| 4.1 | Introduction | 77 |
| 4.2 | Materials and methods | 79 |
| 4.2.1 | Buffers and reagents | 79 |
| 4.2.2 | Methods | 80 |
| 4.2.2.1 | FO-SPR platform and preparation of fiber probes | 80 |
| 4.2.2.2 | Surface functionalization of the FO probes with antibodies | 80 |
| 4.2.2.3 | Surface functionalization of AuNPs with antibodies..... | 83 |
| 4.2.2.4 | Establishing FO-SPR assay for IFX detection in buffer and serum | 83 |
| 4.2.2.5 | IFX quantification in IFX treated patients' sera using FO-SPR | 84 |
| 4.2.2.6 | IFX quantification in IFX treated patients' sera using ELISA | 84 |
| 4.3 | Results and discussion | 85 |
| 4.3.1 | Immobilization of IFX-specific antibody on the surface of FO probes | 85 |
| 4.3.2 | Controlling the nonspecific binding on the surface of FO probes | 86 |

4.3.3 Detecting IFX spiked in buffer and serum using FO-SPR platform88

4.3.4 Validation of established FO-SPR bioassay with sera from IFX treated patients 91

4.4 Conclusions 92

4.4 Supplementary information..... 94

4.4.1 FO-SPR platform and preparation of fiber probes..... 94

4.4.2 Results 95

4.4.2.1 Selection of blocking buffer 95

4.4.2.2 FO-SPR signal amplification with AuNPs 96

4.4.2.3 Controlling nonspecific binding 96

4.4.2.4 Evaluation of the fitting model..... 97

4.4.2.5 Calibration curve in 200-fold diluted serum..... 98

4.4.2.6 Evaluation of established FO-SPR assay with IBD patient samples..... 99

4.5 References..... 101

5. Immunoassay for detection of infliximab in whole blood using a fiber-optic surface plasmon resonance biosensor 105

5.1 Introduction..... 107

5.2 Materials and methods 108

5.2.1 Buffers and reagents 108

5.2.2 FO-SPR platform and preparation of FO-SPR sensors..... 109

5.2.3 Detection of IFX spiked in 10-fold diluted whole blood.. 109

5.2.4 Preparation and extraction of DBS samples 110

5.2.5 Establishing a POC FO-SPR bioassay for IFX detection . 111

| | | |
|---------|---|-----|
| 5.2.6 | Validation of the POC FO-SPR bioassay using serum and plasma samples from IFX-treated patients..... | 111 |
| 5.2.7 | IFX quantification in serum and plasma samples from IFX-treated patients using ELISA..... | 111 |
| 5.2.8 | Data analysis..... | 111 |
| 5.3 | Results and discussion | 112 |
| 5.3.1 | FO-SPR bioassay for detection of IFX in 10-fold diluted whole blood..... | 112 |
| 5.3.2 | Accelerated POC FO-SPR bioassay for detection of IFX in 10-fold diluted whole blood | 113 |
| 5.3.3 | POC FO-SPR bioassay for detection of IFX in 100-fold diluted serum, plasma and whole blood | 115 |
| 5.3.4 | POC FO-SPR bioassay for detection of IFX in 100-fold diluted DBS..... | 116 |
| 5.3.4 | Comparison of the POC FO-SPR bioassay performance in different matrices | 118 |
| 5.3.5 | Validation of the POC FO-SPR bioassay with plasma and serum samples from IFX treated patients..... | 119 |
| 5.4 | Conclusions..... | 121 |
| 5.5 | Supplementary information..... | 124 |
| 5.5.1 | Materials and Methods | 124 |
| 5.5.1.1 | FO-SPR platform and preparation of FO-SPR sensors | 124 |
| 5.5.1.2 | FO-SPR bioassay and POC FO-SPR bioassay steps | 124 |
| 5.5.1.3 | Determining limit of detection | 126 |
| 5.5.2 | Results | 127 |
| 5.5.2.1 | Binding kinetics of AuNPs in the POC FO-SPR bioassay | 127 |
| 5.5.2.2 | Correlation between spiked and reference DBS samples | 128 |

5.5.2.3 Studying the impact of different sample matrices on the POC FO-SPR bioassay 128

5.5.2.4 Validation of the POC FO-SPR bioassay with plasma and serum samples from IFX treated patients..... 132

5.6 References..... 134

6. General conclusions and future perspectives 137

6.1 General conclusions 137

6.2 Future perspectives 140

6.2.1 Long-range SPR for detection of whole cells 142

6.2.2 Self-referenced sensor 146

6.2.3 FO-SPR biosensor toward POC..... 147

6.2.4 DBS sample collection using a glass capillary..... 148

6.3 Reference 151

Publications..... 153

Chapter 1

General introduction

Biotechnology is the field of science that has existed since the dawn of human civilization, even before its name was coined by the Hungarian agricultural engineer Károly Ereky in 1919. By definition, biotechnology is the use of living organisms to develop products and processes. Humans have been constantly striving to develop new methods using biological resources in order to make life more comfortable and convenient. Dating back to 7000 years ago, people living in Mesopotamia and Egypt used bacteria to convert wine into vinegar and utilized yeast for brewing beer and baking bread. Subsequently, humans began exploiting soil organisms to improve crop yields, to breed animals for meat and to manufacture by-products from animals, such as cheese. As civilization continued to advance, humans gained more knowledge on biology and technology, and implemented biotechnology techniques in a wide range of applications such as the manufacturing of antibiotics, the production of vaccines, and the synthesis and amplification of DNA for medical diagnosis. In fact, biotechnology has been utilized to improve the environment and to raise living standards in practically every aspect of our lives.

To further improve the quality of life, we can benefit from sensing technology in areas such as food and medical sciences, which has driven the development of devices known as biosensors. A wide variety of applications

have exploited biosensors ranging from food production and medical diagnosis to environmental monitoring. In this thesis, we will focus on two of these applications, namely the agro-food and the healthcare sectors. Over the years, both fields have witnessed a trend of continuous technical innovations to address various challenges, such as (i) maximizing production yield in the agriculture industry and thus allow farmers to remain competitive or (ii) in the healthcare sector, improving patients' wellbeing by enabling early diagnosis and monitoring of chronic diseases. In the context of this, we use in the thesis an in-house established fiber optic surface plasmon resonance (FO-SPR) biosensor to address some of the remaining challenges in these fields.

In this chapter we will give a general overview of biosensors, followed by a detailed description of a subset of biosensors, known as point-of-care (POC) devices, as well as the discussion on the current POC market situation and technical limitations. Furthermore, two target analytes (i.e. progesterone hormone and infliximab antibody (IFX)) from two different applications (agriculture and healthcare sector, respectively) along with state-of-the-art detection techniques are discussed. Finally, an overview of the thesis and the objectives of each chapter are given.

1.1 Biosensors

A biosensor is an analytical device that converts a biological response into a measurable signal using two of its major components: a biological recognition element and a transduction system. The biological recognition element, also known as a bioreceptor, is directly linked to a transducer and can be an enzyme, nucleic acid, antibody, cell or biomimetic material (for instance aptamers, peptide nucleic acids, nanobodies, etc., Figure 1.1). The first biosensor was developed in 1962 by Clark [1], when using an electrode coated with enzymes to monitor blood parameters such as glucose concentration [2]. This publication was highly significant for the development of modern biosensors for a number of reasons. First, it has defined important biosensing criteria, such as rapid response, ease-of-use and portability of the biosensing device. Next, the technique was successfully deployed for monitoring blood chemistry of surgical patients in a hospital, and finally, it inspired the development of the commercial blood glucose biosensor, which is still recognized as the greatest success in the biosensor market. Since then, several

other criteria have been widely accepted as highly desired and important in the biosensing field, such as high specificity and sensitivity for the analyte detection.

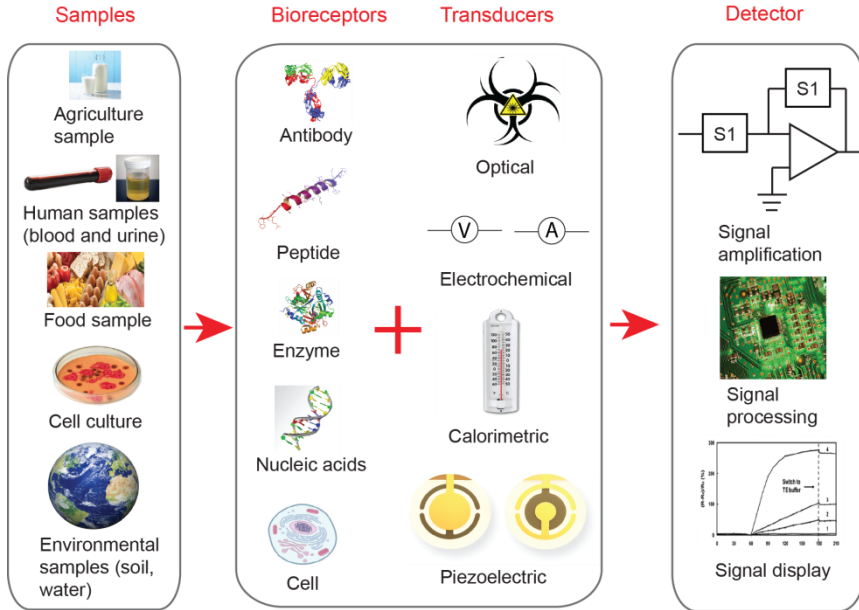


Figure 1.1 A scheme of components in biosensors, adapted with the permission from [3], Copyright (2008) MDPI.

Following this first example, numerous other biosensing platforms have been developed for a broad range of applications from medical diagnosis to food safety and environmental monitoring. As analytes can exist in various matrices such as blood, urine, milk or soil, different types of biosensors are used depending on the application. The classification of biosensors can be based on the type of selected bioreceptor molecule (enzyme sensors, immunosensors, DNA sensors, etc.) or on the measured physical property (Figure 1.1). The latter classification recognizes the following biosensors: (i) electrochemical, such as amperometric and potentiometric biosensors, which use bioreceptors immobilized on the electrode to measure the current or voltage change [4, 5]; (ii) calorimetric biosensors, which measure the temperature change as a result of the interaction between target and receptor [6]; (iii) piezoelectric biosensors are often based on quartz-crystal coated gold

electrodes to measure the change of mass change-induced resonant frequency [7]; and (iv) optical biosensors, which measure for instance changes in absorption, luminescence or scattering of the light, optical images of the target analytes, SPR, etc. [8-10].

Biosensors are employed in a wide variety of applications as seen in Figure 1.1, and many of these applications require fast results, less work on sample preparation, and performing tests near the source of the samples. Therefore, portable biosensors which can provide fast, reliable and accurate results and which can be transported easily to the location where tests are conducted, are highly desirable.

1.2 Portable biosensors and point-of-care testing

Traditionally, tests for almost all the applications mentioned in the previous section are conducted in a central laboratory. This requires sample collection and transportation, which can substantially delay the time to result. However, this can be evaded with portable biosensors that allow performance of tests near the source of the samples, such as farms (agriculture industry), rivers and forests (environmental monitoring), food factories (food safety) and probably the most important, near the patients (healthcare sector). Substantial research and development has been dedicated to portable biosensors for so-called point-of-care-testing (POCT). POCT includes diagnostic tests that are performed near the patient or used for self-testing at home. It offers rapid and reliable results, which facilitates immediate diagnostic decisions, reduces patient follow-up visits, improves therapeutic outcomes, and reduces the length of time spent by patients in hospitals. There are a few essential criteria that differentiate POCT from conventional central laboratory tests: (i) testing body fluids should be in the immediate proximity of the patient, (ii) dedicated devices should be capable of performing single rather than serial analyses and (iii) tests results should allow immediate therapeutic actions to be taken [11]. However, for resource-limited environments, requirements are even stricter considering the circumstances. Therefore, the World Health Organization (WHO) specifically defined criteria for POC devices that are encapsulated in the acronym, ASSURED (Affordable, Sensitive, Specific, User-friendly, Rapid and robust, Equipment-free and Deliverable to end users). Examples of commercialized POC devices are illustrated in Figure 1.2. A smartphone-

based quantitative lateral flow reader (HRDR-200) developed by Holomic offers features including high sensitivity and accuracy, ease-of-use and low cost as illustrated in Figure 1.2 A [12]. This reader can be utilized for a variety of lateral flow assays. Another example of commercialized POC device is the i-STAT Alinity blood analyzer developed by Abbott (Figure 1.2 B) [13]. This blood analyzer provides a comprehensive list of the characteristics of patient blood samples, including pH, glucose, hematocrit, lactate and partial pressure of oxygen and carbon dioxide etc.

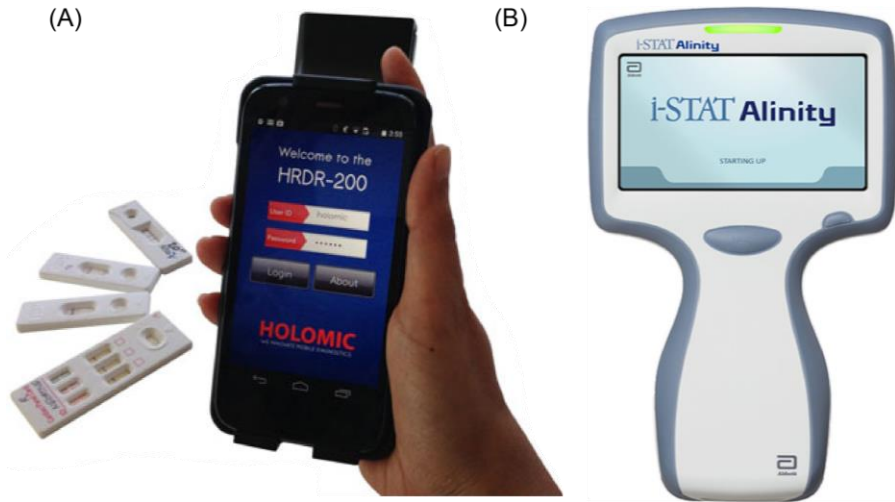


Figure 1.2 Examples of handheld POC devices: (A) smartphone-based quantitative lateral flow reader, HRDR-200, developed by Holomic, and (B) handheld blood analyzer, i-STAT Alinity, developed by Abbott.

Numerous global challenges draw increasing attention and financial support for developing POCT devices, including the rise of antibiotic resistance, the high cost of effective drugs, the rising incidence of lifestyle diseases, such as cardiac and diabetes in developed countries, and the increased threat of infectious diseases, such as malaria and HIV spreading from low-resource countries due to globalization. The global POCT market is expected to grow at a compound annual growth rate of 9.8% from 2016 to 2021, and is projected to reach \$37 billion USD by 2021 [14].

The POCT market is organized according to specific conditions or diseases [15]. Currently, glucose testing, which allows diabetic patients to

perform tests at home, holds the largest segment in the POCT market [16]. Although the general public might have the impression that all POC devices should and will only be available at home, the reality is that in the near future a lot of POCT will still be used within traditional test settings for a number of applications. One example is diagnostics and monitoring of cardiology and oncology diseases, with predictions that POC devices will still be seen in traditional care settings for at least next five to ten years [15]. On the contrary, for diagnosis of acute and infectious disease in low-resource countries, due to limited access to central laboratories and a lack of medical expertise, patients often cannot be treated in time. Therefore, POC devices that fulfill the ASSURED criteria are highly desired.

Despite this great need, there are still numerous barriers that limit expansion of the POCT market, with economics being the primary limitation. The high cost associated with the development and commercialization of a POC device makes it difficult to replace conventional testing devices. Moreover, the fact that most POC technologies are only developed for a specific disease, further adds to this high cost. Additional challenges include lower analytical sensitivity compared to the assays performed in the central laboratory, inadequate regulation for quality control and, for low resource countries, a lack of resources to train personnel on using the devices which may cause lower accuracy in results [17, 18]. Thus, rapid, sensitive and reliable POC devices that can be used for multiple applications are highly desirable in the market to reduce development costs. In this thesis, we explore an in-house established FO-SPR platform, for its capacity to accommodate different applications and potential to be miniaturized to be a portable biosensor. Two specific targets used in the thesis are discussed in more detail in the next section while a detailed discussion on the physical principles of SPR, the state-of-the-art of portable SPR biosensors and the FO-SPR platform is shown in Chapter 2.

1.3 Diagnostic targets

Our in-house developed FO-SPR platform has been already demonstrated for its capacity to detect a variety of different targets (e.g. DNA, antibodies, proteins, phages, etc.) [19-21] next to having other advantages, such as being fully automated, and easy to miniaturize. All these features offer great

potential to develop a unique sensing platform that can be used for multiple applications requiring portable biosensors. However, the developed FO-SPR bioassays mainly remained at the proof-of-concept level without extensive validation using complex biological samples. Therefore, in this thesis we focus on the development and implementation of novel bioassays that are specific and sensitive, and at the same time robust enough to detect targets directly in complex biological matrices. In this work two target molecules are used, namely progesterone and infliximab (IFX), representing different classes of targets with respect to the size (i.e. small molecule and antibody, respectively). Moreover, the two targets impose detection in different matrices (i.e. milk and serum/plasma/blood, respectively). This poses major challenges for the development of the immunoassays on the FO-SPR platform.

1.3.1 Progesterone detection in the agriculture industry

The rate of cattle reproduction is a major factor that influences profitability for dairy and livestock producers. When a cow is not pregnant after 90 days of post-calving, the dairy farm loses daily between \$2 to \$7 per cow since the cow is not producing milk during this period [22]. Due to the low natural conception rate, most herd owners now use artificial insemination [23]. To achieve a higher rate of conception it is important to accurately detect estrus. One of the most reliable methods to determine estrus is to detect the progesterone (a hormone produced by the corpus luteum) level in blood or milk. Since a good correlation between progesterone concentration in milk and blood is found, detection of progesterone in milk is often performed, as milk is an easy source of samples.

Traditionally, the progesterone concentration is determined by radioimmunoassay (RIA) but these tests are expensive, they take days to obtain results, and they require a special facility to dispose the associated radioactive waste. Instead, herd owners would prefer to obtain the results for measuring progesterone immediately on the farm. In recent years, more techniques have become available on the market, including an on-farm used enzyme linked immunosorbent assay (ELISA) [24], a fluorescence-based immunoassay [25], and a lateral flow immunoassay (LFIA) [26, 27]. However, many of these techniques still suffer from problems such as bulkiness and an inability to provide quantitative results [28]. An exception to

this is the Herd Navigator® (Lattec, Hillerød, Denmark), a LFIA test which offers quantitative testing although at a lower sensitivity than the traditional ELISA [27]. Therefore, there is still room on the market for devices that provide direct quantification of progesterone in milk in a specific, sensitive, automated and cost-effective fashion to allow rapid off-laboratory inspection of milk samples. The FO-SPR biosensor will be explored in this thesis as a candidate for developing a progesterone specific bioassay since it satisfies most of the critically important criteria, as described in Chapter 3.

1.3.2 Infliximab detection in the healthcare sector

Therapeutic drug monitoring (TDM) is the clinical practice of measuring drug concentrations in serum, plasma or blood, and adjusting individual dosage to maintain drug concentrations within an optimal range. This approach is mainly used for drugs with narrow therapeutic ranges, a reasonable relationship between blood concentrations and clinical effects, and drugs known to cause therapeutic effects [18]. As such, TDM is beneficial for improving therapeutic outcomes, avoiding toxicity, monitoring and evaluating drug-drug interactions. In this thesis, we aim to develop a FO-SPR based immunoassay for detecting a biologic agent known as IFX, used for treating patients with inflammatory bowel disease (IBD).

One of the main causes of IBD is the overproduction of tumor necrosis factor (TNF) in mucosal tissue [11]. To suppress the symptoms, non-steroidal anti-inflammatory drugs, antibiotics, steroids or anti-TNF biologic agents are prescribed to patients depending on the severity of the symptoms [29]. Two types of commonly used biologic agents are IFX and adalimumab (ADM), both being monoclonal antibodies that specifically target TNF. At induction phase, an IFX infusion dose of 5 mg/kg is typically administered at week 0, 2 and 6, and followed by maintenance therapy at 8 week intervals [30]. Due to the fact that some patients initially respond to induction therapy but lose the response over time, TDM is practiced for dosage adjustment to improve long-term therapeutic outcomes.

Conventional methods for detection of IFX include ELISA, radioimmunoassay (RIA) and homogeneous mobility shift assay (HMSA) [30-32]. However, all of these techniques are nowadays typically performed in a central laboratory so immediate dosage adaption is not feasible. To date,

only a limited number of publications have been reported on a POC device as alternative to the conventional methods [33-35]. In this thesis, we will investigate the potential of the FO-SPR platform for sensitive and accurate determination of IFX concentrations in clinical samples within the timeframe of a patient's visit to the hospital. The detailed development of these immunoassays is described in Chapter 4 and 5.

1.4 Outline and objectives

As discussed above, portable biosensors market are expanding and devices that are sensitive, specific, reliable, affordable, and versatile are in high demand. Although conventional methods such as ELISA and RIA exploit the simplicity of an immunoassay and are applicable to many different applications, they are unfortunately not suitable for applications that require portable biosensors. Our in house developed FO-SPR platform has numerous desirable features next to the proven capacity to accommodate diverse bioassays for detecting a range of different targets (e.g. DNA, antibodies, proteins, phages, etc.) [19-21]. However, the FO-SPR platform has never been challenged for developing bioassays in real biological samples that regardless of the complexity of the sample matrix, maintain high specificity and sensitivity while offering the desired fast and reproducible interaction between bioreceptors and targets.

In this context, **the general aim of this thesis is to investigate the capability of the FO-SPR platform for the development of sensitive and rapid immunoassays that can specifically detect a variety of target analytes in complex biological matrices.** Immunoassays are selected in the thesis as the type of bioassay to be implemented on the platform since (i) the generation of antibodies is a mature technology often resulting in antibodies with high affinity and specificity toward their respective antigens, and (ii) binding events between an antibody, especially monoclonal antibody, and an antigen are specific, simple and fast [36]. More specifically, in this work two target molecules are selected, namely progesterone (small molecule) and IFX (antibody), each with their own particular objectives:

- The FO-SPR platform is explored for implementation of a competitive immunoassay for the detection of a small molecule, namely progesterone. The current on-farm LFIA technique provides testing results

within 15 minutes, but with a lower sensitivity than ELISA. The objective is to develop an immunoassay using the FO-SPR platform for determining the progesterone level in milk, which can achieve a comparable sensitivity as ELISA and with a similar detection time as LFIA. To achieve the sensitive detection of such small molecules, the capability of implementing a competitive immunoassay on the FO-SPR platform is explored (Chapter 3).

– The FO-SPR platform is further explored for detecting a therapeutic antibody, IFX. Detection of IFX is still mainly performed in a central laboratory, which requires sample collection and transportation, leading to delay in obtaining results. The objective for IFX detection is to develop a rapid, specific and sensitive immunoassay using the FO-SPR platform. For validation of the immunoassay, tests are carried out with clinical samples.

An overview of the structure of this thesis is illustrated in Figure 1.5. A literature review on the SPR phenomenon and the state-of-the-art SPR biosensors is discussed in **Chapter 2**. The chapter describes the physics of SPR, state-of-the-art SPR sensors, miniaturized SPR biosensors and gold surface modification with bioreceptors.

As introduced in Section 1.3.1, progesterone is a small molecule, hence it is challenging to obtain sensitive detection using a direct sandwich immunoassay. Therefore, in **Chapter 3** a competitive immunoassay is described to attain sensitive detection of progesterone in milk. To achieve this, progesterone (P4) mixed with bovine serum albumin (BSA) is immobilized on the sensor surface. Milk samples containing progesterone are then mixed with antibodies (anti-P4) that specific target progesterone. This way, there is a binding competition to the anti-P4 between P4 immobilized on the sensor surface and P4 in the sample. The concentrations of P4-BSA and anti-P4 are carefully chosen to achieve the optimal binding condition. For signal amplification, gold nanoparticles (AuNPs) are employed.

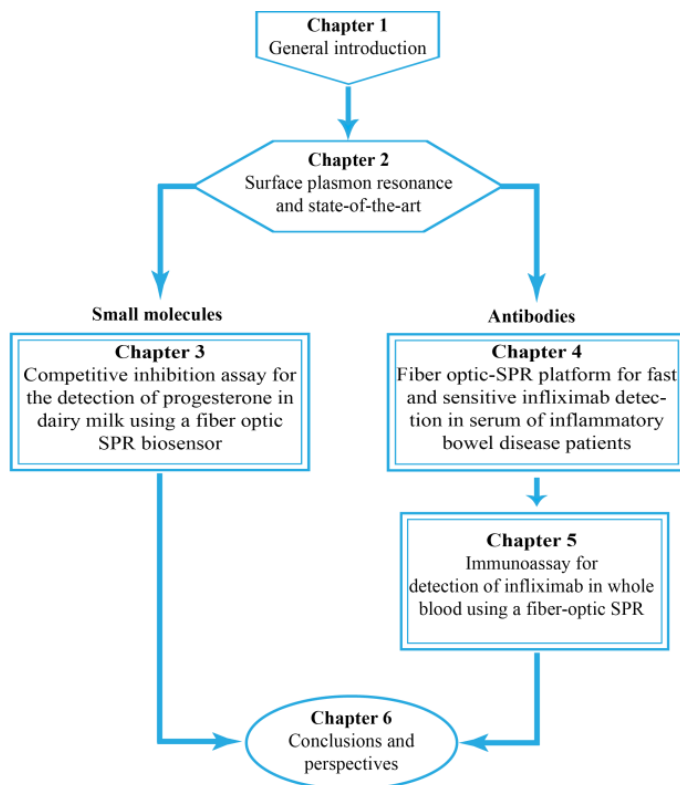


Figure 1.5 Schematic overview of the thesis.

The development of a sandwich immunoassay for detection of IFX is reported in **Chapter 4**. Antibodies specifically targeting IFX are immobilized on the sensor surface. Detailed optimization of buffer and concentration of the capture antibody for immobilization of the capture antibody is discussed. For preventing undesired nonspecific adsorption from patient serum samples to the sensor surface, a blocking buffer is carefully chosen. To achieve an LOD that is within the clinically relevant range, AuNPs conjugated to the detection antibody are introduced to the assay. The developed immunoassay is validated with serum samples from patients.

The immunoassay described in Chapter 4 demonstrates that the FO-SPR is capable of sensitive detection of IFX. However, the total detection time is suboptimal for POCT. In **Chapter 5**, to further reduce the detection time, a novel approach has been implemented for data analysis without influencing

the sensitivity of the assay, leading to a reduction in the total detection time compared to the method in Chapter 4. Since patients' blood samples need to be collected and processed into serum/plasma, this delays the turnaround time. Therefore, direct detection of IFX in blood has been demonstrated, hence shortening the turnaround time. Moreover, by collecting dried blood spots (DBS) samples, patients can avoid going to the hospital. Therefore, the shortened immunoassay is performed in both citrated-treated whole blood and DBS. The validation of the shortened assay is accomplished with 10 clinical samples.

A summary of the thesis is given in **Chapter 6**. All the contents displayed in the thesis demonstrates that the FO-SPR biosensor can be deployed for POCT for various applications. Also, future work that can improve the immunoassay and the FO-SPR sensor is discussed here.

1.5 References

1. Clark, L.C. and C. Lyons, *Electrode systems for continuous monitoring in cardiovascular surgery*. Annals of the New York Academy of sciences, 1962. **102**(1): p. 29-45.
2. Clark Jr, L., *Monitor and control of blood and tissue oxygen tensions*. ASAIO Journal, 1956. **2**(1): p. 41-48.
3. Grieshaber, D., *et al.*, *Electrochemical biosensors-sensor principles and architectures*. Sensors, 2008. **8**(3): p. 1400-1458.
4. Dzyadevych, S., *et al.*, *Amperometric enzyme biosensors: past, present and future*. Irbm, 2008. **29**(2): p. 171-180.
5. Trivedi, U.B., *et al.*, *Potentiometric biosensor for urea determination in milk*. Sensors and Actuators B: Chemical, 2009. **140**(1): p. 260-266.
6. Gardikis, K., *et al.*, *Microbial biosensors to monitor the encapsulation effectiveness of Doxorubicin in chimeric advanced Drug Delivery Nano Systems: A calorimetric approach*. International Journal of Pharmaceutics, 2017. **516**(1-2): p. 178-184.
7. Yamaguchi, S., *et al.*, *Adsorption, immobilization, and hybridization of DNA studied by the use of quartz crystal oscillators*. Analytical Chemistry, 1993. **65**(14): p. 1925-1927.
8. Monošík, R., M. Stred'anský, and E. Šturdík, *Biosensors-classification, characterization and new trends*. Acta Chimica Slovaca, 2012. **5**(1): p. 109-120.
9. Strianese, M., *et al.*, *Fluorescence-based biosensors*. Spectroscopic Methods of Analysis: Methods and Protocols, 2012: p. 193-216.
10. Sahoo, P.R., *et al.*, *Surface plasmon resonance based biosensor: A new platform for rapid diagnosis of livestock diseases*. Veterinary World, 2016. **9**(12): p. 1338-1342.
11. Luppa, P.B., *et al.*, *Clinically relevant analytical techniques, organizational concepts for application and future perspectives of point-of-care testing*. Biotechnology advances, 2016. **34**(3): p. 139-160.
12. Mudanyali, O., *et al.*, *Integrated rapid-diagnostic-test reader platform on a cellphone*. Lab on a Chip, 2012. **12**(15): p. 2678-2686.
13. Breeze, S., *et al.*, *evaluation Of The Next Generation I-stat® Point-of-care Instrument (i-stat Alinity) For Blood Gases: Cod: T077*. Clinical Chemistry and Laboratory Medicine, 2017. **55**: p. S577.
14. Wood, R.W., *On a Remarkable Case of Uneven Distribution of Light in a Diffraction Grating Spectrum*. Proceedings of the Physical Society of London, 1902. **18**(1): p. 269.

15. Todorovic, M. *5 Things You Need To Know About The Point-Of-Care Technology Market*. 2014; Available from: <http://www.meddeviceonline.com/doc/things-you-need-to-know-about-the-point-of-care-technology-market-0001>.
16. Cooke, J., *et al.*, *Narrative review of primary care point-of-care testing (POCT) and antibacterial use in respiratory tract infection (RTI)*. *BMJ open respiratory research*, 2015. **2**(1): p. e000086.
17. Pai, N.P., *et al.*, *Barriers to Implementation of Rapid and Point-of-Care Tests for Human Immunodeficiency Virus Infection: Findings From a Systematic Review (1996–2014)*. *Point of Care*, 2015. **14**(3): p. 81-87.
18. Kang, J.-S. and M.-H. Lee, *Overview of Therapeutic Drug Monitoring*. *The Korean Journal of Internal Medicine*, 2009. **24**(1): p. 1-10.
19. Knez, K., *et al.*, *Spherical nucleic acid enhanced FO-SPR DNA melting for detection of mutations in Legionella pneumophila*. *Analytical chemistry*, 2013. **85**(3): p. 1734-1742.
20. Tran, D.T., *et al.*, *Selection of aptamers against Ara h 1 protein for FO-SPR biosensing of peanut allergens in food matrices*. *Biosensors and Bioelectronics*, 2013. **43**: p. 245-251.
21. Pollet, J., *et al.*, *Fast and accurate peanut allergen detection with nanobead enhanced optical fiber SPR biosensor*. *Talanta*, 2011. **83**(5): p. 1436-1441.
22. Hutjens, M., *Are you leaving money on the table?*, in *Hoards Dairyman*. 2013.
23. Ambrose, D. and M. Colazo. *Reproductive status of dairy herds in Alberta: a closer look*. in *Advances in dairy technology: proceedings of the... Western Canadian Dairy Seminar*. 2007.
24. Wu, L., *et al.*, *Development and Application of an ELISA Kit for the Detection of Milk Progesterone in Dairy Cows*. *Monoclonal antibodies in immunodiagnosis and immunotherapy*, 2014. **33**(5): p. 330-333.
25. Oku, Y., *et al.*, *Validation of a direct time-resolved fluoroimmunoassay for progesterone in milk from dairy and beef cows*. *The Veterinary Journal*, 2011. **190**(2): p. 244-248.
26. Samsonova, J., V. Safronova, and A. Osipov, *Pretreatment-free lateral flow enzyme immunoassay for progesterone detection in whole cows' milk*. *Talanta*, 2015. **132**: p. 685-689.
27. Waldmann, A. and A. Raud, *Comparison of a lateral flow milk progesterone test with enzyme immunoassay as an aid for reproductive status determination in cows*. *The Veterinary record*, 2016. **178**(11): p. 260-260.
28. Nebel, R., *On-farm milk progesterone tests*. *Journal of dairy science*, 1988. **71**(6): p. 1682-1690.

29. Mowat, C., *et al.*, *Guidelines for the management of inflammatory bowel disease in adults*. Gut, 2011. **60**(5): p. 571-607.
30. Sandborn, W.J. and S.B. Hanauer, *Infliximab in the treatment of Crohn's disease: a user's guide for clinicians*. The American journal of gastroenterology, 2002. **97**(12): p. 2962-2972.
29. Tracey, D., *et al.*, *Tumor necrosis factor antagonist mechanisms of action: A comprehensive review*. Pharmacology & Therapeutics, 2008. **117**(2): p. 244-279.
30. Pariente, B., *et al.*, *Trough levels and antibodies to infliximab may not predict response to intensification of infliximab therapy in patients with inflammatory bowel disease*. Inflammatory bowel diseases, 2012. **18**(7): p. 1199-1206.
31. Bendtzen, K., *et al.*, *Individualized monitoring of drug bioavailability and immunogenicity in rheumatoid arthritis patients treated with the tumor necrosis factor α inhibitor infliximab*. Arthritis & Rheumatism, 2006. **54**(12): p. 3782-3789.
32. Castelee, N.V., *et al.*, *Antibody response to infliximab and its impact on pharmacokinetics can be transient*. The American journal of gastroenterology, 2013. **108**(6): p. 962-971.
33. Corstjens, P.L., *et al.*, *A rapid assay for on-site monitoring of infliximab trough levels: a feasibility study*. Analytical and bioanalytical chemistry, 2013. **405**(23): p. 7367-7375.
34. Van Stappen, T., *et al.*, *Rapid Test for Infliximab Drug Concentration Allows Immediate Dose Adaptation*. Clinical and translational gastroenterology, 2016. **7**(12): p. e206.
35. Van Stappen, T., *et al.*, *Rapid Test for Infliximab Drug Concentration Allows Immediate Dose Adaptation*. Clinical and Translational Gastroenterology, 2016. **7**(12): p. e206.
36. Alice Lee, N. and I.R. Kennedy, *Chapter 5 - Immunoassays A2 - Picó, Yolanda*, in *Food Toxicants Analysis*. 2007, Elsevier: Amsterdam. p. 91-145.

Chapter 2

Surface plasmon resonance: state-of-the-art

The initial observation of surface plasmons (SPs) was reported by R.W. Wood in 1902 [1], when polarized light was incident upon a metallic grating. The first theoretical description, which demonstrated that surface plasmons can exist near a metal surface, was published by R.H. Ritchie in 1957 [2]. More than 10 years later, the same author described the anomalous behavior of metal gratings where surface plasmon resonance (SPR) can be generated [3]. In the same year, a significant milestone in the development of modern SPR sensors was reached by the research team of Otto, and the research team of Kretschmann and Reather, with both groups reporting methods for optical excitation of SPR by utilizing a thin silver film coated on one side of a glass prism [4, 5]. Thereafter, research on SPR has gradually transitioned from fundamental studies towards practical applications with real-time monitoring of biomolecular interactions (IgG/anti-IgG binding) reported for the first time in 1983 [6]. The widespread implementation of SPR techniques for biosensing began with the launch of the first commercial SPR-based sensor, namely Biacore in the early 1990s [7]. Since then, there has been an ever increasing amount of publications on SPR-based sensors for detection of biomolecules.

In this chapter, detailed discussions are presented on the physics of surface plasmons, various configurations for achieving excitation of SPR and

corresponding SPR sensors, state-of-the-art of miniaturized SPR biosensors, and strategies for surface modifications of the SPR sensor surface.

2.1 Plasma oscillations and SPs

As mentioned previously, the SPR phenomenon occurs at a metal/dielectric interface under certain conditions as will be explained further. In a metal, an equal quantity of positively charged ions and negatively charged electrons results in the net charge of a metal being zero and metal being electronically neutral. Locally, due to the relatively light weight of electrons compared to the positive ions, electrons are pulled toward ions by electrostatic force while picking up kinetic energy. The kinetic force reaches a maximum when the electrons pass the ions, so they continue to move forward and eventually are pulled back toward ions by restoring forces, thereby generating plasma oscillations [8]. A plasmon is a quantum of plasma oscillations. Unlike bulk plasmons, which occur throughout the entire volume of a piece of metal, SPs or surface plasmon polaritons (SPPs) are confined to a metal/dielectric interface. The optical excitation of SPs is commonly known as SPR.

When using light to excite SPs, the energy of incident photons needs to be transferred to electrons in the metal, which requires a certain wavelength of light at a certain angle of incidence. As illustrated in Figure 2.1, the metal and the dielectrics are stacked along the z axis and SP waves are transmitted along the interface of the metal and dielectric 2. Therefore, when light is transmitted from the dielectric 1 onto the metal surface, within a given plane of incidence (x - z plane), the electric field that is normal to the x axis is expressed as follows:

$$\vec{E} = E_0 \exp[i(\vec{k}_{in}\vec{r}-\omega t)] = E_0 \exp[i(k_{in,x}x \pm k_{in,z}z - \omega t)] \quad (2.1)$$

$$k_{in} = \frac{2\pi}{\lambda_0} \sqrt{\varepsilon_d} = \frac{\omega}{c} \sqrt{\varepsilon_d} = \sqrt{k_{in,x}^2 + k_{in,z}^2} \quad (2.2)$$

where E_0 is the amplitude of the electric field, $k_{in,x}$ and $k_{in,z}$ are the wave vectors of the incident light along the x and z axes respectively, ε_d is the permittivity of the dielectric, ω is the angular frequency of the incident light in free space, λ_0 is the wavelength of incident light in free space and c is the speed of light in vacuum. The symbol “ \pm ” represents the direction of the electric field: when

“+” is used, the equation represents the electric field in the dielectric region.
 “-” is used for the metal region.

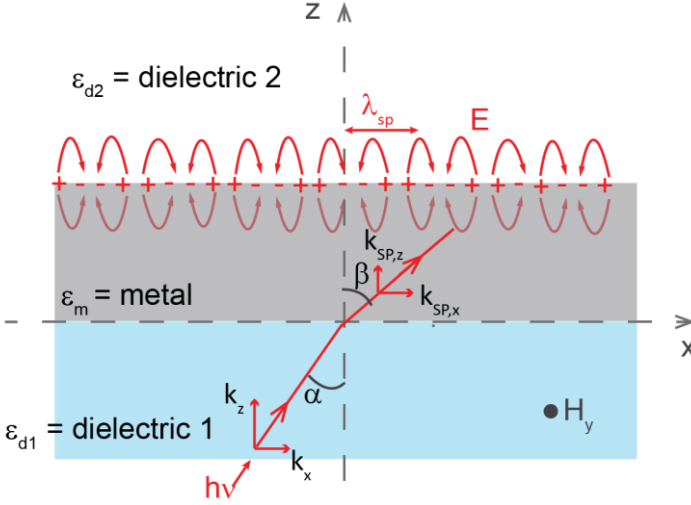


Figure 2.1 Interfaces of dielectric/metal and metal/dielectric. Light is incident onto the metal from dielectric 1, and the SPs are excited on the interface of the metal and dielectric 2.

As seen in Equation 2.1, p-polarized light (parallel to the plane of incidence) is therefore the primary condition for exciting SPs. Since the electric and magnetic field must satisfy Maxwell’s equations [9], by combining with the continuous boundary conditions and Equation 2.2, the wave vectors of the SP waves can be solved as follows:

$$k_{SP,x} = \frac{2\pi}{\lambda_0} \sqrt{\frac{\epsilon_d \epsilon_m}{\epsilon_d + \epsilon_m}} \quad (2.3)$$

$$k_{SP,z1} = \frac{2\pi}{\lambda_0} \sqrt{\frac{\epsilon_d^2}{\epsilon_d + \epsilon_m}}, k_{SP,z2} = \frac{2\pi}{\lambda_0} \sqrt{\frac{\epsilon_m^2}{\epsilon_d + \epsilon_m}} \quad (2.4)$$

where ϵ_m is the permittivity of the metal, $k_{SP,x}$ denotes the wave vector of SPs along the x axis, also known as the propagation constant of the SP waves, $k_{SP,z1}$ and $k_{SP,z2}$ represent the electric field of the SP waves decaying along the z direction in the dielectric and the metal region, respectively. The permittivity of the metal is complex, but in this thesis ϵ_m only represents the real part. For sensing purpose, the penetration depths (the distance from the incident point

at the metal/dielectric interface where the SP waves decay exponentially along $+z$ or $-z$ direction) of the SP waves in the dielectric is critical, which is indicated in Equation 2.5,

$$\delta_{SP,z1} = \frac{1}{k_{SP,z1}} = \frac{\lambda_0}{2\pi} \sqrt{\frac{\epsilon_d + \epsilon_m}{\epsilon_d^2}} \quad (2.5)$$

As the frequency range of the visible light region is greater than that of the near infrared (NIR) light region, this equation explains that the penetration depth of SP waves in NIR region is greater than that in the visible light region. Using a gold (Au)/water interface as an example to estimate the penetration depth of the SP waves with Equation 2.5, when the incident wavelength is 600 nm, the penetration depth in water is approximately 149 nm. Here, ω is $3.14 \times 10^{15} \text{ s}^{-1}$, the permittivity of Au and water at 600 nm are approximately -9.39 and 1.77, respectively. To further investigate the relation between SP and incident photons, Snell's law is exploited, as give in Equation 2.6

$$n_d \sin\alpha = n_m \sin\beta \quad (n_d = \sqrt{\epsilon_d}, n_m = \sqrt{\epsilon_m}) \quad (2.6)$$

To fulfill the condition for exciting the SPs, combining Equation 2.2 and 2.3 together with Equation 2.6, this leads to the equation below:

$$n_d \frac{k_{in,x}}{k_{in}} = n_m \frac{k_{SP,x}}{k_{SP}} \quad (k_{in,x} = \frac{\omega}{c} \sqrt{\epsilon_d} \sin\alpha) \quad (2.7)$$

where n_d and n_m are the refractive indices of the dielectric and metal, k_{SP} is the wave vector of SPs. By combining Equations 2.2 and 2.7, the relation between the wave vector of the incident light and SPs along x axis is found to be

$$k_{in,x} = k_{SP,x} \quad (2.8)$$

Equations 2.1 and 2.8 indicate that p-polarized light with a wave vector along the x axis that matches the propagation constant of the SPs is required in order to excite SPs.

As seen from Equations 2.3 and 2.8, ϵ_m is negative and ϵ_d is positive, so for a given ω or λ_0 , the wave vector of incident light in free space is always smaller than that of the SPs. Hence, excitation of SPs by directly shining light onto a metal is not achievable. The wave vector in free space can be increased

by diffraction of the incident light or by using evanescent waves generated by total internal reflection (TIF).

SPR sensors exploit the phenomenon of SPR to achieve sensitive detection of any change in refractive index (RI) of the analyte. As seen from Equation 2.3, even a small change in the permittivity/refractive index (RI) of the dielectric, leads to a corresponding change in $k_{SP,x}$. Therefore, to achieve matching wave vectors to fulfill the condition for excitation of the SP waves, the characteristics of the incident light needs to be adjusted, as explained below. SPR sensors exploit this characteristic of the SPs to determine the RI change of the sample of interest. When SPs are excited, the law of conservation of momentum must be fulfilled as shown in Equation 2.9

$$\frac{\omega}{c} \sqrt{\frac{n_s^2 \epsilon_m}{n_s^2 + \epsilon_m}} = \frac{\omega}{c} \sqrt{\epsilon_d} \sin \alpha = \frac{2\pi}{\lambda_0} \sqrt{\epsilon_d} \sin \alpha \quad (2.9)$$

where n_s is the RI of the sample. The angle or wavelength where SPs are excited is known as the resonant angle or resonant wavelength. The excitation of SPs leads to a drop in intensity (known as the SPR dip, as seen in Figure 2.4) in the angular or wavelength spectrum of the reflected light at the resonant angle or wavelength, due to the energy transfer from photons to SPs. Depending on whether resonant angle or wavelength is measured, the SPR sensors can be based on angular or wavelength interrogation, which are the most commonly used interrogation modes. However, the excitation of SPs can also be observed from a change of intensity, phase or polarization of the incident light.

2.2 Characteristics of SPR sensors

For estimating the performance of an SPR based biosensor, there are several parameters, such as RI resolution (R_n), refractometric sensitivity, limit of detection (LOD), specificity and dynamic range. When the RI of the sample (n_s) is changed by δn_s , as a result the resonant angle or wavelength is altered by $\delta \theta_{res}$, or $\delta \lambda_{res}$ respectively. R_n is the smallest change measurable by the sensor (degree or nanometer) when there is change in the bulk refractive index, $R_n = \sigma S_b$, where σ is the noise of the sensor output. The refractometric sensitivity (or bulk sensitivity (S_b)), and the surface sensitivity (S_s), are defined as follows in Equation 2.10

$$S_b = \frac{\delta\theta}{\delta n_s} \text{ or } \frac{\delta\lambda}{\delta n_s} \text{ and } S_s = \frac{\delta\theta}{\delta t} \text{ or } \frac{\delta\lambda}{\delta t} \quad (2.10)$$

where t is the thickness of a layer of analytes absorbed onto the metal surface. Sensitivity is an important parameter to be considered when designing a sensor.

For biosensors, the limit of detection (LOD) is one indicator of the sensitivity. A low LOD indicates the biosensor has a good sensitivity. There are different ways of calculating the LOD. Some papers refer to the resolution as the LOD of the system, where the LOD represents the smallest change in RI unit (RIU). However in this thesis, LOD is defined as the lowest detectable concentration of the target. To calculate the LOD, a calibration curve with a series of analyte concentration is required. The calibration curve is fitted with either a linear regression or a non-linear regression using a selected model. The LOD can be calculated using the fitted equation and the sensor response for the nonspecific binding. A more detailed calculation is given in Chapter 4, Section 4.3.3. Specificity indicates the response of the sensor that is exclusively due to a specific target analyte to the sensor. When detecting target molecules in complex matrix, such as serum, blood or milk, which contains proteins may interact with targets or bioreceptors, leading to undesirable nonspecific interactions. Minimizing such nonspecific binding is essential to obtain a good sensitivity.

The dynamic range describes the range of the concentrations of the analytes that can be reliably measured by the SPR sensor [10].

2.3 Classifications of SPR sensors

In this section, state-of-the-art SPR sensors are introduced, classified into diffraction grating-coupled SPR (Section 2.3.1), prism-coupled SPR (Section 2.3.2) and FO-SPR sensors (Section 2.3.3). This classification is based on the excitation mechanisms of the SPR that can be either diffraction of incident light on a metallic grating or generation of evanescent waves by total internal reflection (TIR) using prism or optical fibers.

2.3.1 Diffraction grating-coupled SPR

The first scientific observation of SPs was the anomalous reflected bright and dark pattern from a metallic diffraction grating when shone with polarized light [1]. This section gives a general background of the diffraction grating-coupled SPR (GC-SPR) and discusses a few GC-SPR sensors.

When light is incident upon the grating, the wave vector of the diffracted light is the sum of light waves diffracted by each element of the grating (illustrated in Figure 2.2), as indicated below:

$$k = k_x + m \frac{2\pi}{\Lambda} = \frac{2\pi}{\lambda} n_s \sin \alpha + m \frac{2\pi}{\Lambda} \quad (m = 0, \pm 1, \pm 2, \dots) \quad (2.11)$$

where m represents the order of diffraction, Λ is the grating period. When Equation 2.9 is satisfied, it gives the excitation condition as

$$\sin \alpha + m \frac{\lambda}{\Lambda} = \sqrt{\frac{n_s^2 \epsilon_m}{n_s^2 + \epsilon_m}} \quad (2.12)$$

Equation 2.12 shows that for a given grating (fixed grating period), excitation of SPR can be achieved by adjusting either the incident angle or incident wavelength. The GC-SPR configuration can be in either angular or wavelength interrogation mode. This coupling configuration has been employed for biosensing since 1987 [11], but has never been widely employed for sensing applications, due to lower sensitivity compared to the prism-coupled SPR (PC-SPR) [12].

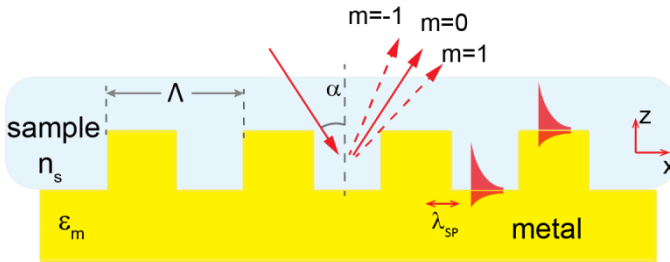


Figure 2.2 Schematic drawing of GC-SPR.

In recent years, theoretical and experimental work has been carried out on improving the sensitivity of GC-SPR. Hu *et al.* proposed depositing a

bimetallic layer on the grating by employing aluminum (Al) as the active metal for excitation of SPR and a thin layer of Au to prevent oxidation of the Al [13]. Compared to the previously published sensitivity of 70 °/RIU [14], an improved sensitivity of 187.2 °/RIU was achieved in this paper. Ruffato *et al.* have reported their exhaustive research from design and simulation of a nanostructure metallic grating to nanofabrication and characterization of the sensor [15]. This work introduced fabrication of gratings using soft-lithography, which produces highly reproducible gratings in a fast and cheap manner. The sensitivity of such sensor was up to 1000 °/RIU. Wang *et al.* reported a GC-SPR biosensor for detection of β human chorionic gonadotropin (β hCG) [16]. In this work, by utilizing magnetic nanoparticles conjugated to detection antibody for signal amplification, an LOD of 0.45 pM of β hCG in buffer was achieved.

2.3.2 Prism-coupled SPR

PC-SPR devices are by far the most commonly deployed SPR sensors. In this section, the physical principle of three types of PC-SPR sensors is introduced, being angular, intensity and wavelength interrogation. All prism-coupled SPR sensors employ a prism with high RI to achieve TIR and excite SPs by evanescent waves. This way the momentum of the incident light is increased, to fulfil the condition indicated in Equation 2.8 for excitation of SPR. As derived from Equation 2.9, the excitation condition of SPs is given below,

$$\sqrt{\varepsilon_p} \sin\alpha = \sqrt{\frac{\varepsilon_s \varepsilon_m}{\varepsilon_s + \varepsilon_m}} \quad (2.13)$$

where α is the incident angle, and ε_p , ε_s , and ε_m are the permittivity of the prism, sample medium and metal ($\varepsilon_p > \varepsilon_s$), respectively. Equation 2.13 indicates that for a given prism and metal, the incident angle must be adjusted when the RI of the detection dielectric changes in order to achieve matching wave vectors. In 1968, two prism-coupled configurations were reported by A. Otto (Figure 2.3 A), and E. Kretschmann and H. Reather (Figure 2.3 B).

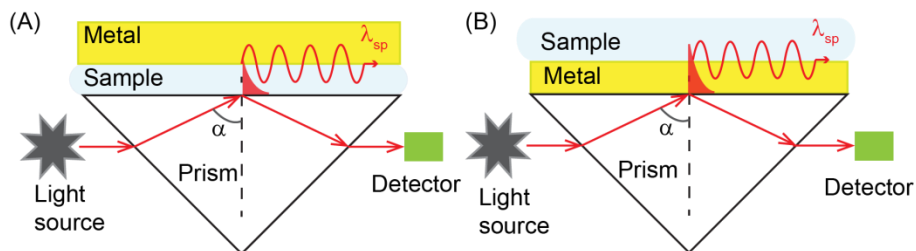


Figure 2.3 Schematic drawings of prism-coupled SPR sensors: (A) Otto configuration and (B) Kretschmann configuration.

In the Otto configuration, a thin layer of metal was placed at a short gap from the prism, where the evanescent waves generated at the prism/air interface ended at the surface of the metal. The sample was placed inside the gap between the prism and the metal layer. The gap width required careful control since a too big gap prevented the evanescent wave to excite the SPs, while a too thin gap led to radiation damping of the SP. However, because sample placing in between the two interfaces is experimentally challenging, this configuration has been rarely employed in sensors. In the Kretschmann configuration, the metal was directly deposited onto one side of the prism. The evanescent waves, generated at the prism/metal interface, penetrated through the metal layer and excited SPs at the metal/sample interface. Similarly to the Otto configuration, the thickness of the metal layer required careful control. The metal layer employed in both configurations was silver. Due to the relatively high permittivity of silver, the penetration depth of the SP waves in the dielectric region was longer compared to a metal with a lower permittivity. However, easy oxidation of silver [17] and its cytotoxicity [18] are suboptimal for biosensing applications. Therefore, Au has been used more frequently in SPR biosensors, owing to its chemical stability and ease of functionalization with bioreceptors.

The Kretschmann configuration is by far the most commonly employed configuration in SPR biosensors. In the early 1990s, Pharmacia Biosensor AB deployed this configuration and launched the first commercially available SPR biosensor, namely the Biacore (now GE Life Sciences) instrument. The Biacore instruments demonstrated the advantages of SPR biosensors including sensitive, accurate, and reproducible label-free detection and real-time kinetic monitoring of biomolecular interactions, which made them the

leader on the market. The Biacore instrument employs a monochromatic light source that is incident on a fixed prism. A removable sensor chip coated with Au is inserted at the bottom of the prism for SPR excitation. As illustrated in Figure 2.4 A, the incident angle can be adjusted to fulfill the SPR excitation condition, and the reflected light is collected by an array of photodetectors. These instruments are based on angular interrogation. Another feature of the Biacore instrument that attracted interest from researchers is that it enables fully automated operation, as it exploits a microfluidic system to deliver samples and reagents to the chip, and to channel the waste to a waste bottle. Biacore systems have been widely employed for a variety of applications, ranging from DNA and small proteins to antibodies and viruses [20-24]. The resolution is typically between 10^{-6} to 10^{-7} RIU [25]. Although these instruments offer superior advantages, there are limitations. Due to the high cost of the sensing chips, regeneration of the sensor surface is applied to be re-used. However, optimized regeneration conditions might be required for each individual target, which is time consuming. Moreover, the instruments are bulky and heavy, which confine the measurements to be performed only in central laboratories.

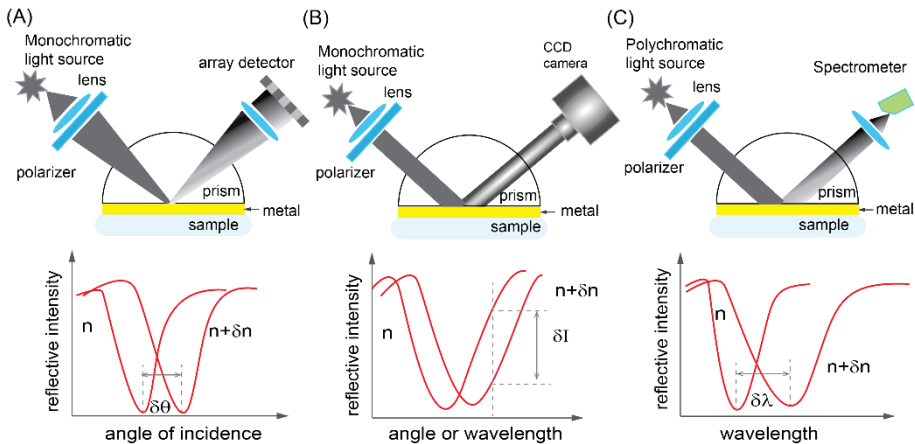


Figure 2.4 Schematic drawing of PC-SPR sensors with angular (A), intensity (B) and wavelength interrogation (C), which measure the change in resonant angle, wavelength and intensity as a function the change in RI of the sample, respectively. Recreated with permission from [19], Copyright (2006) Springer-Verlag Berlin Heidelberg.

Another frequently deployed modulation, so-called SP microscopy or SPR imaging (SPRi), is based on intensity interrogation. The concept was initially proposed by Yeatman and Ash in 1987 [26] and realized by Rothenhausler and Knoll in 1988 [27]. SPRi is performed at a fixed incident angle and wavelength. The reflected light intensity alters as the change of the refractive index, which is recorded by a CCD camera, as illustrated in Figure 2.4 B. The main advantages of the SPRi are: (i) the CCD camera allows recording of both sensorgrams (resonant signal vs. time) and images of the arrayed chip in real time and (ii) high throughput, i.e. multiple samples (up to hundreds) can be measured simultaneously [28].

Lastly, wavelength interrogation based SPR sensors utilize a polychromatic light source so that the incident wavelength can be altered, but with a fixed incident angle [29, 30], as shown in Figure 2.4 C. However, this type of modulation is more commonly employed in waveguide coupled SPR sensors rather than PC-SPR sensors. One example is the fiber-optic SPR (FO-SPR) sensor, which is exploited in this thesis and explained further in detail.

2.3.3 FO-SPR sensors

Since the late 1980s, optical fibers started being used in SPR sensors for light delivery and signal collection [31, 32], owing to their advantages, such as small scale, possibility of remote sensing, low cost, and high flexibility (they can operate under extreme conditions such as high temperature, high pressure and toxic environments). In the context of this thesis, an important feature of optical fibers to be used for exciting SPR is that the propagation of light in the core is based on TIR, so they are naturally chosen as an alternative candidate. Contrary to PC-SPR sensors, which need a separate chip, FO-SPR sensors do not require separate optical components, making them easier to miniaturize. Similar to wavelength interrogation in a PC-SPR, a polychromatic light source is introduced into an optical fiber, where the cladding is removed and coated with a noble metal (silver or Au), and the signal is detected by a spectrometer. Since there is no fixed angle of incidence when light propagates in an optical fiber, FO-SPR sensors are based on wavelength interrogation.

A few examples of FO-SPR configurations are given in Figure 2.5, which illustrates that the metal layer is directly deposited on the core. Removal of the cladding of the sensing region is necessary, otherwise the evanescent wave

at the core/cladding interface usually cannot reach the metal layer to excite the SPs. The cladding of standard single mode telecommunication optical fibers is made of pure glass, which can be removed by etching or polishing, whereas the cladding of multimode fibers (MMFs) is typically made of polymer, which can be simply removed by a chemical solvent. In this section, three subgroups of FO-SPR sensors are introduced: (i) using conventional optical fibers which propagate light based on TIR (Figure 2.5), (ii) using microstructured optical fibers (MOFs), which propagate light based on either TIR or photonic bandgap effect (Figure 2.6), and (iii) using fiber gratings (Figure 2.7).

The realization of using optical fibers for excitation of SPR was achieved by Jorgenson and Ye in 1993, using a transmission mode configuration (Figure 2.5 A) [33]. Both theoretical simulation and experimental results demonstrated that the SPR dip quality (full width at half maximum (FWHM) and intensity/depth) is influenced by the mode propagation angle and number of reflections of propagated light. In the case of PC-SPR, only p-polarized light is sent to excite SPR. However, for FO-SPR, both s- and p-polarized light propagate in the core, this leads to a broader FWHM and shallower dip compared to the prism-coupled SPR sensors. Therefore, the maximum achievable dip in intensity/depth was to 0.5 (50%) for FO-SPR rather than to 0 (100%) for PC-SPR. The paper also showed a reflection mode FO-SPR setup (Figure 2.5 B), that allows the possibility of disposable sensors and *in-vivo* testing. The FO-SPR platform exploited in this thesis is based on this configuration. The number of reflections is determined by the mode propagation angle α , the diameter of the optical fiber d and the sensing length L , given by $L/d * \tan(\alpha)$. As illustrated in Figure 2.5 A and B, for the same sensing length at a given propagation angle, the reflection mode has double the number of reflections compared to the transmission mode. The paper demonstrated that an SPR dip with good FWHM and depth can be achieved with the sensing length between 10 and 18 mm for a MMF with a diameter of 400 μm . In further work conducted by the authors, they explained the design criteria of an FO-SPR sensor including (i) the dynamic range is dependent on the RI of the fiber core (high RI core leads to the measuring dynamic range shift to higher RI and vice versa), (ii) it is preferable to choose optical fibers with a numerical aperture (NA) from 0.2 to 0.4, and core diameters between

200 to 40 μm , (iii) Au thickness of 55 nm [34-36]. In this thesis, an SPR sensor with an MMF fiber core diameter of 400 μm and NA of 0.39 coated with approximately 45 nm of Au has been employed, and the sensing length was chosen to be 6 mm. Arghir *et al.* reported a sensitivity of 1723 nm/RIU was achieved using the same FO-SPR platform employed in this thesis [37]. The sensitivity was improved to 1931 nm/RIU by adding an additional layer of silane to improve the adhesion between glass and Au.

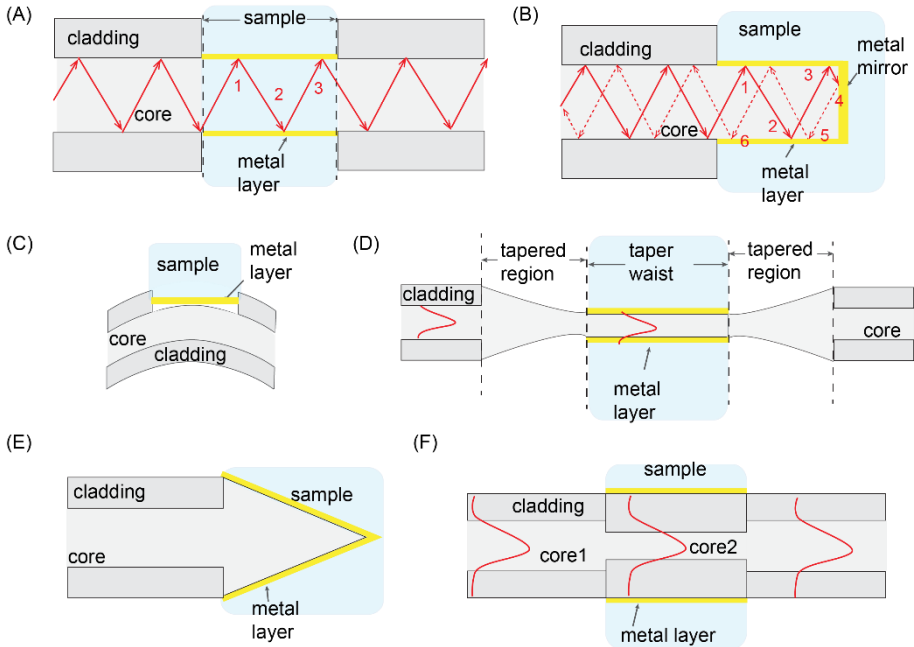


Figure 2.5 Schematic drawing of a few configurations of FO-SPR sensors. (A) transmission mode, (B) reflection mode, (C) side-polished structure, (D) tapered fiber structure, (E) tapered fiber tip structure, (F) hetero-core structure.

The research group of Homola reported a side-polished configuration using a single mode fiber (SMF) as seen in Figure 2.5 C [38-40]. A thin layer of chromium was deposited on the SMF to improve the adhesion of Au to the surface of SMF. The apparatus exploits polarized light for excitation of the SPR in the SMF, and achieved a sensitivity of 3300 nm/RIU and a resolution of 3×10^{-5} RIU. [39, 40]. Moreover, by adding a thin dielectric overlayer of tantalum pentoxide, the dynamic range of the sensor can be tuned. Therefore,

by altering the thickness of the tantalum pentoxide, the SPR sensor can be utilized for detecting targets lying within a broad range of RI. The drawback of this type of sensor is that the imperfection in polishing the cladding can introduce variation in the SPR dip depth and more importantly, the resonant wavelength [39]. In the work of Zhao *et al.*, the transmission spectrum of the SMF was monitored during the polishing process [41]. When the SMF is polished near the core and the power loss reaches approximately 1 dB, the polishing stops. This way the variation in the thickness of residue cladding is minimized. Theoretical work has been published utilizing MMF as side-polished SPR probes, but has not yet been experimentally demonstrated [42]. Recently, Liu *et al.* proposed an “eccentric core fiber”, which consists of two SMFs spliced together [43]. The spliced ends of the two SMFs were side-polished and coated with two different thicknesses of Au, one for excitation of SPR and the other for reflecting the signal. By adjusting the grinding angle, the incident angle is altered, which changes the resonant wavelength and dynamic range. The achieved sensitivity using this configuration was 4738 nm/RIU.

The tapered fiber structure is an alternative option to avoid etching or polishing the cladding. A tapered fiber can be achieved by stretching and heating a piece of SMF with an oscillating flame torch in a controlled manner, resulting in a precisely controlled dimension of a uniform taper waist where a metallic film is deposited, as seen in Figure 2.5 D. The power loss due to the tapering process is demonstrated to be typically lower than 0.2 dB [44]. At the sensing region, the cladding is thin enough to allow evanescent waves to reach the metal layer. Monzon-Hernandez and Villatoro presented a tapered SMF SPR sensor with multiple resonance dips, which resulted from a broader fundamental mode in the tapered fiber. They compared the sensor performance when only depositing Au on one side of the taper waist and on both sides of the waist, which indicated that the resonant wavelength remained the same, but the depth of the SPR dip doubled when both sides were coated with Au. A resolution of 7×10^{-7} RIU was achieved [45]. As described by Homola *et al.*, the sensing dynamic range can be tuned by adding an overlayer of dielectric material [39]. Esteban *et al.* demonstrated the same principle on the tapered fiber, where an average sensitivity of 4300 nm/RIU and 11800 ng/RIU in the RI regime between 1.415 and 1.429 were obtained [46]. Another type of tapered fiber structure is the reflection mode, meaning the optical fiber

is tapered at the tip, as illustrated in Figure 2.5 E. Kim *et al.* proposed a modified tapered tip geometry that results in two SPR dips, which enables simultaneous detection of vapor and liquid [47]. Coelho *et al.* compared the performance of tapered structure in transmission and reflective modes, and achieved sensitivities of 5100 and 3800 nm/RIU respectively, for RI range between 1.33 to 1.37 [48].

The drawback of the tapered structure in transmission mode is the thin taper waist (typically less than a few tens of micrometers), which makes this structure rather fragile. An alternative approach is to employ a so-called hetero-core fiber. This type of fiber consists of a MMF with a large core which is cleaved into two pieces and a piece of SMF with smaller core but the same diameter of cladding. The SMF is inserted in between the two identical fibers and the three pieces are spliced together as seen in Figure 2.5 F. When light propagates from the large core MMF to the small core SMF, a significant proportion of the light escapes to the cladding of the SMF due to the big difference in size between the two cores. Therefore, by directly depositing metal film onto the cladding of the SMF, the escaped light can excite the SPs. This type of fiber structure is easy to fabricate compared to the tapered fiber structure. Due to light transmission from the MMF, more modes are present in the SMF, leading to a broader FWHM of the SPR dip and poor sensitivity [49, 50].

Light propagation in conventional optical fibers is a result of RI difference between the core and cladding made of two materials that generates TIR. In the mid-1990s, a new class of optical fiber was invented known as microstructured optical fibers (MOFs). They are made of a single material (typically silica) and they guide light by manipulating the arrangements of air holes ($RI = 1$) in the fiber. There are two main classes of MOF, which are categorized based on the principle of light propagation, namely TIR and the photonic bandgap (PBG) effect. The latter is alternatively referred to as the photonic crystal fiber (PCF). There are a variety of structures for MOF, and the ones that are used for SPR sensing are usually with large air holes which can be used as a microfluidic channel. A few examples of MOF that are exploited in SPR sensors are illustrated in Figure 2.6. Suspended core MOF has a structure of a solid silica core surrounded by three air holes, as illustrated in Figure 2.6 A. Due to the large RI contrast between the core and the air holes, light is confined in the core by TIR and only evanescent waves can exist in

the air holes. Hautakorpi *et al.* presented a theoretical design of depositing Au on the edge of the air holes and injecting samples into the air holes, but this has yet to be experimentally demonstrated [51]. The size of the three holes can differ, but the ones with large holes shown in Figure 2.6 A tend to be more fragile. Deposition of Au on the air holes can be performed by a technique called high pressure chemical deposition [52]. Hassani and Skorobogatiy proposed a MOF as illustrated in Figure 2.6 B, where the air holes in the center acted as the core and the air channels acted as the cladding, which were then filled with samples. The maximum achievable resolution was 3×10^{-5} RIU [53, 54]. When changing the structure of the air holes in the center, i.e. the core, the effective RI changes, hence the dynamic range can be tuned. The same authors presented a modified version of Figure 2.6 B to achieve this purpose. Moreover, a honeycomb structured PCF with two air channels was described, where a biolayer with a thickness of 10 nm was immobilized on the Au surface and resulted in a 23 nm shift in resonant wavelength [55]. Liu *et al.* presented a hollow fiber structure, which is only suitable for detection in liquids with high RI that is similar to the RI of the cladding, since the light needs to be confined in the core, and it achieved good sensitivity up to 6607 nm/RIU [56]. Despite the interesting features of MOFs i.e. no need to remove cladding and the optical fiber facilitates both signal detection and sample delivery, most of the research still remains in the theoretical domain due to the challenge of depositing metal inside the air holes. Light propagation in PCFs is obtained via constructive interference of scattered light from the periodic array of air holes, as seen in Figure 2.6 C. Recently, PCF has been integrated in a hetero-core structured fiber, meaning a piece of PCF is inserted in between two pieces of identical MMF. A bioassay for detection of IgG using a protein G immobilization strategy has been implemented on this structure and reached an LOD of 0.267 $\mu\text{g}/\text{mL}$ [57].

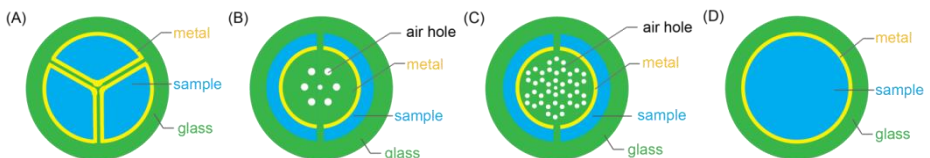


Figure 2.6 Cross-sections of a few MOFs: (A) Suspended core MOF, (B) solid core MOF, (C) PCF, (D) hollow core fiber.

In recent years, grating-assisted SPR sensors have attracted more attention from researchers. A fiber grating consists of a periodic variation in the RI of the fiber core that generates a wavelength-specific dielectric mirror which reflects particular wavelengths of the incident light and transmits all others. By contrast with GC-SPR sensors where the grating is used for excitation of the SPs, in grating-assisted SPR sensors the grating is used to guide light to the cladding. One approach is to employ long period fiber grating (LPFG) as indicated in Figure 2.7 A, which has the advantage of ease of fabrication. Moreover, the core modes couple to the cladding modes so removal of cladding is unnecessary. However, these sensors are very sensitive to changes in temperature and any substance that can nonspecifically bind to the surface. Therefore, they are only found in studies for the design of new sensor structures [58], but not for real biosensing applications. Using fiber Bragg gratings (FBG) still requires polishing or etching the cladding, whose disadvantages have been discussed earlier in this chapter. An alternative method is to use tilted FBG (TFBG) as displayed in Figure 2.7 B, which diffracts light from the core into the cladding. The sensitivity of SPR using TFBG is generally lower compared to other SPR sensors, between 400 to 1000 nm/RIU [59]. However, owing to the extremely narrow SPR dips, a higher detection accuracy can be potentially achieved. The TFBG assisted SPR sensor [59] has been implemented for detecting tumor marker, namely cytokeratins 7. This work showed an LOD of 1 ng/mL (0.4 nM) for small molecule cytokeratins 7 peptide (2.5 kDa) in 10% of fetal bovin serum [60].

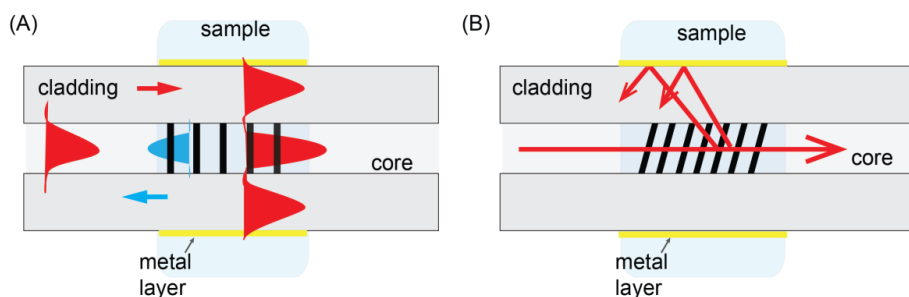


Figure 2.7 (A) Schematic drawing of LPFG where transmitted light is indicated in red and reflected light is labelled as blue, and (B) TFBG FO-SRP configuration.

2.4 Miniaturized SPR biosensors

Ever since the successful launch of the Biacore instrument, companies and research groups have attempted to meet the high standards set by this device. Over the course of the last decade, a few manufacturers such as Reichert (SR7500) [61], Nomadics (SensiQ) [62], and Sensia (Indicator) [63] have introduced to the market SPR instruments with modified optical and liquid handling designs, which provide signals with better resolution, lower noise level, larger dynamic range and relatively lower cost. However, these devices are still bulky and expensive, so they are only utilized in research laboratories. Due to the increasing demand for POC devices, miniaturization of conventional bench-top SPR biosensors is desirable for rapid diagnostics in clinics or for fast analysis in the field. A few miniaturized PC- and FO-SPR biosensors are introduced in this section. For each listed system, one example of application for the system is described. However, this is not an exhaustive list of applications for each system.

The Spreeta system, manufactured by Texas Instruments Inc, was one of the earliest miniaturized prism-coupled SPR sensors to be successfully commercialized. One of the models, Spreeta 2000, integrates all the optical and electronic components into an inexpensive molded plastic package with a size slightly bigger than a coin ($1.5\text{ cm} \times 0.7\text{ cm} \times 3\text{ cm}$, Figure 2.8 A, top). Inside this plastic package is a plastic prism molded onto an electronic circuit on a printed circuit board. The circuit consists of a monochromatic LED, an array detector and a memory chip for recording data. The LED emits light through a polarizer, which is incident upon the sensor surface at a range of angles above the critical angle and then reflected by the mirror into the array detector (Figure 2.8 B, bottom) [64]. Another example is the SPIRIT system (Seattle sensing systems) that enables multiple-channel measurements and incorporates portable Spreeta 2000 SPR sensors, a flow injection system for sample delivery, a signal processing system and a display into a portable box that weighs less than 3 kg (Figure 2.8 C). The system has been tested with a variety of targets including small molecules (2,4-Dinitrophenol), proteins (bacterial toxin *Staphylococcus enterotoxin B* and ricin A chain), viruses (Norwalk virus) and bacteria (*Francisella tularensis* LVS), reaching respectively LOD values in buffer of $1\text{ }\mu\text{M}$, 1 nM , 10 ng/mL (0.31 nM), 10^9 VLPs/mL , and 10^4 CFU/mL [65]. Recently the SPIRIT system has been

successfully employed to differentiate a biological warfare agent, namely *Bacillus anthracis* in a mixture of different species of *Bacillus* [66].

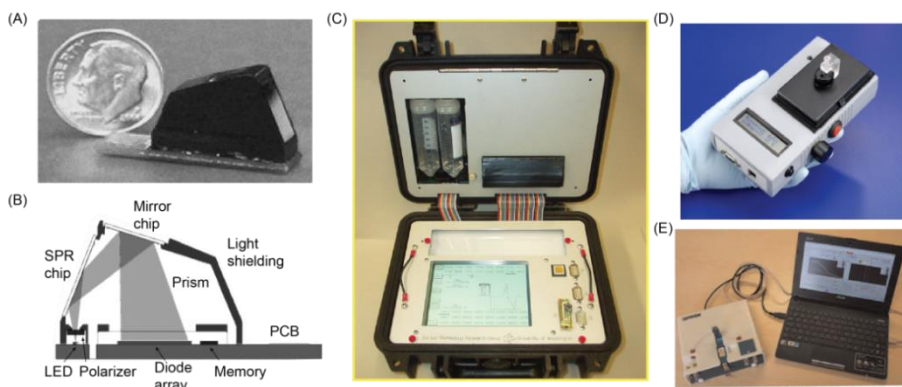


Figure 2.8 Images of (A) Spreeta 2000 system and (B) its working principle, reprinted with permission from [64], Copyright (2003) Elsevier, (C) SPIRIT system reprinted with permission from [65], Copyright (2006) Elsevier, (D) a hand-held SPR biosensor presented by Feltis *et al.*, reprinted with permission from [69], Copyright (2007) Elsevier, (E) a miniaturized SPR biosensor proposed by Masson *et al.*, reprinted with permission from [71], Copyright (2015) Elsevier.

A few more portable PC-SPR biosensors with multiple channels are available on the market, including SensiQ Discovery (SensiQ Technologies), Biosuplar 6 (Analytical μ -systems/Mivitec), and Smart SPR SS-1001 (NTT Advanced Technology). SensiQ Discovery system is a semi-automated and dual channel PC-SPR instrument. Using this portable instrument, Wu *et al.* reported an immunoassay for detection of a small molecule, melamine, in infant formula where milk fat was removed [67]. The lowest LOD was 0.02 $\mu\text{g}/\text{mL}$ with a dynamic range of 0.06 to 1 $\mu\text{g}/\text{mL}$ and a detection time of 15 min. This LOD was similar to that of the conventional methods (HPLC and ELISA) for quantifying the level of melamine. Biosuplar 6 is a two-channel system that has been employed for instance in monitoring cell volume changes by directly culturing the cells on the SPR chips. One channel of the Biosuplar was used as reference and the buffer was kept the same. The other channel was used as the measurement channel, where the buffer was changed to induce the volume change [68]. SPR SS-1001 consists of a portable PC-SPR sensor with an instrument dimensions of 29 cm \times 16 cm \times 12 cm and a microfluidic chip dimensions of 1.6 cm \times 16 cm \times 0.4 cm, both in centimeters. In this

system, the flow of buffers and samples is passively driven by the capillary force. With this instrument, Horiuchi *et al.* demonstrated detection of IgG in homogenized milk with an LOD of 1 $\mu\text{g/mL}$ [69].

Some research groups in academia have also been working on development of miniaturized SPR biosensors. Feltis *et al.* proposed a hand-held SPR biosensor, which integrates a glass prism, a laser, optical and electronic components, and an LCD display into a fully portable device with a weight of 600 g that can be powered by a single 9 V battery [70]. As illustrated in Figure 2.8 D, the sample is introduced from the plastic cylinder at the top. This biosensor was capable of detecting the bio-toxic compound, ricin, in buffer with the lowest detectable concentration of 200 ng/mL and a coefficient of variation of 15%. This system was found to be 2 orders of magnitude less sensitive than the Biacore. Despite offering the advantage of portability, the sensitivity of the above SPR sensors is still not as good as bench-top SPR devices. However, this limitation can be overcome through signal amplification by using Au nanoparticles (AuNPs) as proposed in a miniaturized 4-channel SPR biosensor with a size similar to a laptop (Figure 2.8 E). A competitive immunoassay utilizing AuNP for signal enhancement was implemented on the system for detecting an anti-cancer drug, methotrexate, in 10-fold diluted serum, ranging from 1 nM to 1 μM . The final dynamic range was determined between 28 to 500 nM with an LOD of 28 nM. The system was also successfully validated with 6 clinical samples from cancerous patients [71].

GC- and FO-SPR sensors have also been developed into portable devices. The research group of Homola has exploited a diffraction grating structure, referred to as SPR coupler and disperser (SPRCD), which couples the incident light into SPs via second-order diffraction and simultaneously disperses the first order diffracted light for spectral readout. All the components, as shown in Figure 2.9 A, can fit into a unit with a footprint smaller than 15 cm \times 15 cm. The sensitivity, resolution and dynamic range are 680 nm/RIU, 3×10^{-7} RIU and 0.02 RIU, respectively [72]. The system with 6 channels proved to be capable of detecting antibiotics in milk with LOD below 0.3 ng/mL in 5-fold diluted milk [73]. Another example of a portable SPR device is an FO-SPR biosensor based on a smart phone. This system utilizes the transmission mode configuration, where a built-in LED flash from the phone emits light into an optical fiber, which is connected to the sensing fiber, and the signal is

collected by the CMOS camera on the phone. All the optical components and sensing elements are fixed on a phone case via the optical fiber (Figure 2.9 B). To counteract against the instability of the LED flash, a control channel (CC) and reference channel (RC) were added, where the intensities from the two channels were then used to correct the intensity from the measurement channel. The resolution and sensitivity of this system were 7.4×10^{-5} RIU and 1136 %/RIU, respectively and the LOD of label-free detection of IgG was 47.4 nM. By comparison to Biosuplar 6, the obtained LOD was approximately 3 times higher, but the cost was nearly 1000-fold lower [74].

Unfortunately, not all the miniaturized SPR biosensors mentioned above have been implemented using clinical samples. In our group, an in-house built fully automated FO-SPR platform has been continuously explored for detecting a variety of targets in complex matrices e.g. milk, serum and blood. As mentioned in Section 1.3, the FO-SPR platform has great potential for various applications using antibody- or DNA-based bioassays. Recently, the FO-SPR set-up was fully integrated and miniaturized into a benchtop device (FOx Biosystems) with dimensions of 42 cm \times 40 cm \times 40 cm, which enables single or multiple (up to 4) channel measurements (Figure 2.9 C). In this thesis, two applications are described using the FO-SPR platform. The obtained results demonstrated the capability of the FO-SPR platform for detection a wide range of target analytes. Although the results presented in this thesis were not obtained from the FOx system, it has been proven that the results from the FO-SPR platform are transferable to the FOx Biosystems biosensor (data not shown). Thus, the work described in this thesis can be easily reproduced with the FOx Biosystems biosensor.

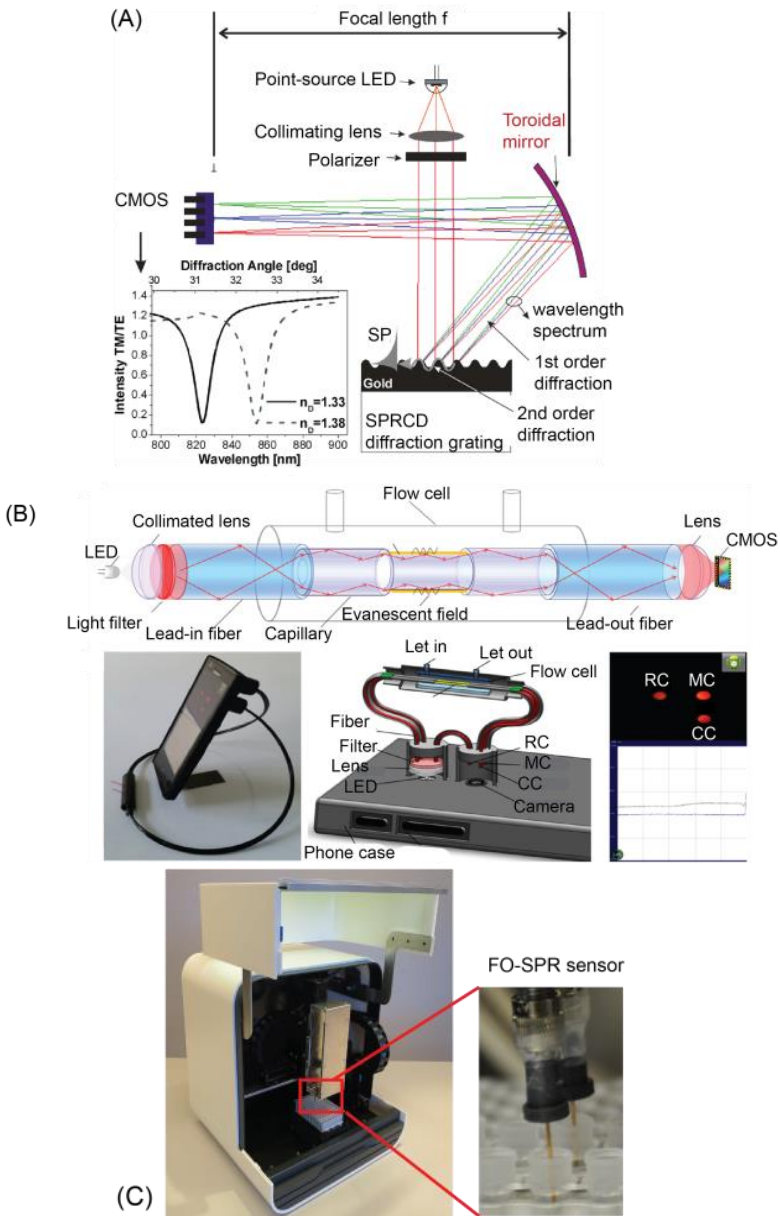


Figure 2.9 (A) image of an SPRCD chip, reprinted with permission from ref. [72] Copyright (2009) Elsevier, (B) working principle of the smart phone-based SPR biosensor, where RC, MC and CC are the acronyms of reference channel, measurement channel and control channel respectively, reprinted with permission from Liu et al. [74], (C) FOx Biosystems FO-SPR platform.

2.5 Surface modification of the sensor surface

Whereas previous sections have been focusing on the physics of SPR and different categories of SPR biosensors, this section gives information on the surface modification approaches on the SPR sensors. As introduced in Chapter 1, biosensors require bioreceptors on the transducer for capturing target analytes. This step is crucial as it influences the sensitivity and specificity of the sensor. In the case of SPR biosensors, gold-coated prisms or optical fibers act as the transducer element. A variety of methods can be employed for immobilizing bioreceptors, which can be DNA, antigens, antibodies, cells or biomimetic material. Since this thesis is focused on immunoassays, common methods for antibody immobilization on Au surface are presented in this section. There are several methods for immobilization of antibodies including physical adsorption, biochemical affinity binding, covalent binding, as well as other strategies. A schematic drawing of the three approaches is illustrated in Figure 2.10.

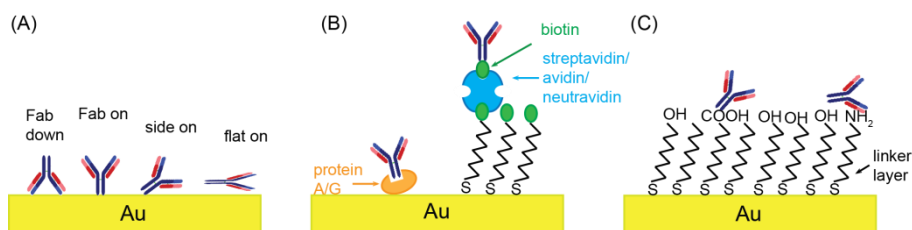


Figure 2.10 Schematic drawing of three immobilization strategies: (A) physical adsorption, where random orientation is shown, adapted with permission from [75], Copyright (2012) American Chemical Society, (B) biochemical affinity binding via protein A/G, and streptavidin/avidin/neutravidin which is attached to Au surface via biotinylated SAM, and (C) covalent binding using a linker layer, where the terminator groups of the linker layer are usually a mixture of hydrogen groups and functional groups, such as carboxyl or amine groups.

Antibodies (and proteins in general) can directly adsorb to Au surfaces via ionic bonds, hydrophobic interactions, electrostatic and van der Waals forces (Figure 2.10 A). These interactions are collectively referred to as physical adsorption (otherwise known as physisorption or passive adsorption). Although this is the easiest approach to immobilize antibodies, as no chemical modification of the sensor surface or antibody is required, this method is also

associated with number of disadvantages: (i) antibodies can dissociate from the surface during washing steps, (ii) denaturation may occur when the antibodies get in contact with Au, (iii) the surface density affects the binding efficiency and (iv) random orientation of immobilized molecules [75]. Both (i) and (ii) lead to poor reproducibility and (iii) means that binding efficiency cannot be controlled with this approach [76].

An alternative approach is to exploit biochemical affinity binding, which includes using protein A, G, avidin/streptavidin-biotin (Figure 2.10 B). These proteins are immobilized on the sensor surface and bind to the fragment crystallizable (Fc) region of the antibodies, hence leaving the antigen-binding fragment (Fab) free for the targets. This approach requires pre-functionalization of the surface with these proteins that can be achieved through (i) a dative covalent bonding where thiol groups on the proteins can form a strong bond with the Au surface or (ii) a self-assembled monolayer (SAM) terminated with functional groups or biotin. Lee *et al.* reported immobilization of IgG on the SPR surface using cysteine-tagged protein G, which increased the SPR shift for immobilization of IgG by 5 fold and the IgG-antigen binding by 10 fold compared to using non-tagged protein G [77]. Another way to attach protein A/G onto the sensor surface is to exploit amine groups on protein A/G bind to the 1-ethyl-3-(3-dimethylaminopropyl) carbodiimide hydrochloride (EDC)/ N-hydroxysuccinimide (NHS)-activated carboxyl groups of the SAM. SAM provides various advantages for immobilization of biomolecules. To begin with, a selection of terminal functional groups are available for different biomolecules. Also, it can form stable covalent binding with the biomolecules. Furthermore, it has been demonstrated that SAM can effectively minimize nonspecific adsorption [78]. Vashist *et al.* compared the immobilization efficiency when using free protein A, protein A via SAM, physical adsorption and covalent binding via SAM, where the SPR shifts induced by immobilization and binding were 1112, 1457, 816, and 1536 response units (RU) and 113, 194, 63 and 149 RU respectively [79]. Although the immobilization response was greater from covalent binding, the target binding response was lower than the protein A strategy via SAM. Since the latter strategy provided oriented antibody binding, the Fab sites are therefore better available for target binding. For avidin-biotin strategy, a common method to attach avidin/streptavidin to the sensor surface is to exploit biotinylated SAM, where SAM is terminated with

biotin. Walper *et al.* compared immobilization strategies of single domain antibodies (sdAbs), where streptavidin-conjugated sdAbs which were covalently bond to the surface gave the best binding efficiency [80]. With this immobilization strategy, the LODs were 1.6 ng/mL and 0.32 ng/mL for detection of the S-layer protein EA1 of *Bacillus anthracis* and ricin respectively. This was a 100-fold and 5-fold improve in LOD respectively by comparison with other monoclonal antibody-based assays. Moreover, by washing with regeneration buffer (0.5% SDS) on the surface, the sensor could be reused up to 45 times. The limitation of avidin/streptavidin-biotin approach is that it not only requires surface modification to attach avidin/streptavidin, it also requires biotinylation of the antibody, which leads to increase in both preparation time and cost.

The last approach to immobilize antibodies is via covalent bonding with a linker layer (Figure 2.10 C). A commonly used linker layer is SAM. As described above, SAM has been employed for covalent binding of protein A/G and streptavidin. The principle of antibody immobilization via SAM is identical to protein A/G, by using EDC/NHS strategy. The most common approach is via EDC/NHS activation of terminal functional (i.e. carboxyl) groups. Beside SAM, covalent binding of antibodies can be also achieved through a polymer, with dextran-based hydrogel being most commonly used polymer for this purpose. The commercially available Biacore chips are usually functionalized with dextran hydrogel, and these chips are often employed as a reference for evaluating other immobilization strategies [79, 81]. Another type of polymer for immobilizing antibodies is p-xylylene. Jeon *et al.* reported p-xylene modified with a primary amine group, named parylene-A film. They compared the immobilization efficiency of the parylene-A film with physical adsorption and SAM using horseradish peroxidase (HRP) [75]. Both parylene-A film and SAM gave a much higher immobilization efficiency than the physical adsorption approach. In other words, the HRP concentration when using physical adsorption had to be 10-fold higher compared to the covalent immobilization with parylene-A film to achieve similar SPR signal.

In recent years, fusion proteins have been exploited to achieve a reproducible and improved immobilization efficiency. Juan-Franco *et al.* proposed a protein A fused with an Au binding peptide (PAG), which attached directly onto the Au surface. By comparison with free protein A and covalent

binding via SAM, PAG showed at least twice higher efficiency for both immobilization and target binding [82]. Kausaite-Minkstimiene *et al.* presented a modified antibody (specific for anti-human growth hormone), where the antibodies were chemically divided into two parts and each fragment contains both Fc and Fab region [81]. The fragments of the antibody were directly attached onto the Au surface via thiol groups on the hinge region of the antibody. This way, all the antibody fragments are immobilized in a oriented manner so that the Fab regions of all the antibodies are available for binding. Although the immobilization of antibodies from this approach was less efficient than when using SAM or hydrogel strategies, the binding of target was at least 7 times higher because of the orientation of the antibodies.

2.6 Conclusions

In this chapter, the physical principles of the SPR phenomenon have been explained in detail next to introducing three methods for exciting SPR, being GC-, PC- and FO-SPR, and the state-of-the-art of each type of SPR sensor was reviewed. As portable biosensors are increasingly desirable for a variety of applications, a few miniaturized SPR biosensors were discussed. Finally, a variety of methods for sensor surface functionalization were described.

PC-SPR sensors provide better resolution and sensitivity compared to GC- and FO-SPR sensors. GC-SPR sensors are rarely exploited in biosensing applications. This is primarily because the incident light is unavoidably transmitted through the sample, which can be potentially absorbed, especially in the case of blood samples. FO-SPR sensors have been increasingly deployed in biosensing, as discussed in Section 2.3.3. Three categories of FO-SPR sensors are introduced, being conventional optical fibers with modified structures, MOFs and fiber gratings. For conventional optical fibers, modified structures such as tapered or side-polished structures are used to improve the sensitivity. In both cases, the change of geometry makes the incident angles closer to the critical angle, thus maximize the excitation efficiency. However, the most practical and widely deployed structure for biosensing remains the transmission and reflection modes. The latter has been employed in this thesis. MOFs and fiber gratings are only recently developed kinds of optical fibers, so research on them has mainly been confined to fundamental studies. The hollow core or cladding in MOFs offer the possibility of being used as

microfluidic channels, which can potentially be advantageous for biosensing. Grating-assisted FO-SPR has the advantage of easier fabrication compared to conventional optical fibers with modified structure and MOFs, but the sensitivity remains unsatisfactory [59]. Portable biosensors are advantageous for obtaining results near the source of samples. Therefore, there are an increasing number of miniaturized PC-SPR biosensors commercially available on the market at present. The main trade-off associated with portable PC-SPR biosensors is a reduction in resolution and LOD compared to the bench-top versions, but the performance is quite similar to FO-SPR sensors. Since FO-SPR sensors do not require separated prisms and Au coated chips, the sensing element, being the optical fiber, is affordable, easy to miniaturize, and thus they have great potential to be developed as portable devices. A summary of the performance of SPR sensors is indicated in Table 2.1, where a selection of work is presented. The key take-home message is that there is a large number of PC-SPR sensors that have been miniaturized and implemented in biosensing applications, whereas most of GC-and FO-SPR sensors are still in the stage of fundamental research.

Lastly, strategies for surface modification of the SPR sensor surface were discussed. Since a reliable and reproducible immobilization protocol is the foundation for specific and sensitive detection, there has been an increasing amount of research on bioreceptors with a modified structure to obtain better immobilization outcome as explained in ref [81, 82]. Based on the literature review, it seems that a more sensitive detection can be achieved via oriented antibody immobilization, whereas better surface density can be obtained by random covalent immobilization strategy [75, 79]. However, the improvement in sensitivity depends on the particular system. Therefore, a universal immobilization strategy for all applications is still unavailable. In the remaining chapters of this thesis, discussions on the optimization of immobilizing capture antibodies using covalent binding strategy is described.

*Table 2.1 Performance summary of a variety of SPR sensors. *Direct assay structure: bioreceptors-target molecules, no signal amplification.*

| | Portable (Yes/No) | Molecule size | With bio-applications | | Without bio-applications | | | |
|--------|-------------------|---------------------------------|--|------------------------|--------------------------|-----------------|------------------------------|----------------------|
| | | | Type of immunoassay | Detection matrix | LOD | RI range | Resolution (RU) | Sensitivity (nm/RIU) |
| GC-SPR | No | βhCG (22 kDa) | Sandwich with MNP enhancement | buffer | 0.45 pM | | | |
| | Yes | ricin A chain (32 kDa) | Sandwich | buffer | 10 ng/mL (0.31 nM) | | | |
| PC-SPR | Yes | melamin (126 Da) | Competitive enhance with BSA conjugated melamine | | | | 10 ⁻⁶ | |
| | Yes | Methotrexate (454 Da) | Competitive with AuNP enhancement | serum | 28 nM | | 10 ⁻⁶ | |
| | Yes | Thrombin (36 kDa) | Direct* | buffer | 34 nM | 1.333 – 1.352 | 1.5 × 10 ⁻⁵ | 1931 |
| FO-SPR | No | | | | | 1.324 – 1.335 | 2 × 10 ⁻⁵ | 3300 |
| | No | | | | | 1.3252 – 1.3905 | 8 × 10 ⁻⁵ | 4300 |
| | No | | | | | 1.494 – 1.697 | 1.4 – 5.1 × 10 ⁻⁴ | 1189 – 4356 |
| | No | IgG (150kDa) | Direct* (protein G) | buffer | 0.267 µg/mL (1.8 nM) | 1.330 – 1.377 | 2.7 × 10 ⁻⁴ | 2018 - 3692 |
| TFBG | No | Cyokeratins 7 peptide (2.5 kDa) | Direct* | 10% fetal bovine serum | 1 ng/mL | 1.31 – 1.38 | 1 × 10 ⁻⁵ | 673 |

2.7 References

1. Wood, R.W., On a Remarkable Case of Uneven Distribution of Light in a Diffraction Grating Spectrum. Proceedings of the Physical Society of London, 1902. 18(1): p. 269.
2. Ritchie, R., Plasma losses by fast electrons in thin films. Physical Review, 1957. 106(5): p. 874.
3. Ritchie, R., *et al.*, Surface-plasmon resonance effect in grating diffraction. Physical Review Letters, 1968. 21(22): p. 1530.
4. Otto, A., Excitation of nonradiative surface plasma waves in silver by the method of frustrated total reflection. Zeitschrift für Physik, 1968. 216(4): p. 398-410.
5. Kretschmann, E. and H. Raether, Radiative decay of non radiative surface plasmons excited by light. Zeitschrift für Naturforschung A, 1968. 23(12): p. 2135-2136.
6. Liedberg, B., C. Nylander, and I. Lunström, Surface plasmon resonance for gas detection and biosensing. Sensors and Actuators, 1983. 4: p. 299-304.
7. Jönsson, U., *et al.*, Real-time biospecific interaction analysis using surface plasmon resonance and a sensor chip technology. Biotechniques, 1991. 11(5): p. 620-627.
8. Francis, F.C., Introduction to Plasma Physics and Controlled Fusion. Plasma Physics, 1984.
9. Novotny, L. and B. Hecht, Principles of nano-optics. 2012: Cambridge university press.
10. Homola, J. and M. Piliarik, Surface Plasmon Resonance (SPR) Sensors, in Surface Plasmon Resonance Based Sensors, J. Homola, Editor. 2006, Springer Berlin Heidelberg: Berlin, Heidelberg. p. 45-67.
11. Cullen, D.C., R.G.W. Brown, and C.R. Lowe, Detection of immuno-complex formation via surface plasmon resonance on gold-coated diffraction gratings. Biosensors, 1987. 3(4): p. 211-225.
12. Homola, J., I. Koudela, and S.S. Yee, Surface plasmon resonance sensors based on diffraction gratings and prism couplers: sensitivity comparison. Sensors and Actuators B: Chemical, 1999. 54(1-2): p. 16-24.
13. Hu, C. and D. Liu, High-performance grating coupled surface plasmon resonance sensor based on Al-Au Bimetallic layer. Modern Applied Science, 2010. 4(6): p. 8.
14. Byun, K.M., S.J. Kim, and D. Kim, Grating-coupled transmission-type surface plasmon resonance sensors based on dielectric and metallic gratings. Applied optics, 2007. 46(23): p. 5703-5708.

15. Ruffato, G., F. Romanato, and G. Zacco, Innovative exploitation of grating-coupled surface plasmon resonance for sensing. 2012: INTECH Open Access Publisher.
16. Wang, Y., J. Dostalek, and W. Knoll, Magnetic nanoparticle-enhanced biosensor based on grating-coupled surface plasmon resonance. *Analytical chemistry*, 2011. 83(16): p. 6202-6207.
17. Zhu, X.-M., *et al.*, Surface treatments for surface plasmon resonance biosensors. *Sensors and Actuators B: Chemical*, 2002. 84(2): p. 106-112.
18. Foldbjerg, R., D.A. Dang, and H. Autrup, Cytotoxicity and genotoxicity of silver nanoparticles in the human lung cancer cell line, A549. *Archives of toxicology*, 2011. 85(7): p. 743-750.
19. Piliarik, M. and J. Homola, SPR sensor instrumentation. *Surface Plasmon Resonance Based Sensors*, 2006: p. 95-116.
20. Mitchell, J., Small molecule immunosensing using surface plasmon resonance. *Sensors*, 2010. 10(8): p. 7323-7346.
21. Huang, J., *et al.*, Broad and potent neutralization of HIV-1 by a gp41-specific human antibody. *Nature*, 2012. 491(7424): p. 406-412.
22. Baker, T., L. Kevorkian, and A. Nesbitt, FRI0162 Investigation into the binding affinity of certolizumab pegol to fc γ n and functional consequences for fc γ n-mediated transcytosis: comparison to infliximab, adalimumab and etanercept. *Annals of the Rheumatic Diseases*, 2013. 72(Suppl 3): p. A426-A426.
23. Ding, X., *et al.*, Surface plasmon resonance biosensor for highly sensitive detection of microRNA based on DNA super-sandwich assemblies and streptavidin signal amplification. *Analytica chimica acta*, 2015. 874: p. 59-65.
24. Jason-Moller, L., M. Murphy, and J. Bruno, Overview of Biacore systems and their applications. *Current protocols in protein science*, 2006: p. 19.13. 1-19.13. 14.
25. Fan, X., *et al.*, Sensitive optical biosensors for unlabeled targets: A review. *Analytica Chimica Acta*, 2008. 620(1-2): p. 8-26.
26. Yeatman, E. and E.A. Ash, Surface plasmon microscopy. *Electronics Letters*, 1987. 23(20): p. 1091-1092.
27. Rothenhausler, B. and W. Knoll, Surface-plasmon microscopy. *Nature*, 1988. 332(6165): p. 615-617.
28. Beusink, J.B., *et al.*, Angle-scanning SPR imaging for detection of biomolecular interactions on microarrays. *Biosensors and Bioelectronics*, 2008. 23(6): p. 839-844.

29. Gwon, H.R. and S.H. Lee, Spectral and angular responses of surface plasmon resonance based on the Kretschmann prism configuration. *Materials transactions*, 2010. 51(6): p. 1150-1155.
30. Sun, Y., et al., Design and performances of immunoassay based on SPR biosensor with magnetic microbeads. *Biosensors and Bioelectronics*, 2007. 23(4): p. 473-478.
31. Villuendas, F. and J. Pelayo, Optical fibre device for chemical sensing based on surface plasmon excitation. *Sensors and Actuators A: Physical*, 1990. 23(1-3): p. 1142-1145.
32. van Gent, J., et al., Optimization of a chemo-optical surface plasmon resonance based sensor. *Applied optics*, 1990. 29(19): p. 2843-2849.
33. Jorgenson, R. and S. Yee, A fiber-optic chemical sensor based on surface plasmon resonance. *Sensors and Actuators B: Chemical*, 1993. 12(3): p. 213-220.
34. Jorgenson, R.C. and S.S. Yee, Fiber optic sensor and methods and apparatus relating thereto. 1994, Google Patents.
35. Jorgenson, R.C. and S.S. Yee, Fiber optic sensor and methods and apparatus relating thereto. 1997, Google Patents.
36. Jorgenson, R.C. and S.S. Yee, Fiber optic sensor and methods and apparatus relating thereto. 1998, Google Patents.
37. Arghir, I., et al., Improved surface plasmon resonance biosensing using silanized optical fibers. *Sensors and Actuators B: Chemical*, 2015. 216: p. 518-526.
38. Homola, J., Optical fiber sensor based on surface plasmon excitation. *Sensors and actuators B: chemical*, 1995. 29(1-3): p. 401-405.
39. Slavík, R., J. Homola, and J. Čtyroký, Single-mode optical fiber surface plasmon resonance sensor. *Sensors and Actuators B: Chemical*, 1999. 54(1): p. 74-79.
40. Slavík, R., et al., Novel spectral fiber optic sensor based on surface plasmon resonance. *Sensors and Actuators B: Chemical*, 2001. 74(1): p. 106-111.
41. Zhao, J., et al., Surface plasmon resonance refractive sensor based on silver-coated side-polished fiber. *Sensors and Actuators B: Chemical*, 2016. 230: p. 206-211.
42. Ahn, J.H., et al., Fiber-optic waveguide coupled surface plasmon resonance sensor. *Optics express*, 2012. 20(19): p. 21729-21738.
43. Liu, Z., et al., Distributed fiber surface plasmon resonance sensor based on the incident angle adjusting method. *Optics letters*, 2015. 40(19): p. 4452-4455.

44. Villatoro, J., D. Monzón-Hernández, and E. Mejía, Fabrication and modeling of uniform-waist single-mode tapered optical fiber sensors. *Applied Optics*, 2003. 42(13): p. 2278-2283.
45. Monzón-Hernández, D. and J. Villatoro, High-resolution refractive index sensing by means of a multiple-peak surface plasmon resonance optical fiber sensor. *Sensors and Actuators B: Chemical*, 2006. 115(1): p. 227-231.
46. Esteban, Ó., *et al.*, High-sensitive SPR sensing with Indium Nitride as a dielectric overlay of optical fibers. *Sensors and Actuators B: Chemical*, 2011. 158(1): p. 372-376.
47. Kim, Y.-C., *et al.*, Tapered fiber optic surface plasmon resonance sensor for analyses of vapor and liquid phases. *Optics letters*, 2005. 30(17): p. 2218-2220.
48. Coelho, L., *et al.*, Sensing structure based on surface plasmon resonance in chemically etched single mode optical fibres. *Plasmonics*, 2015. 10(2): p. 319-327.
49. Iga, M., A. Seki, and K. Watanabe, Hetero-core structured fiber optic surface plasmon resonance sensor with silver film. *Sensors and Actuators B: Chemical*, 2004. 101(3): p. 368-372.
50. Hosoki, A., *et al.*, A surface plasmon resonance hydrogen sensor using Au/Ta₂O₅/Pd multi-layers on hetero-core optical fiber structures. *Sensors and Actuators B: Chemical*, 2013. 185: p. 53-58.
51. Hautakorpi, M., M. Mattinen, and H. Ludvigsen, Surface-plasmon-resonance sensor based on three-hole microstructured optical fiber. *Optics Express*, 2008. 16(12): p. 8427-8432.
52. Sazio, P.J.A., *et al.*, Microstructured Optical Fibers as High-Pressure Microfluidic Reactors. *Science*, 2006. 311(5767): p. 1583-1586.
53. Hassani, A. and M. Skorobogatiy, Design of the Microstructured Optical Fiber-based Surface Plasmon Resonance sensors with enhanced microfluidics. *Optics Express*, 2006. 14(24): p. 11616-11621.
54. Hassani, A. and M. Skorobogatiy, Design criteria for microstructured-optical-fiber-based surface-plasmon-resonance sensors. *JOSA B*, 2007. 24(6): p. 1423-1429.
55. Hassani, A. and M. Skorobogatiy, Photonic crystal fiber-based plasmonic sensors for the detection of biolayer thickness. *JOSA B*, 2009. 26(8): p. 1550-1557.
56. Liu, B.-H., *et al.*, Hollow fiber surface plasmon resonance sensor for the detection of liquid with high refractive index. *Optics express*, 2013. 21(26): p. 32349-32357.


57. Wong, W.C., *et al.*, Photonic crystal fiber surface plasmon resonance biosensor based on protein G immobilization. *IEEE Journal of Selected Topics in Quantum Electronics*, 2013. 19(3): p. 4602107-4602107.
58. Schuster, T., *et al.*, Miniaturized long-period fiber grating assisted surface plasmon resonance sensor. *Journal of lightwave Technology*, 2012. 30(8): p. 1003-1008.
59. Caucheteur, C., *et al.*, High resolution interrogation of tilted fiber grating SPR sensors from polarization properties measurement. *Optics Express*, 2011. 19(2): p. 1656-1664.
60. Ribaut, C., *et al.*, Small biomolecule immunosensing with plasmonic optical fiber grating sensor, *Biosensors and Bioelectronics*, 2016. 77: p. 315-322.
61. Hwang, Y.H., *et al.*, HMGB1 modulation in pancreatic islets using a cell-permeable A-box fragment. *Journal of Controlled Release*, 2017. 246: p. 155-163.
62. Rich, R.L., *et al.*, Biosensor-based fragment screening using FastStep injections. *Analytical biochemistry*, 2010. 407(2): p. 270-277.
63. Zagorodko, O., *et al.*, Highly sensitive detection of DNA hybridization on commercialized graphene-coated surface plasmon resonance interfaces. *Analytical chemistry*, 2014. 86(22): p. 11211-11216.
64. Chinowsky, T.M., *et al.*, Performance of the Spreeta 2000 integrated surface plasmon resonance affinity sensor. *Sensors and Actuators B: Chemical*, 2003. 91(1-3): p. 266-274.
65. Chinowsky, T.M., *et al.*, Portable 24-analyte surface plasmon resonance instruments for rapid, versatile biodetection. *Biosensors and Bioelectronics*, 2007. 22(9): p. 2268-2275.
66. Adducci, B.A., *et al.*, Differential detection of a surrogate biological threat agent (*Bacillus globigii*) with a portable surface plasmon resonance biosensor. *Biosensors and Bioelectronics*, 2016. 78: p. 160-166.
67. Wu, H., *et al.*, Rapid detection of melamine based on immunoassay using portable surface plasmon resonance biosensor. *Sensors and Actuators B: Chemical*, 2013. 178: p. 541-546.
68. Robelek, R. and J. Wegener, Label-free and time-resolved measurements of cell volume changes by surface plasmon resonance (SPR) spectroscopy. *Biosensors and Bioelectronics*, 2010. 25(5): p. 1221-1224.
69. Horiuchi, T., *et al.*, Passive fluidic chip composed of integrated vertical capillary tubes developed for on-Site SPR immunoassay analysis targeting real samples. *Sensors*, 2012. 12(6): p. 7095-7108.

70. Feltis, B.N., *et al.*, A hand-held surface plasmon resonance biosensor for the detection of ricin and other biological agents. *Biosensors and Bioelectronics*, 2008. 23(7): p. 1131-1136.
71. Zhao, S.S., *et al.*, Miniature multi-channel SPR instrument for methotrexate monitoring in clinical samples. *Biosensors and Bioelectronics*, 2015. 64: p. 664-670.
72. Piliarik, M., *et al.*, Compact and low-cost biosensor based on novel approach to spectroscopy of surface plasmons. *Biosensors and Bioelectronics*, 2009. 24(12): p. 3430-3435.
73. Fernández, F., *et al.*, A label-free and portable multichannel surface plasmon resonance immunosensor for on site analysis of antibiotics in milk samples. *Biosensors and Bioelectronics*, 2010. 26(4): p. 1231-1238.
74. Liu, Y., *et al.*, Surface Plasmon Resonance Biosensor Based on Smart Phone Platforms. *Scientific Reports*, 2015. 5: p. 12864.
75. Wiseman, M.E. and C.W. Frank, Antibody adsorption and orientation on hydrophobic surfaces. *Langmuir*, 2012. 28(3): p. 1765-1774.
76. Jeon, B.-J., M.-H. Kim, and J.-C. Pyun, Application of a functionalized parylene film as a linker layer of SPR biosensor. *Sensors and Actuators B: Chemical*, 2011. 154(2): p. 89-95.
77. Lee, J.M., *et al.*, Direct immobilization of protein G variants with various numbers of cysteine residues on a gold surface. *Analytical chemistry*, 2007. 79(7): p. 2680-2687.
78. Masson, J.-F., *et al.*, Reduction of nonspecific protein binding on surface plasmon resonance biosensors. *Analytical and Bioanalytical Chemistry*, 2006. 386(7): p. 1951-1959.
79. Vashist, S.K., *et al.*, Effect of antibody immobilization strategies on the analytical performance of a surface plasmon resonance-based immunoassay. *Analyst*, 2011. 136(21): p. 4431-4436.
80. Walper, S.A., *et al.*, Comparison of single domain antibody immobilization strategies evaluated by surface plasmon resonance. *Journal of immunological methods*, 2013. 388(1): p. 68-77.
81. Kausaite-Minkstimiene, A., *et al.*, Comparative Study of Random and Oriented Antibody Immobilization Techniques on the Binding Capacity of Immunosensor. *Analytical Chemistry*, 2010. 82(15): p. 6401-6408.
82. de Juan-Franco, E., *et al.*, Site-directed antibody immobilization using a protein A-gold binding domain fusion protein for enhanced SPR immunosensing. *Analyst*, 2013. 138(7): p. 2023-2031.

Chapter 3

Competitive inhibition assay for the detection of progesterone in dairy milk using a fiber optic SPR biosensor

The work presented in this chapter is adapted from:



Daems D., Lu J., Delport F.,
Marien N., Orbie L.,
Aernouts B., I. Adriaens, Huybrechts T., Saeys W., Spasic D and Lammertyn J (2017).

Competitive inhibition assay for the detection of progesterone in dairy milk using a fiber optic SPR biosensor.

Analityca Chemica Acta, 2017 Jan 15; 950: 1 - 6

Contribution of Lu J. to the manuscript: Assisting Daems D. in fabrication of FO-SPR sensors, surface functionalization, carrying out experiments, data processing and analysis, and editing the manuscript.

Abstract

Analytical methods that are often used for the quantification of progesterone in bovine milk include immunoassays and chromatographic techniques. Depending on the selected method, the main disadvantages are the cost, time-to-result, labor intensity and usability as an automated at-line device. This chapter reports for the first time on a robust and practical method to quantify small molecules, such as progesterone, in complex biological samples using an automated fiber optic surface plasmon resonance (FO-SPR) biosensor. A FO-SPR competitive inhibition assay was developed to determine biologically relevant concentrations of progesterone in bovine milk (1e10 ng/mL), after optimizing the immobilization of progesterone-bovine serum albumin (P4-BSA) conjugate, the specific detection with anti-progesterone antibody and the signal amplification with goat anti-mouse gold nanoparticles (GAM-AuNPs). The progesterone was detected in a bovine milk sample with minimal sample preparation, namely $\frac{1}{2}$ dilution of the sample. Furthermore, the developed bioassay was benchmarked against a commercially available ELISA, showing excellent agreement ($R^2 = 0.95$). Therefore, it is concluded that the automated FO-SPR platform can combine the advantages of the different existing methods for quantification of progesterone: sensitivity, accuracy, cost, time-to-result and ease-of-use.

Keywords: fiber optics, surface plasma resonance, biosensor, competitive inhibition assay, progesterone

3.1 Introduction

In dairy industry, optimal reproductive performance of cows is a crucial factor for profitability [1, 2]. In order to avoid long calving intervals and the related economic losses, accurate estrus detection is essential. However, not only do the modern high-productive dairy cows show their external estrous symptoms less clearly, the visual signs are also regularly missed due to the insufficient inspection of the cows on large farms. Therefore, in order to improve the detection of heat in dairy cows, one solution is to use a biosensor for measuring hormone levels related to ovulation and heat, such as progesterone (P4), which is independent of the external symptoms [1-3]. The concentration of this important biomarker in milk correlates well with the level of this reproduction hormone in blood. The concentration of P4 is typically below 3.5 ng/mL in milk during estrus (as seen in Figure 3.1), while it is high for pregnant cows (>7 ng/mL) and remains high throughout gestation [1, 4]. Hence, regular monitoring of milk P4 levels is very useful for dairy farmers to accurately identify cows in heat and optimize the timing of artificial insemination as well as to detect pregnancy in an early stage or abnormalities in the estrous cycle [3, 5].

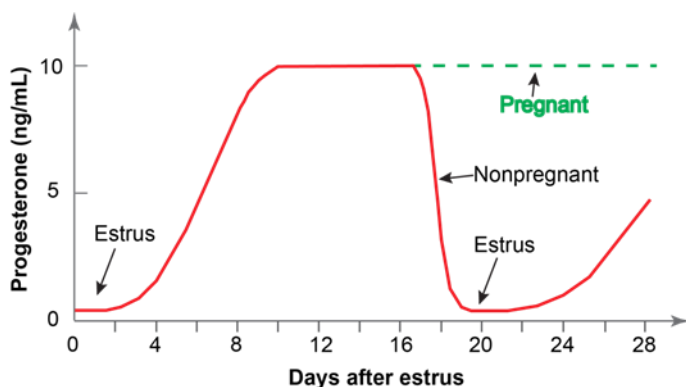


Figure 3.1 Schematic drawing of progesterone concentration change during the estrus cycle.

Standard analytical techniques frequently used in the past for P4 monitoring, like thin layer chromatography and gas chromatography [6], isotope dilution in combination with mass spectrometry [7] and high

performance liquid chromatography [8, 9] suffered from a number of drawbacks such as high costs, extensive sample preparation and their limitation to be only used in a lab environment. More recently, sensitive bio-analytical methods based on immunologic concepts were developed and commercialized [10, 11]: radioimmunoassays (RIA) [12], lateral flow immunoassays (LFIA) [13, 14], fluorescence immunoassays (FIA) [15, 16], electrochemical immunosensors [17], and enzyme immunoassays (EIA) [1, 10, 18, 19]. The advantages of these methods are mainly their specificity and sensitivity in the targeted concentration range (1 - 10 ng/mL) [13]. Among these, the two most commonly used are ELISA and LFIA tests, which have both been shown to provide reliable measurement results for P4 detection with minimal sample preparation. The major drawbacks of the reference ELISA tests are the time-to-result (1 h) and the laborious handling steps [1, 2, 20]. On the other hand, the sensitivity of the fast (15 min) LFIA tests (0.8 - 5 ng/mL [13, 14, 21]) is considerably lower than that of ELISA (0.2 - 1.3 ng/mL [1, 20]). Although the dynamic range of the LFIA is sufficient for this application, accurate determination of P4 in the lower concentration range (0.2 to 1 ng/mL) allows a higher successful rate of artificial insemination. Therefore, a lower LOD of the biosensor is desirable. The LFIA technology has already been used in dairy farming for monitoring the reproductive status of a cow by means of an automated online tool, called the Herd Navigator (Lattec, Hillerød, Denmark) [3, 22].

Immunoassays for P4 detection can also be implemented on a surface plasmon resonance (SPR) based transduction platform [23]. SPR is an advanced label-free, real-time detection technology that provides accurate information on analyte concentrations and binding kinetics [24, 25]. Although SPR is already widely used to detect proteins, peptides and nucleic acids, monitoring small molecules still remains challenging [5], as their direct binding to the sensor surface results in a weak signal [5, 26].

In this work, the use of one such SPR platform, being an in-house developed fiber optic (FO)-SPR, is demonstrated for the first time for the detection of low molecular weight targets. This FO-SPR sensor platform has been previously reported as a cost-effective and easy to use alternative to the expensive and more complex SPR systems [27] for (i) studying the binding kinetics of bacterio-phages on the sensor surface [28], (ii) the implementation of antibody and aptamer based assays on the fiber surface [29-31], and (iii)

the implementation of DNA/RNA based assays including the real time monitoring of nucleic acid amplification and high-resolution melting for single nucleotide polymorphism detection [27, 32-34]. Here, the development of a competitive inhibition bioassay for detection of P4 in bovine milk samples (Figure 3.2) on the FO-SPR platform (ciFO-SPR) is described. In the ciFO-SPR, a detection antibody competes to bind either P4 from the sample or its derivative immobilized on the sensor surface. To improve the limit of detection (LOD), the signal is amplified by means of gold nanoparticles (AuNPs) functionalized with a goat anti-mouse antibody (GAM), similar to other competitive immunoassays for small molecules [5, 24, 26]. The established ciFO-SPR is validated against a competitive commercially available ELISA (cELISA).

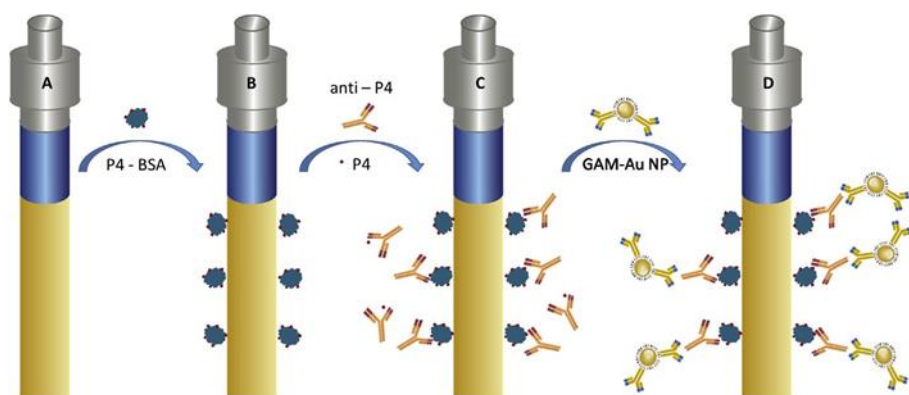


Figure 3.2 Conceptual overview of the ciFO-SPR bioassay. Starting from a FO-SPR biosensor (A), the P4-BSA is covalently immobilized on the surface of a gold coated fiber with carboxyl SAM through EDC/NHS activated carboxyl groups (B). The free P4 in solution and the immobilized P4-BSA on the FO-SPR sensor compete for the detection antibody (anti-P4) (C). The signal is enhanced by AuNPs functionalized with GAM-AuNPs (D).

3.2 Materials and methods

3.2.1 Reagents

All chemicals were of analytical reagent grade. Progesterone (P4) and buffer reagents were supplied by Sigma-Aldrich (Belgium), unless stated otherwise. Solutions were prepared with deionized water purified by a Milli-Q Plus

system (Millipore, Marlborough, MA, USA). Acetic acid, hydrochloric acid and sodium hydroxide were purchased from Chem-Lab (Belgium). Sodium chloride, 1-ethyl-3-(3-dimethylaminopropyl) carbodiimide (EDC) and N-hydroxysuccinimide (NHS) were supplied by Fischer Scientific (Belgium) and Tween-20 by Applichem (Germany). Progesterone-BSA conjugate (P4-BSA) and mouse anti-progesterone antibody (anti-P4 Ab) were purchased from AbD Serotec (UK). Goat anti-mouse antibody (GAM Ab) was supplied by Life Technologies (Belgium). AuNPs (\varnothing 20 nm) were produced by BBI Solutions (UK) and carboxylic acid-SAM formation reagent was purchased from Dojindo (Japan). The milk progesterone enzyme-immunoassay (M-kit Elisa) and ELISA milk standards were purchased from Ridgeway Science (UK). A milk sample was collected for 6 cow (numbered Cow 1e6) selected from a 50 headed herd on an experimental farm (Hooibeekhoeve, Geel) in Flanders, Belgium. These samples were taken from cows in heat.

3.2.2 FO-SPR setup

The FO-SPR device and FO-SPR sensor tips were manufactured as previously described in detail [27, 32]. In short, the FO-SPR device consists of a HL-FHSA tungsten halogen lamp (Ocean optics, USA), a UV-VIS spectrophotometer (USB4000, Ocean Optics, USA) and a FO-SPR sensor tip. All the components were installed on a High-Z S400 CNC/T router (CNC-Step, Germany) to allow automated handling. A modified T1 thermocycler (Biometra, Germany) was used to control the temperature of the samples. The replaceable FO-SPR sensor tips were coupled by means of an SMA-type connector to a bifurcated optical FO-SPR sensor to guide white light from the halogen lamp into the FO-SPR sensor tip, and back to the spectrophotometer [32, 33]. Binding phenomena at the gold surface of the sensor tip result in a shift of the typical spectral resonance SPR-dip recorded by the spectrophotometer.

The manufacturing of a FO-SPR sensor tip consisted of several steps. Briefly, the jacket and the cladding of a 400 μm multimode TEQS fiber (Thorlabs, Germany) were respectively removed with pliers and acetone. Subsequently, the fiber was cleaved with a LDC-400 device (Vytran, UK) to make a FO-SPR sensor with a total length of 4.3 cm (a middle part with cladding of 3.6 cm and two ends of 0.6 cm and 0.1 cm). Next, a 50 nm gold

coating was deposited onto the 0.6 cm end of the FO-SPR sensor surface using a sputter coater (Quorum Q150T ES, UK). The freshly prepared FO-SPR sensor tips were incubated overnight with a 100 mM mixed self-assembling monolayer (Carboxylic acid-SAM formation reagent), washed in ethanol, and stored in 50 mM MES buffer (pH 6) until further use.

3.2.3 Immobilization of goat anti-mouse antibody on gold nanoparticles

GAM Ab was coupled to AuNPs (ϕ 20 nm) by passive adsorption. First, the pH of the AuNPs (initial concentration of 7×10^{11} particles per mL) was adjusted to pH 9.2 with a 0.2 M Na_2CO_3 solution. Following, the GAM Abs were added to the AuNPs at final concentration of 5 $\mu\text{g}/\text{mL}$ and incubated on a rotator (Grant-Bio PRT-30, Keison products, UK) at room temperature for 20 min. In a next step, 500 μL of 0.5% BSA in PBS was added to the AuNPs and incubated on the rotator for 1 h to reduce nonspecific binding of the AuNPs to the FO-SPR sensor tip during detection. After centrifugation of the AuNP-solution for 40 min at 7000 rpm at 20 $^\circ\text{C}$, the supernatant was discarded and the GAM-AuNPs were diluted in PBS buffer to a final optical density (OD) of 0.5 or 1.0 (wavelength = 530 nm), corresponding to the concentration of 7×10^{11} or 14×10^{11} AuNPs per mL, respectively. The OD was measured with a SpectraMax M2 spectrophotometer (Molecular Devices LLC., USA). The prepared AuNPs were stored at 4 $^\circ\text{C}$ until use.

3.2.4 Competitive inhibition assay on the FO-SPR

The FO-SPR sensor tip was immersed in 50 mM MES buffer to reach a stable baseline, followed by activation of the carboxyl groups on the FO-SPR sensor tip surface using 150 μL of 0.4 M EDC and 0.1 M NHS in 50 mM MES solution for 10 min. Next, the FO-SPR sensor tip was immersed in the P4-BSA conjugate solution with a concentration of 25, 50 or 100 $\mu\text{g}/\text{mL}$ in 10 mM sodium acetate (pH 4.5) for 30 min, followed by a short washing step of 30 s in a regeneration buffer (1 M NaCl and 50 mM NaOH). The unreacted activated groups were blocked with 150 μL of 50 mM ethanolamine in PBS for 8 min.

In the first step of the ciFO-SPR bioassay, the P4-BSA function-alized FO-SPR sensor tip was put in 150 mL of a pre-incubated mixture of anti-P4 Ab in PBS buffer with 0.5% BSA and (i) a P4 dilution in PBS or (ii) a milk sample for 15 min. Milk standards and bovine milk samples were incubated for 10 min at 37 °C and vortexed before use. Next, the signal of the anti-P4 Abs, captured onto the P4-BSA sensor tip surface, was amplified for 30 min by binding with the GAM-AuNPs. The complete protocol for detecting P4 is shown in Section 3.5.1 Table S3.1.

3.2.5 ELISA procedure

A commercially available competitive ELISA (M-Kit, cELISA) was applied as a reference technology for P4 quantification in bovine milk samples in this study. The wells of a microtiter plate were loaded with either 10 µL of milk standard or sample solution. These milk standards were derived from an anoestrus or ovariectomized cow in which there will be little or negligible amounts of P4 and spiked with P4 (0 - 10 ng/mL). Following, 200 µL of progesterone labeled enzyme was added to each well and incubated for 1 h at room temperature. The microtiter plate was washed 3 times with 200 µL cold demiwater (5 °C). Finally, 200 µL of the substrate solution was added to each well and after 20 min the color change was quantified in terms of the absorption at 570 nm as measured with a spectrophotometer (SpectraMax M2, Molecular Devices LLC., USA).

3.2.6 Data processing

FO-SPR data were recorded with LabView (National Instruments, USA) and further processed using Origin 8 (OriginLab, USA). Calibration curves were fitted with a logistic fit [35], as shown in Equation 3.1

$$y = A_2 + \frac{(A_1 - A_2)}{1 + (x/x_0)^p} \quad (3.1)$$

where A_1 is the minimum asymptote (response value at zero standard concentration), A_2 is the maximum asymptote (response value for infinite standard concentration), x is the target concentration, x_0 is the inflection point,

p is the Hill's slope (refers to the steepness of the curve), and y is the FO-SPR shift.

Equation 3.2 was used to calculate the LOD of the established bioassays:

$$LOD_x = x_0 \times \sqrt[p]{\frac{(A_1 - A_2)}{((LOD_y - A_2) - 1)}} \tag{3.2}$$

where $LOD_y = y_0 - 3 \times \sigma_0$, with y_0 is the average response for 0 ng/mL P4 of a certain number of repetitions ($n = 4$ for buffer, $n = 3$ for milk) and σ_0 is the mean standard deviation for y_0 . To be more specific, as seen in Figure 3.3, a calibration curve has been generated. By using Origin 8 with Equation 3.1, a logistic curve can be fitted for the calibration curve and the values of all the parameters (A_1 , A_2 , x_0 , and p) were given by the software (as seen in the inset table). Since LOD_y can be easily calculated, by using all the given parameters, the LOD in concentration (LOD_x) can be calculated using Equation 3.2.

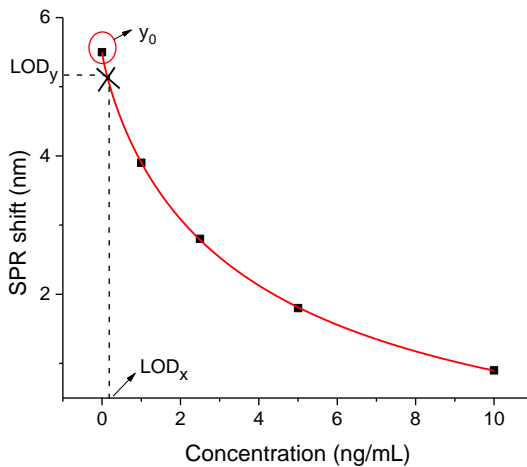


Figure 3.3 An example of how the LOD was calculated from the calibration curve and Equation 3.2.

The intraclass correlation coefficient (ICC) [36], which assesses the reliability of ratings by comparing the variability of different ratings of the same object, was calculated with the statistical package R (version 2.11.1, The R foundation for Statistical Computing, Vienna, Austria).

3.3 Results and discussion

3.3.1 FO-SPR competitive inhibition assay development

A competitive inhibition bioassay was implemented on the FO-SPR to quantify the concentration of P4 in milk samples. This type of bioassay was chosen as the sensitivity of SPR based sensors is generally not adequate for detection of low molecular weight targets. As indicated in Figure 3.1, the free P4 in solution and the P4-BSA conjugate immobilized on the FO-SPR sensor tip surface get in competition for the detection antibody (anti-P4). To improve the LOD, the signal generated by the binding of the detection antibody to the FO-SPR sensor tip was amplified through the binding of AuNPs functionalized with GAM antibody (GAM-AuNP) (Figure S3.1). In order to achieve a reproducible calibration curve for the ciFO-SPR bioassay, three main aspects of the assay were first optimized in buffer conditions: (i) immobilization of P4-BSA conjugate to the FO-SPR sensor tip surface, (ii) signal amplification by GAM-AuNPs and (iii) specific detection by monoclonal anti-P4 Ab. These parameters were evaluated based on the size of the FO-SPR shift, reproducibility, sensitivity, and LOD.

Firstly, the FO-SPR sensor tip was functionalized with three different P4-BSA concentrations (25, 50 and 100 $\mu\text{g}/\text{mL}$) (Figure 3.4A). The immobilization with both 50 and 100 $\mu\text{g}/\text{mL}$ of P4-BSA conjugate resulted in the highest and most reproducible FO-SPR shifts with coefficients of variation (CV) below 5%. In order to minimize the cost of the bioassay, 50 $\mu\text{g}/\text{mL}$ was selected for immobilization, unless stated otherwise. To quantify the level of nonspecific binding, tests were performed in absence of the P4-BSA conjugate on the FO-SPR sensor tip surface. This resulted in a negligible shift of 0.06 nm with a CV of 2.4% (data not shown). Moreover, the anti-P4 Ab was specific for P4 as no significant FO-SPR shift was observed when BSA without P4 was immobilized on the FO-SPR sensor tip surface (data not shown).

Secondly, the role of AuNPs on the signal amplification was studied by comparing the direct binding of free anti-P4 Ab to the FO-SPR sensor tip surface and the same antibody when functionalized to AuNPs. In both cases, the FO-SPR sensor tip surface was functionalized with a 100 $\mu\text{g}/\text{mL}$ P4-BSA conjugate. A 3.3 times increase in FO-SPR shift was obtained when anti-P4

Ab was immobilized on AuNPs (11 ± 1 nm, $n = 3$) compared to free anti-P4 Ab (3.4 ± 0.2 nm, $n = 3$) (Figure 3.4B). Moreover, it was also observed that the concentration of AuNPs plays an important role in the signal amplification efficiency. By doubling the initial concentration of GAM-AuNPs from 0.5 to 1 OD in the ciFO-SPR bioassay, the FO-SPR shift was doubled after 30 min (Figure S3.2). Since GAM Ab is polyclonal, to exam if there was nonspecific binding between GAM-AuNPs and the FO-SPR sensor surface, tests were performed by immersing the FO-SPR sensor functionalized with P4-BSA into a suspension of bare AuNPs or GAM-AuNPs. Results showed negligible FO-SPR shifts, proving there is no nonspecific binding (data not shown). Sensitivity of the bioassay may be improved by using a monoclonal Ab which is specific to anti-P4 Ab.

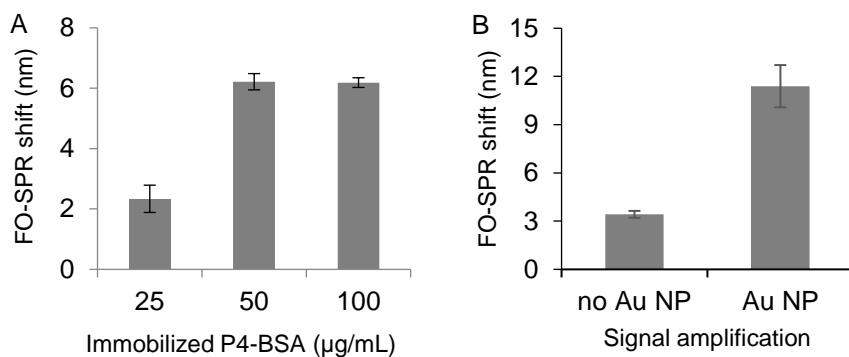


Figure 3.4 (A) FO-SPR shift from immobilization of different P4-BSA conjugate concentrations. Error bars represent one standard deviation ($n = 3$). (B) Comparison of a ciFO-SPR bioassay using anti-P4 Ab with or without AuNPs for signal amplification as detection antibody. Error bars represent one standard deviation ($n = 3$).

Thirdly, the influence of the anti-P4 Ab concentration on the shape of the calibration curve, and correspondingly the LOD, was studied. Four different concentrations of anti-P4 Ab were tested in buffer conditions: 0.1, 0.2, 0.4 and 0.8 $\mu\text{g/mL}$. This concentration range was chosen based on a competitive assay reported in ref [37], where 0.4 $\mu\text{g/mL}$ of conjugate against target molecule was used. Therefore, for optimization of the concentration of anti-P4 Ab, testing concentrations were chosen around 0.4 $\mu\text{g/mL}$. For the first two conditions, GAM-AuNP concentration was doubled (from 7×10^{11} to $14 \times$

10^{11} AuNPs per mL) to accelerate binding kinetics. The FO-SPR shifts obtained from different anti-P4 Ab concentrations were plotted as a function of the P4 concentrations (0, 1, 2, 5, and 10 ng/mL). A logistic fit (Equation 3.1) was used to establish the calibration curves (Figure S3.3). The steepness of the calibration curves (p-value from Equation 3.1) was used as a criterion for the sensitivity of the bioassay, with steeper calibration curves having lower p-value. Thus, the p-value decreased from 2.0 ± 0.6 nm for 0.8 $\mu\text{g/mL}$ anti-P4 Ab to 1.1 ± 0.2 for 0.1 $\mu\text{g/mL}$ anti-P4, resulting in a more sensitive calibration curve. Correspondingly, the LOD decreased from 5.7 ng/mL to 0.7 ng/mL of P4. Moreover, the CV was the lowest for 0.1 and 0.2 $\mu\text{g/mL}$ of detection Ab, namely 9%. In conclusion, the lowest anti-P4 Ab concentration (0.1 $\mu\text{g/mL}$) showed the best reproducibility, highest sensitivity and lowest LOD (Table S3.2).

3.3.2 Progesterone detection in buffer and milk standards with ciFO-SPR assay

Using the optimized parameters of the ciFO-SPR bioassay, a calibration curve was established for measurement of P4 concentrations in the range of 1 to 10 ng/mL in PBS buffer and milk standards (Figure 3.5C), starting from their FO-SPR sensorgrams (Figure 3.5A and B). In Figure 3.3A, an overshoot can be observed between step i and ii. This was caused by moving the FO-SPR sensor from the solution of P4 in PBS buffer to PBS buffer. The evaporation of the liquid on the sensor surface led to disappearance of the SPR dip and hence the change in fitting of the SPR dip by the software. Although the signal amplification step with GAM-AuNPs was 30 min in both cases, the FO-SPR shift was higher for buffer compared to the milk samples. This difference can be explained by the matrix effect of a milk sample. Interfering components prevented the GAM-AuNPs to bind to the target on the FO-SPR sensor surface, resulting in a lower binding signal intensity for measurements in milk samples compared to buffer. However, the overall ΔRI [38], between PBS buffer before and after the dipping step, is similar for experiments in buffer and milk. This observation indicated that no milk residues are sticking to the FO-SPR sensor tip. In Figure 3.5C, a logistic curve (Equation 3.1) was fitted on the measurements for both buffer ($R^2 = 0.99$, $n = 4$) and milk standards ($R^2 = 0.99$, $n = 3$), resulting in LOD values of 0.6 and 0.5 ng/mL and CVs of 8%

and 16%, respectively. Furthermore, zooming into the most relevant concentration range (0 - 5 ng/mL), linked to the heat in cows, decreased the average variation both for buffer samples (7%) and for milk standards (9%). As the steepness was maximized over the most important interval of the ciFO-SPR calibration curve, the signal variation of the higher P4 concentrations is increased using the logistic fit. In the remainder of this chapter, the calibration curve for milk will be used to determine the P4 concentrations in raw bovine milk samples with the FO-SPR sensor.

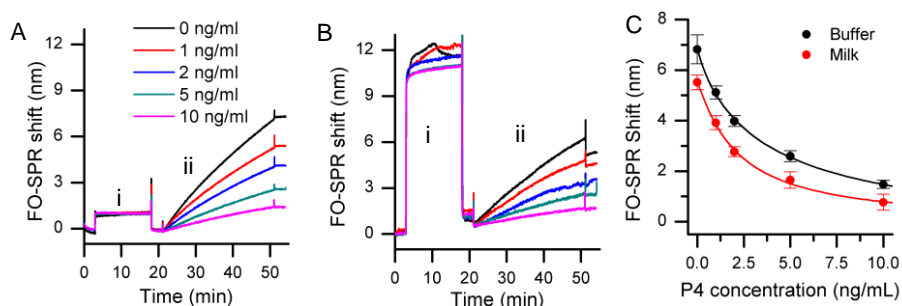


Figure 3.5 ciFO-SPR bioassay performed with series of P4 concentrations in PBS buffer and milk standards by (i) dipping the FO-SPR sensor tip in the sample and (ii) amplifying the signal with GAM-AuNPs. (A) FO-SPR sensorgrams for the range of P4 concentrations in PBS buffer (from 0 ng/mL of P4 (upper curve) to 10 ng/mL (the lowest curve)). (B) FO-SPR sensorgrams for the same range of P4 concentrations in milk standards. (C) The FO-SPR shifts (nm) for buffer (●) and milk standards (●) are plotted as a function of the P4 concentrations, yielding a logistic fit calibration curve (based on Equation 3.1). Error bars represent one standard deviation ($n = 4$ in buffer and $n = 3$ in milk standards).

The potential of the FO-SPR platform as a field device with limited sample preparation was further explored by shortening the measurement time of the established ciFO-SPR bioassay. Besides the functionalization of the FO-SPR sensor tip, which can be done in advance, the signal amplification with GAM-AuNPs is the most time consuming step, being 30 min in the presented bioassay. Therefore, the effect of shortening this amplification step on the calibration curve was evaluated based on reproducibility, sensitivity and LOD (Figure 3.6). The experiment was performed on milk standards with various duration of the amplification step, ranging from 1 to 30 min. The steepness of the calibration curves (p-value Equation 3.1) was again used as a criterion for sensitivity. The p-value was similar for signal amplification

during 10 min (1.3 ± 0.2 nm), 20 min (1.1 ± 0.1 nm) and 30 min (1.1 ± 0.2 nm), resulting in a similar sensitivity. As can be seen in Figure 3.5, the difference in SPR shift between 1 min and 30 min was higher for low concentrations of P4 (e.g. 0 ng/mL) compared to higher concentrations of P4 (e.g. 10 ng/mL). This is due to the competitive nature of the bioassay and the binding kinetics of the Ab-coated AuNPs. In case of a low number of binding sites for AuNPs (high P4 concentration), equilibrium is reached quickly, reducing the effect of time on the signal. In case of a low P4 concentration many binding spots for AuNPs are available and saturation is reached only after a considerable time, making the timing more important. Moreover, based on Equation 3.2, similar LODs were obtained for these bioassays: 0.6 ng/mL for 10 and 20 min and 0.5 ng/mL for 30 min. However, the average CV over the P4 concentration range 0 – 5 ng/mL increased from 9% (30 min, $R^2 = 0.99$) to 14% (20 min, $R^2 = 0.99$) and 22% (10 min, $R^2 = 0.99$). Further decrease in time affected the quality of the fit ($R^2 < 0.99$), the reproducibility ($CV > 25\%$), the sensitivity (p-value ≥ 2 nm) and the LOD (> 1.3 ng/mL). In conclusion, combining independent pre-functionalization of the FO-SPR sensor tip with a signal amplification step of 10 min can bring the total detection time under 20 min, offering the possibility to determine the P4 concentration in raw milk shortly after the milking of a cow.

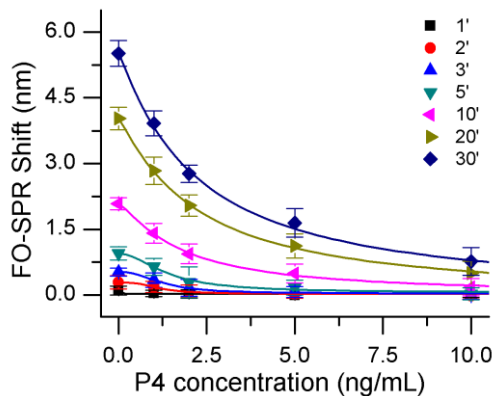


Figure 3.6 Calibration curves for P4 established with different duration of the signal amplification step (1, 2, 3, 5, 10, 20 and 30 min). Error bars represent one standard deviation ($n = 3$).

3.3.3 Screening of biological samples

The established ciFO-SPR bioassay for quantification of P4 in milk was further validated against the cELISA, the most commonly used method for P4 quantification in milk, by measuring six bovine milk samples taken from six different cows. These samples were taken from cows in heat, thus typically having a low P4 level (< 3.5 ng/mL). The samples were processed with a minimal sample preparation procedure consisting of two steps: (i) incubating for 10 min at 37 °C and (ii) diluting the sample with anti-P4 Ab in buffer (Section 3.2.4). The P4 concentrations in the six bovine samples were determined with the ciFO-SPR biosensor using the calibration curve in milk standards shown in Figure 3.5C. All the values obtained for the FO-SPR shifts (nm) and the ELISA absorbance signals (AU) are shown for each sample in Figure S3.4. The average CV was 14% and 22% for ciFO-SPR ($n = 4$) and cELISA ($n = 6$), respectively. As shown in Figure 3.7, the P4 concentrations quantified with the ciFO-SPR bioassay correlated linearly with the corresponding cELISA results ($R^2 = 0.95$). Moreover, the ICC was calculated to be 0.97 ($n = 6$).

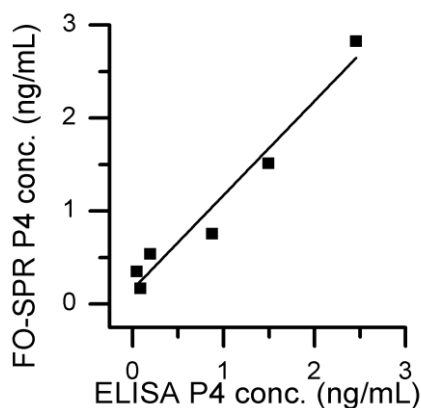


Figure 3.7 Comparison of the P4 levels determined with the in-house developed ciFO-SPR biosensor and the commercial cELISA test.

3.4 Conclusions

Despite advances in accuracy and time-to-result, off-laboratory screening of P4 with automated and cost-effective assays is still challenging. In search of new techniques to quantify P4 in bovine milk, an in-house developed FO-SPR biosensor was explored for establishing a competitive inhibition bioassay. The designed ciFO-SPR bioassay was first optimized by determining the concentration of (i) P4-BSA conjugate to be immobilized on the FO-SPR sensor tip, (ii) anti-P4 antibody and (iii) GAM-AuNPs. Calibration curves were established with the ciFO-SPR bioassay for spiked buffer samples and milk standards in the biologically relevant concentration range between 1 and 10 ng/mL, resulting in LODs of 0.6 ng/mL and 0.5 ng/mL P4, respectively. Furthermore, the time-to-result of the established ciFO-SPR bioassay was reduced under 20 min resulting in a similar LOD and sensitivity of the assay. Finally, the bioassay was validated against a reference cELISA technique. In the low concentration range corresponding to heat, the results obtained with the ciFO-SPR biosensor for bovine milk samples correlated very well with those of the cELISA, resulting in ICC of 0.97. In conclusion, the developed platform combines the ease-of-use and cost efficiency of a LFIA with the accuracy, sensitivity and possibility for automation of an ELISA test. Future work will focus on integrating this ciFO-SPR bioassay in an automated milking robot on a dairy farm to monitor the reproductive cycle of dairy cows.

3.5 Supplementary information


3.5.1 Detection protocol

Detection of the small molecule progesterone (P4) with FO-SPR biosensor was performed with a competitive inhibition assay (ciFO-SPR). Calibration curves were established in different matrices: PBS buffer with 0.5% BSA and bovine milk standards (Ridgeway Science, UK). The samples were always diluted $\frac{1}{2}$ during sample preparation. The five tested P4 concentrations to establish the calibration curve were: 10, 5, 2, 1 and 0 ng/mL.

The complete protocol for detecting P4 is shown in Table S3.1. The five concentrations of P4 (between 0 and 10 ng/mL) to establish the calibration curves were measured during a fully automated process on the same FO-SPR sensor tip with regeneration between the different concentrations. All tests were performed at room temperature. After an initial baseline step in 50 mM of MES buffer pH 6.0 (step 1), the FO-SPR sensor tip was activated with freshly prepared 400 mM EDC and 100 mM NHS in MES buffer (step 2). 50 μ g/mL P4-BSA in 10 mM NaAc pH 4.5 was immobilized on the surface of the FO-SPR sensor tip during step 5. Subsequently the FO-SPR sensor tip was washed with 1 M NaCl and 50 mM NaOH (NaCl/OH) (step 7) and blocked with 50 mM ethanolamine (EtAm) in PBS pH 7.4 (step 9). The P4-BSA functionalized FO-SPR sensor tip was immersed in 150 μ L of a pre-incubated mixture (step 12) of anti-P4 Ab in PBS buffer with 0.5 % BSA and (i) a P4 dilution in PBS or (ii) a milk sample for 15 min. Finally, GAM-AuNP (suspended in PBS) were used for signal amplification (step 14). A regeneration step with 1 M NaCl and 50 mM NaOH to remove the bounded anti-P4 Ab and GAM-AuNPs was added to the protocol (step 16) if several samples were measured with the same FO-SPR sensor. Step 4, 6, 8, 10, 11, 13, 14 and 17 were washing steps.

Table S3.1 Protocol to detect P4 with a ciFO-SPR bioassay. Because 5 repetition were done on the same FO-SPR sensor, step 11 till 17 were repeated 4 times after the first complete run. The used volume was 150 μ L per step.

| | Step | Time (min) | Sample* | Action |
|-----------------------------|------|------------|----------|----------------------------------|
| Functionalization | 1 | 15 | MES | |
| | 2 | 10 | EDC/NHS | Activation |
| | 3 | 3 | MES | |
| | 4 | 3 | NaAc | |
| | 5 | 30 | P4-BSA | Immobilization |
| | 6 | 3 | NaAc | |
| | 7 | 0.5 | NaCl/OH | Washing |
| | 8 | 3 | NaAc | |
| | 9 | 8 | EtAm | Blocking |
| | 10 | 3 | NaAc | |
| | 11 | 3 | PBS | |
| Interaction | 12 | 15 | Sample | Interaction with sample |
| | 13 | 3 | PBS | |
| Signal amplification | 14 | 30 | GAM-AuNP | Signal amplification by GAM-AuNP |
| | 15 | 3 | PBS | |
| Regeneration | 16 | 0.5 | NaCl/OH | Regeneration |
| | 17 | 3 | PBS | |



* Used labels for the samples: MES, 50 mM MES-buffer pH 6.0; EDC/NHS, 400 mM EDC and 100 mM NHS in MES; NaAc, 10 mM NaAc pH 4.5; P4-BSA, 50 μ g/mL P4-BSA in 10 mM NaAc pH 4.5; NaCl/OH, 1 M NaCl and 50 mM NaOH; EtAm, 50 mM EtAm in PBS pH 7.4; PBS, PBS pH 7.4; sample, P4 in buffer or sample with 0.1 μ g/mL P4-Ab added; GAM-AuNP, GAM-AuNP in PBS.

3.5.2 Results and discussion

3.5.2.1 FO-SPR competitive inhibition assay development

The concept of a ciFO-SPR assay was demonstrated by comparing the FO-SPR shift obtained in the absence of free P4 with the one generated in the presence of a high concentration of P4 (20 μ g/mL). As expected, the ciFO-

SPR assay gives a significant increase in signal when P4 is absent (Figure S3.1).

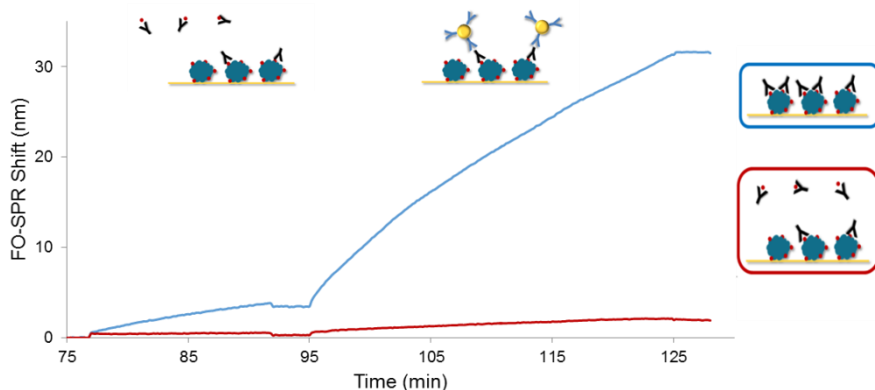


Figure S3.1 Binding events during step 12 and 14 from the competitive inhibition assay (Table S3.1). The *ciFO-SPR* assay gives a higher signal in the absence of P4 (blue curve) compared to the presence of 10 $\mu\text{g/mL}$ P4 (red curve). Both measurements are performed with 10 $\mu\text{g/mL}$ anti-P4 antibody in step 12.

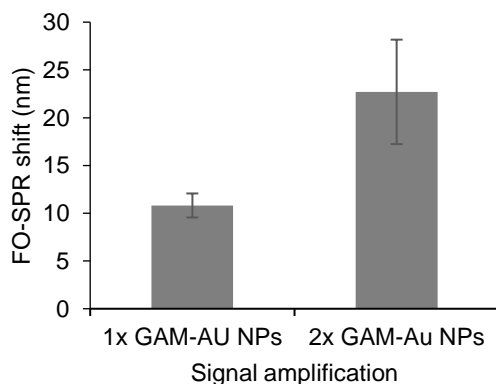


Figure S3.2 Comparison of a *ciFO-SPR* bioassay using 1 \times GAM-AuNPs or 2 \times GAM-AuNPs for signal amplification. Error bars represent one standard deviation ($n = 3$).

The concentration of GAM-AuNPs plays an important role in the signal amplification efficiency. By doubling the initial concentration of GAM-AuNP from 7×10^{11} to 14×10^{11} AuNPs per mL, the observed FO-SPR shift was increased after 30 min with a factor 2.1 ± 0.3 ($n = 3$) (Figure S3.2). Although

an excess of GAM-AuNPs was present in both cases, this increase in FO-SPR shift can be explained by the enhanced mass transport of the GAM-AuNPs and the accelerated association kinetics of the biomolecular interactions at the FO-SPR sensor tip surface [1, 2-4]. By fitting the association reaction kinetics, it was observed that for both concentrations of GAM-AuNPs eventually the same equilibrium value was reached, but that the way towards this equilibrium was different.

The influence of the concentration of the detection Ab (anti-P4) on the shape of the calibration curve, and correspondingly the LOD, was studied for the developed ciFO-SPR bioassay (Figure S3.3).

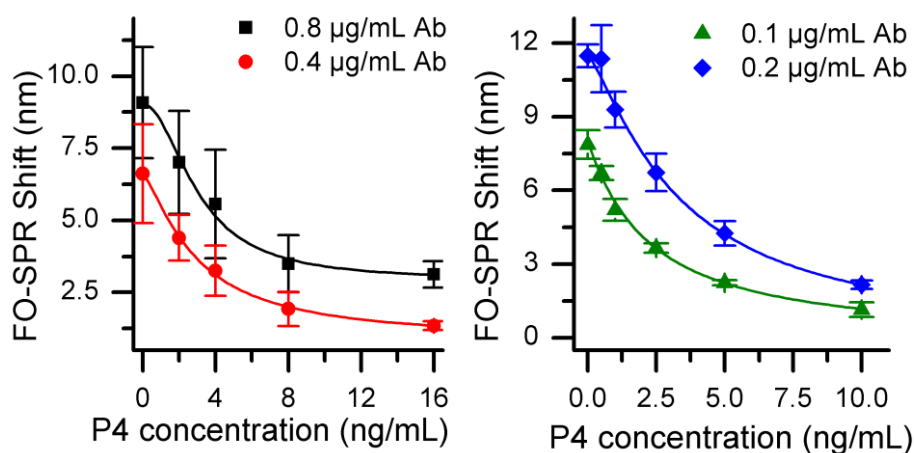


Figure S3.3 Evaluation of different concentrations of anti-P4 detecting Ab. The FO-SPR shifts (nm) obtained in PBS buffer are plotted in function of the P4 concentrations (ng/mL), yielding a logistic fit calibration curve (Equation 3.1). Error bars represent one standard deviation ($n = 3$).

Four different concentrations of anti-P4 detecting Ab were tested (0.1, 0.2, 0.4 and 0.8 µg/mL) and evaluated in buffer conditions based on FO-SPR shift, reproducibility, sensitivity and limit of detection (LOD) (Table S3.2). For the low concentrations of anti-P4 Ab (0.1 and 0.2 µg/mL), the concentration of secondary GAM-AuNPs was doubled from 7×10^{11} to 14×10^{11} AuNPs per mL to accelerate binding kinetics, resulting in higher FO-SPR shifts after 30 min assay time. A typical logistic fit (Equation 3.1) was used to establish the preliminary calibration curves for the different concentrations of

anti-P4 Abs by plotting the FO-SPR shifts as a function of the P4 concentrations.

Table S3.2: Four different concentrations of anti-P4 detecting Ab were tested and evaluated in buffer conditions.

| Anti-P4 Ab ($\mu\text{g/mL}$) | R ² | CV (%) | p value (nm) | LOD (ng/mL) |
|------------------------------------|----------------|-----------|-----------------|----------------|
| 0.8 | 0.999 | 21 | 2.0 \pm 0.6 | 5.7 |
| 0.4 | 0.999 | 18 | 1.4 \pm 0.2 | 4.9 |
| 0.2 | 0.998 | 9 | 1.3 \pm 0.2 | 0.7 |
| 0.1 | 0.995 | 9 | 1.1 \pm 0.2 | 0.7 |

3.5.2.2 Screening of biological samples

Six bovine milk samples taken from six different cows were measured both with the cELISA and ciFO-SPR. The obtained FO-SPR shifts (nm) as well as the ELISA absorbance signals (AU) are shown for each sample in Figure S3.4.

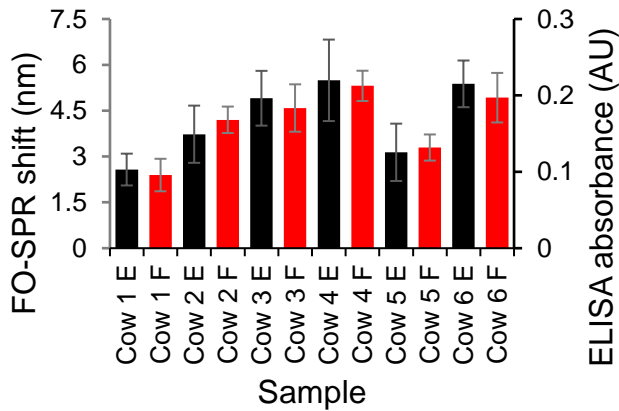


Figure S3.4: Comparison of cELISA (E columns) and ciFO-SPR (F columns) signals for 6 different cows. Errors represent one standard error ($n = 6$ in ELISA and $n = 4$ in FO-SPR).

3.6 References

1. Claycomb, R.W., *et al.*, *Rapid enzyme immunoassay for measurement of bovine progesterone*. Biosensors and Bioelectronics, 1998. **13**(11): p. 1165-1171.
2. Simersky, R., *et al.*, *Development of an ELISA-based kit for the on-farm determination of progesterone in milk*. VETERINARNI MEDICINA-PRAHA-, 2007. **52**(1): p. 19.
3. Frigens, N.C. and M.G. Chagunda, *Prediction of the reproductive status of cattle on the basis of milk progesterone measures: model description*. Theriogenology, 2005. **64**(1): p. 155-190.
4. Chanvallon, A., *et al.*, *Comparison of three devices for the automated detection of estrus in dairy cows*. Theriogenology, 2014. **82**(5): p. 734-741.
5. Mitchell, J., *Small molecule immunosensing using surface plasmon resonance*. Sensors, 2010. **10**(8): p. 7323-7346.
6. Darling, J., A. Laing, and R. Harkness, *A SURVEY OF THE STEROIDS IN COWS'MILK*. Journal of endocrinology, 1974. **62**(2): p. 291-297.
7. Siekmann, L., *Determination of steroid hormones by the use of isotope dilution-mass spectrometry: a definitive method in clinical chemistry*. Journal of steroid biochemistry, 1979. **11**(1): p. 117-123.
8. Purdy, R.H., *et al.*, *Analysis of metabolites of progesterone in bovine liver, kidney, kidney fat, and milk by high performance liquid chromatography*. Journal of steroid biochemistry, 1980. **13**(11): p. 1307-1315.
9. Díaz-Cruz, M.S., *et al.*, *Determination of estrogens and progestogens by mass spectrometric techniques (GC/MS, LC/MS and LC/MS/MS)*. Journal of Mass Spectrometry, 2003. **38**(9): p. 917-923.
10. Ivanova, T. and T. Godjevargova, *Sensitive progesterone determination using a magnetic particle-based enzyme-linked immunosorbent assay*. Analytical Letters, 2015. **48**(5): p. 843-860.
11. Nebel, R., *et al.*, *Comparisons of eight commercial on-farm milk progesterone tests*. Theriogenology, 1989. **31**(4): p. 753-764.
12. Posthuma-Trumpie, G.A., *et al.*, *Perspectives for on-site monitoring of progesterone*. Trends in biotechnology, 2009. **27**(11): p. 652-660.
13. Samsonova, J., V. Safronova, and A. Osipov, *Pretreatment-free lateral flow enzyme immunoassay for progesterone detection in whole cows' milk*. Talanta, 2015. **132**: p. 685-689.
14. Laitinen, M.P. and M. Vuento, *Immunochemical assay for quantitation of milk progesterone*. Acta Chemica Scandinavica, 1996. **50**(2): p. 141-145.


15. Käppel, N.D., F. Pröll, and G. Gauglitz, *Development of a TIRF-based biosensor for sensitive detection of progesterone in bovine milk*. Biosensors and Bioelectronics, 2007. **22**(9): p. 2295-2300.
16. Trapiella-Alfonso, L., *et al.*, *Development of a quantum dot-based fluorescent immunoassay for progesterone determination in bovine milk*. Biosensors and Bioelectronics, 2011. **26**(12): p. 4753-4759.
17. Zhang, H.Y., *et al.*, *Detection of progesterone in bovine milk using an electrochemical immunosensor*. International journal of dairy technology, 2013. **66**(4): p. 461-467.
18. Van der Lende, T., R. Schasfoort, and R. van der Meer, *Monitoring reproduction using immunological techniques*. Animal Reproduction Science, 1992. **28**(1): p. 179-185.
19. Wu, L., *et al.*, *Development and Application of an ELISA Kit for the Detection of Milk Progesterone in Dairy Cows*. Monoclonal antibodies in immunodiagnosis and immunotherapy, 2014. **33**(5): p. 330-333.
20. Van de Wiel, D. and W. Koops, *Development and validation of an enzyme immunoassay for progesterone in bovine milk or blood plasma*. Animal Reproduction Science, 1986. **10**(3): p. 201-213.
21. Sananikone, K., *et al.*, *Quantitative lateral flow immunoassay for measuring progesterone in bovine milk*. Transactions of the ASAE, 2004. **47**(4): p. 1357.
22. Waldmann, A. and A. Raud, *Comparison of a lateral flow milk progesterone test with enzyme immunoassay as an aid for reproductive status determination in cows*. The Veterinary record, 2016. **178**(11): p. 260-260.
23. Gillis, E.H., *et al.*, *Improvements to a surface plasmon resonance-based immunoassay for the steroid hormone progesterone*. Journal of AOAC International, 2006. **89**(3): p. 838-842.
24. Schasfoort, R. and A. Tudos, *Handbook of Surface Plasmon Resonance* Royal Society of Chemistry. 2008, London.
25. Homola, J., *Surface plasmon resonance sensors for detection of chemical and biological species*. Chemical reviews, 2008. **108**(2): p. 462-493.
26. Homola, J., S.S. Yee, and G. Gauglitz, *Surface plasmon resonance sensors*. Sensors and Actuators B: Chemical, 1999. **54**(1): p. 3-15.
27. Pollet, J., *et al.*, *Real-Time Monitoring of Solid-Phase PCR Using Fiber-Optic SPR*. Small, 2011. **7**(8): p. 1003-1006.
28. Knez, K., *et al.*, *Affinity comparison of p3 and p8 peptide displaying bacteriophages using surface plasmon resonance*. Analytical chemistry, 2013. **85**(21): p. 10075-10082.

29. Lu, J., *et al.*, *Fiber optic-SPR platform for fast and sensitive infliximab detection in serum of inflammatory bowel disease patients*. *Biosensors and Bioelectronics*, 2016. **79**: p. 173-179.
30. Pollet, J., *et al.*, *Fast and accurate peanut allergen detection with nanobead enhanced optical fiber SPR biosensor*. *Talanta*, 2011. **83**(5): p. 1436-1441.
31. Tran, D.T., *et al.*, *Selection of aptamers against Ara h 1 protein for FO-SPR biosensing of peanut allergens in food matrices*. *Biosensors and Bioelectronics*, 2013. **43**: p. 245-251.
32. Knez, K., *et al.*, *Fiber-Optic High-Resolution Genetic Screening Using Gold-Labeled Gene Probes*. *Small*, 2012. **8**(6): p. 868-872.
33. Knez, K., *et al.*, *Spherical nucleic acid enhanced FO-SPR DNA melting for detection of mutations in Legionella pneumophila*. *Analytical chemistry*, 2013. **85**(3): p. 1734-1742.
34. Daems, D., *et al.*, *Real-time PCR melting analysis with fiber optic SPR enables multiplex DNA identification of bacteria*. *Analyst*, 2016. **141**(6): p. 1906-1911.
35. Polenta, G., *et al.*, *Development of a competitive ELISA for the detection of pecan (*Carya illinoensis* (Wangenh.) K. Koch) traces in food*. *Food analytical methods*, 2010. **3**(4): p. 375-381.
36. Koch, G.G., *Intraclass correlation coefficient*. *Encyclopedia of statistical sciences*, 1982: p. 213 - 217.
37. Urusov, A.E., *et al.*, *Immunochromatographic assay for the detection of ochratoxin A*. *Journal of Analytical Chemistry*, 2011. **66**(8): p. 770.
38. Pollet, J., *et al.*, *Fiber optic SPR biosensing of DNA hybridization and DNA-protein interactions*. *Biosensors and Bioelectronics*, 2009. **25**(4): p. 864-869.

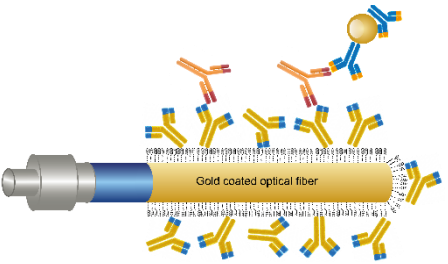
Chapter 4

Fiber optic-SPR platform for fast and sensitive infliximab detection in serum of inflammatory bowel disease patients

The work presented in this chapter is adapted from:



**BIOSENSORS
BIOELECTRONICS**



Gold coated optical fiber

Lu J., Van Stappen T., Spasic D., Delpont F., Vermeire S., Gils A. and Lammertyn J (2016).

Fiber optic-SPR platform for fast and sensitive infliximab detection in serum of inflammatory bowel disease patients.
Biosensors and Bioelectronics 79 173 – 179.

Contribution of Lu J. to the manuscript: Performing the experiments, analyzing data, writing and editing the manuscript.

Abstract

Infliximab (IFX) is a therapeutic monoclonal antibody used for treating patients with inflammatory bowel disease (IBD). In order to improve therapeutic outcomes it is recommended to monitor IFX trough concentrations. Although ELISA is currently widely used for this purpose, this method is not suitable for single patient testing. In this chapter we describe the development of a fast bioassay for determining IFX concentration in serum using an in-house developed fiber-optic surface plasmon resonance (FO-SPR) biosensor. Studies were first conducted to optimize covalent immobilization of the IFX-specific antibody on the sensor surface as well as to select an optimal blocking buffer for restraining the nonspecific binding. In order to reach clinically relevant sensitivity for detecting IFX in patients' serum, the SPR signal was amplified by employing gold nanoparticles functionalized with another set of IFX specific antibodies. Using the optimized sandwich bioassay, calibration curves were made with series of IFX concentrations spiked in buffer and 100-fold diluted serum, reaching the limit of detection of 0.3 and 2.2 ng/mL, respectively. The established bioassay was finally validated using five IFX treated IBD patients samples. Results from the FO-SPR platform were compared with an in-house developed, clinically validated ELISA resulting in excellent Pearson and intraclass correlation coefficient of 0.998 and 0.983, respectively. Furthermore, the assay time of the FO-SPR platform was significantly reduced compared to ELISA, demonstrating the potential of this platform to be used as a point-of-care diagnostic tool for improving therapeutic outcomes of IBD patients.

Keywords: fiber optics, surface plasmon resonance, biosensor, inflammatory bowel disease, infliximab

4.1 Introduction

Inflammatory bowel disease (IBD) is a chronic, relapsing inflammation of the gastrointestinal tract, which limits the life quality of patients affected by the disease. Although incurable, the symptoms can be controlled by medications such as steroids, aminosalicylates, immunomodulators and by using monoclonal antibodies, which target tumor necrosis factor alpha (TNF- α). Infliximab (IFX), a therapeutic monoclonal antibody specifically targeting TNF- α , has been proven as highly effective for inducing and maintaining remission in moderate-to-severe IBD patients. Although the therapy with biologics has revolutionized the management of IBD patients compared to conventional treatments, the average annual cost of IFX per patient is rather high, between \$24000 and \$26000 (approximately €18700 to €20000) [1]. Typically, an IFX infusion dose of 5 mg/kg is administered at week 0, 2 and 6, followed by maintenance therapy at 8 week intervals [2]. A pharmacokinetics profile of serum concentrations of IFX is illustrated in Figure 4.1. However, some patients, who initially respond to the induction therapy, lose the response over time, requiring therefore adjustment of dose and/or interval time. For improving the long-term therapeutic outcomes of IBD patients, it is recommended to monitor the IFX trough concentration, which is defined as the lowest drug concentration immediately before the next infusion is administered [3]. During maintenance therapy, clinical response is associated with IFX trough concentrations in the range from 0.5 to 10 $\mu\text{g/mL}$ in serum (Steenholdt *et al.* 2011). The most commonly used detection method is the enzyme linked immunosorbent assay (ELISA). Although a faster ELISA test is already available on the market (apDia, Turnhout, Belgium), to replace previous ELISA tests taking 1.5 days [4, 5], time to obtain results still requires at least 2 hours and can only take place in well-equipped central laboratories, which hampers immediate dose adaption. Therefore, a faster detection system is highly desired as a point-of-care (POC) diagnostic tool that can replace ELISA without reduction in sensitivity or specificity [6].

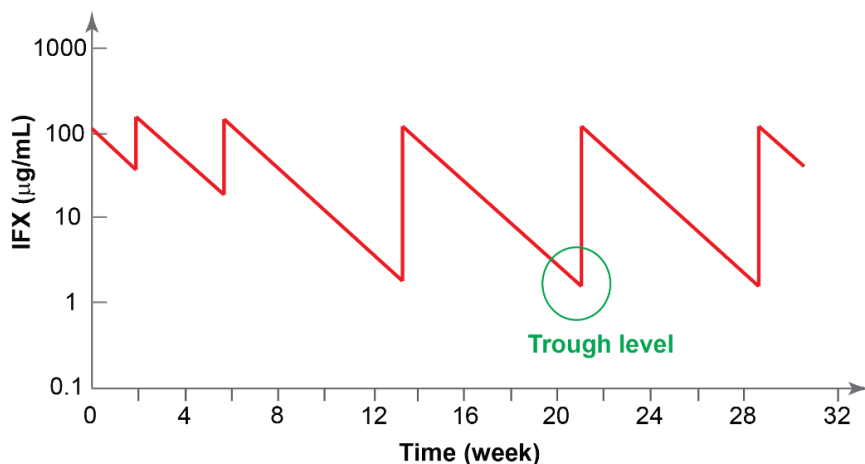


Figure 4.1 Pharmacokinetics profile of serum concentrations of IFX. The circle marks an example of the trough level.

Over the last three decades, optical biosensors based on surface plasmon resonance (SPR) have been increasingly employed in a variety of applications including food safety, clinical diagnostics and environmental monitoring [8-10]. SPR biosensors are optical sensors exploiting electromagnetic waves known as surface plasmon waves to measure local refractive index changes due to interactions between analytes in solution and biomolecules immobilized on the sensor surface. The most commonly used SPR biosensors, including commercially available Biacore instruments, exploit prisms coated with a thin gold layer using the Kretschmann configuration [11]. Although prism-based SPR biosensors are sensitive, reliable and accurate, they are usually bulky and expensive and therefore are not suitable for POC diagnostics which have been highly demanded in recent years. Standard optical fibers have emerged over the years as excellent alternatives that can compete with the sensitivity and specificity of prism-based SPR sensors, while offering the advantage of low cost and small size greatly desired for developing a POC tool. One such platform, namely fiber optic surface plasmon resonance (FO-SPR), has been previously described by our group as a promising biosensor for protein- and DNA-based assays [10, 12-17]. The FO-SPR biosensor makes use of multimode optical fibers that facilitate SPR generation and enable implementation of bioassays. Moreover, the FO-SPR platform offers several advantages compared to many current standard

techniques, including real-time monitoring, fast response time and ease of operation. This, combined with proven high sensitivity and specificity in detecting both proteins and DNA molecules, reveals the vast potential of the FO-SPR platform in developing clinical diagnostic tool for applications such as monitoring IFX trough concentrations in IBD patients.

In this chapter, we present the development of a fast and sensitive FO-SPR-based immunoassay for determining IFX concentrations in serum samples from IBD patients. First, selection of buffers and range of antibody concentrations was studied for immobilizing in-house developed IFX specific antibodies on the sensor surface. Moreover, a blocking buffer was chosen to provide a maximal signal-to-noise ratio for IFX detection in serum. In order to reach clinically relevant sensitivity for detecting IFX in patients' serum, the SPR signal was amplified by employing gold nanoparticles (AuNPs) functionalized with another set of in-house developed IFX specific antibodies. Calibration curves were made with IFX spiked to buffer, 100-fold and 200-fold diluted serum. Finally, the performance of the developed FO-SPR bioassay was evaluated using five serum samples from IFX treated IBD patients and results were compared using an IFX ELISA [18]. The obtained results combined with other intrinsic features of the FO-SPR platform, such as real-time monitoring, fast response time and ease of operation, demonstrate its huge potential for deployment as a POC diagnostic tool in determining biological drugs in patients' sera.

4.2 Materials and methods

4.2.1 Buffers and reagents

All buffer reagents were obtained from Sigma-Aldrich (Bornem, Belgium), unless stated otherwise. All solutions were prepared with deionized water purified by a Milli-Q Plus system (Millipore, Marlborough, MA, USA). Acetone, sulfuric acid (97% H₂SO₄) and acetic acid were purchased from Chemlab (Zedelgem, Belgium). Tween 20 was provided by AppliChem GmbH (Darmstadt, Germany). Carboxylic acid-SAM formation reagent, biotin-SAM formation reagent and amine coupling kit were produced by Dojindo Laboratories (Kumamoto, Japan). 1-ethyl-3-[3-dimethylaminopropyl] carbodiimide (EDC) and N-hydroxysuccinimide

(NHS) were obtained from Thermo Fisher Scientific (Erembodegem, Belgium). *o*-Phenylenediamine was purchased from Acros Organics (Geel, Belgium). AuNPs EMGC20 with the diameter of 20 nm were provided by BBI Solutions (Cardiff, UK). Information on the diameter and coefficient of variation for each batch of the AuNPs was provided by the manufacturer. In this chapter, the average size of the AuNPs was 19.7 nm with 8% of coefficient of variation. Streptavidin and bovin serum albumin (BSA) were supplied by Sigma-Aldrich (Bornem, Belgium). Infliximab (Remicade®) was obtained from Janssen Biologics B.V. (Leiden, the Netherlands) and adalimumab (Humira®) was purchased from Abbvie (North Chicago, IL, USA). Anti-IFX monoclonal antibodies MA-IFX20G2, MA-IFX3D5 and MA-IFX6B7 were generated in the Laboratory of Therapeutic and Diagnostic Antibodies (KU Leuven, Belgium), as previously described [18, 20]. Pooled serum, obtained from 30 healthy volunteers and de-identified serum samples from five IFX treated IBD patients, were taken in the framework of the VLECC study (B322201213950/S53684) after obtaining informed consent. In this chapter, serum refers to pooled serum from healthy volunteers and serum sample refers to IFX treated patient serum. High binding 96-well plates were provided by Costari (Corning Inc., Corning, NY, USA). Phosphate buffer saline (PBS), 2-(*N*-morpholino)ethanesulfonic acid (MES) and sodium acetate buffers were 10 mM at pH 7.4, 50 mM at pH 6.0 and 10 mM at pH 4.5, pH 5.0 and pH 5.5, respectively unless otherwise specified.

4.2.2 Methods

4.2.2.1 FO-SPR platform and preparation of fiber probes

A detailed description of the FO-SPR biosensor platform can be found in Section 4.4.1 and our previous publications [16, 19].

4.2.2.2 Surface functionalization of the FO probes with antibodies

Gold coated optical fibers (FO probes) were functionalized with a carboxyl self-assembling monolayer (SAM) via overnight treatment at 4 °C in a 1 mM mixed solution of ethanol/carboxylic acid-SAM formation reagent (volume ratio of 9:1). FO probes were washed with ethanol after the overnight treatment and stored in MES buffer at 4 °C until use. SAM functionalized FO

probes were immersed in 0.4 M EDC/0.1 M NHS mixture dissolved in MES buffer for 15 minutes to activate carboxylic groups of the SAM. Afterwards, the IFX specific monoclonal antibodies were immobilized on the FO surface for 30 minutes by covalent binding to the activated carboxylic groups. The monoclonal antibody, MA-IFX20G2, was immobilized on the FO probes as capture antibody. The FO probes were immersed twice in regeneration buffer (50 mM NaOH/1 M NaCl) for 30 seconds in order to remove antibodies that were not covalently bound to the surface. This was followed by immersion in blocking buffer (50 mM ethanolamine in PBS) for 8 minutes to deactivate unreacted carboxylic groups. An example of the typical FO-SPR sensorgram representing all the steps from this surface chemistry protocol for covalent immobilization of antibodies is illustrated in Figure 4.2. Measurements in buffer were executed before and after the antibody binding to stabilize the surface, and to wash off any antibodies that were nonspecifically bound to the surface, respectively. FO probes prepared as described were further used for detecting IFX spiked in buffer and serum (see Section 4.2.2.4) as well as for detecting IFX in patient serum samples (see Section 4.2.2.5).

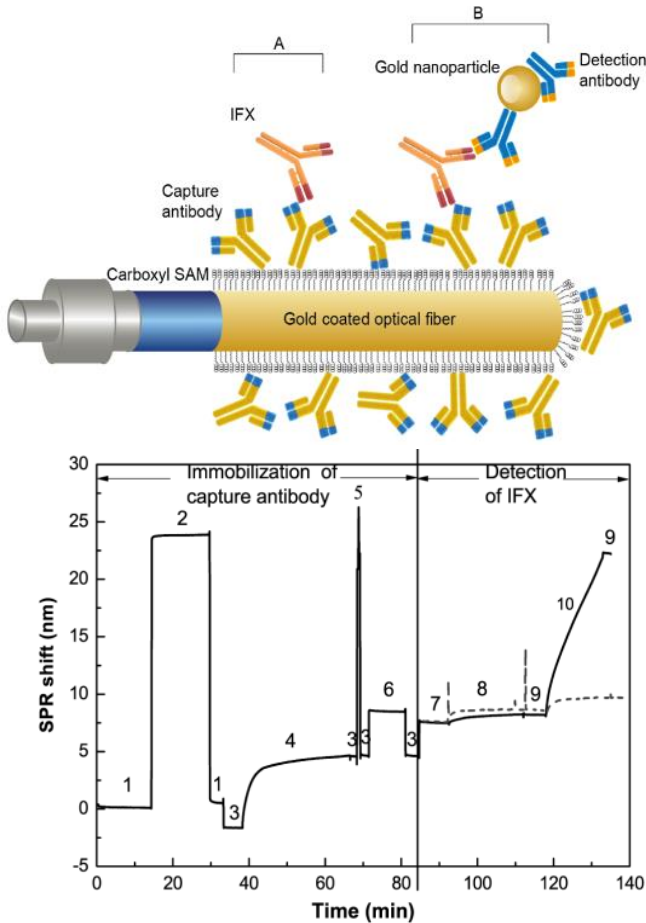


Figure 4.2 Schematic overview of the sandwich bioassay. Left: A schematic representation of the EDC/NHS chemistry-based sandwich bioassay on FO probe surface. Carboxyl SAM was first formed on the surface of a gold coated FO. Capture antibodies were covalently immobilized on the surface through EDC/NHS activated carboxyl groups. IFX molecules were bound to the capture antibodies and the signal was enhanced by AuNPs functionalized with detection antibodies. A) label-free; B) sandwich configuration. Right: Typical FO-SPR sensorgram representing all the steps of EDC/NHS protocol for covalent immobilization of antibodies and IFX detection using sandwich bioassay approach. The dashed line on the detection part represents the detection of 10 $\mu\text{g/mL}$ of IFX using signal amplification with 20 $\mu\text{g/mL}$ of MA-IFX6B7 without AuNPs. (1) MES buffer; (2) EDC/NHS; (3) Sodium acetate buffer pH 5.5; (4) Capture antibody; (5) Regeneration buffer: 50 mM NaOH/1 M NaCl; (6) Blocking buffer: 50 mM ethanolamine in PBS; (7) PBS with 0.01% of Tween 20; (8) IFX; (9) PBS with 0.5% of BSA; (10) AuNPs.

4.2.2.3 Surface functionalization of AuNPs with antibodies

The detection antibodies (MA-IFX3D5 or MA-IFX6B7) were conjugated to AuNPs via physical adsorption. The protocol was based on a previously published paper [20] with several modifications as described here. The pH of the AuNPs was pre-adjusted at pH 9.2 using 0.2 M of sodium carbonate. In a protein low-bind tube, antibodies were added to 800 μL of AuNPs (7×10^{11} particles/mL) to reach a final concentration of 5 $\mu\text{g/mL}$, and incubated on a rotator at room temperature for 20 minutes. Then, 560 μL of BSA (0.5% w/v) was added to stabilize the NPs. After an hour of rotation at room temperature, the NP solution was centrifuged at 7000 rpm and 20 $^{\circ}\text{C}$ for 30 minutes. After discarding the supernatant, containing unbound antibodies, NPs were finally re-suspended in PBS with 0.5% of BSA. In order to ensure reproducibility, the concentration of NPs was controlled to be the same as pre-functionalized NPs, by measuring the optical density (OD) of the NPs using a spectrometer (SpectraMax M2e, Molecular Devices, CA, USA). The OD of purchased AuNPs was 1, corresponding to the concentration of 7×10^{11} particles per mL. After functionalization and re-suspension in the buffer, AuNPs were adjusted to remain the same OD. In each assay, 150 μL of functionalized AuNPs were used. The prepared AuNPs were stored at 4 $^{\circ}\text{C}$ until use.

4.2.2.4 Establishing FO-SPR assay for IFX detection in buffer and serum

FO probes, functionalized with the IFX-specific capture antibody, were used for detecting IFX either directly or through a sandwich bioassay (Figure 4.1). Direct detection of IFX was performed with 10 $\mu\text{g/mL}$ and 1 $\mu\text{g/mL}$ of IFX diluted in PBS with 0.01% Tween 20 for 20 minutes. The sandwich bioassay was established by using AuNPs pre-functionalized with MA-IFX3D5 or MA-IFX6B7 (here referred to as detection antibodies) in order to achieve signal amplification. The sandwich bioassay was performed in two different sample matrices: (i) IFX detection in buffer (PBS with 0.01% of Tween 20 spiked with IFX concentration series from 0 to 100 ng/mL: 0, 2.5, 5, 10, 25, 50, 75 and 100 ng/mL) and (ii) IFX detection in serum (100-fold and 200-fold diluted serum spiked with IFX concentration series from 0 to 75 ng/mL: 0, 2.5, 5, 10, 20, 25, 40, 50, 75 ng/mL). FO probes were functionalized with the capture antibodies as described in Section 4.2.2.2 and were immersed in IFX

dilution for 15 minutes, followed by 20 minutes of signal amplification using functionalized AuNPs. The surface of FO probes was treated with regeneration buffer (two times 30 seconds) in between each IFX concentration in order to wash off the bound IFX and AuNPs. The serum was diluted with PBS containing 0.01% of Tween 20. An example of the typical FO-SPR sensorgram representing all the steps of IFX detection through the sandwich bioassay is illustrated in Figure 4.1, where significant increase in signal is shown with signal amplification by AuNPs. All SPR measurements were conducted at room temperature.

4.2.2.5 IFX quantification in IFX treated patients' sera using FO-SPR

For detecting IFX in infliximab treated patients' sera using FO-SPR, FO probes were functionalized with capture antibodies as described in Section 4.2.2.2 and the sandwich bioassay was similar to Section 4.2.2.4. Here, two concentrations of IFX spiked in 200-fold diluted serum (0 and 5 ng/mL) were first measured as a reference. Using the same FO probe, after removing bound IFX and AuNPs with the regeneration buffer, the IFX concentration was measured in patient serum (diluted 200- or 500-fold) followed by a signal amplification step with AuNPs. Five IFX treated patients' sera were tested and four repetitions were performed for each sample. For these experiments, MA-IFX3D5 was used as the detection antibody conjugated to AuNPs. IFX treated patients' sera were diluted in PBS with 0.01% of Tween 20.

4.2.2.6 IFX quantification in IFX treated patients' sera using ELISA

IFX in serum samples from IFX treated IBD patients was quantified using ELISA as previously described [18]. Taking 150-fold diluted serum into account, the assay cut-off and lower limit of quantification are 0.2 $\mu\text{g/mL}$ and 0.5 $\mu\text{g/mL}$ of IFX, respectively. Each sample was measured three times at different days.

4.3 Results and discussion

4.3.1 Immobilization of IFX-specific antibody on the surface of FO probes

FO probes, functionalized with the IFX-specific capture antibody (MA-IFX20G2), were used in this chapter for detecting IFX either directly at higher concentrations (10 and 1 $\mu\text{g}/\text{mL}$) or through a sandwich bioassay for detecting IFX at lower concentrations (between 2.5 ng/mL and 1 $\mu\text{g}/\text{mL}$). The sandwich bioassay was established by using AuNPs pre-functionalized with detection antibodies (MA-IFX3D5 or MA-IFX6B7) in order to achieve signal amplification (Figure 4.2). These antibodies have been selected based on previously obtained results [18, 21].

In order to develop a highly specific and sensitive FO-SPR based assay for IFX detection, experiments were first carried out to establish protocols for immobilization of IFX-specific capture antibody (MA-IFX20G2) on the sensor surface. As shown previously, the efficiency of antibody immobilization depends on several parameters, such as buffer pH, antibody concentration, ionic strength and reaction time. Thus, increased immobilization efficiency can be achieved in a buffer with low ionic strength and pH close to but smaller than the isoelectric point (pI) of the antibody [22, 23]. Because the pI of the capture antibody, MA-IFX20G2, used in this study was unknown, buffers with low ionic strength (10 mM sodium acetate buffer) and with pH ranging from pH 4.5 to pH 5.5 were tested for covalent immobilization of this antibody at three different concentrations (10, 20 and 40 $\mu\text{g}/\text{mL}$).

The obtained results were analyzed with a two-way Anova statistical test and subsequently Bonferroni correction to determine statistically significant differences between immobilization conditions. The maximum immobilization was achieved when using sodium acetate pH 5.5 for all three tested antibody concentrations (Figure 4.3 A). This can be due to the pI of the capture antibody being slightly higher than pH 5.5, resulting in positively charged antibodies and negatively charged carboxyl groups of SAM at pH 5.5. Moreover, under this condition, the detection of 10 $\mu\text{g}/\text{mL}$ IFX also resulted in the highest SPR shift (Figure 4.3 B). Based on the experimentally obtained SPR shifts and the statistical analysis, 20 $\mu\text{g}/\text{mL}$ of the capture antibody was

immobilized on the FO surface in sodium acetate buffer pH 5.5 in all further experiments.

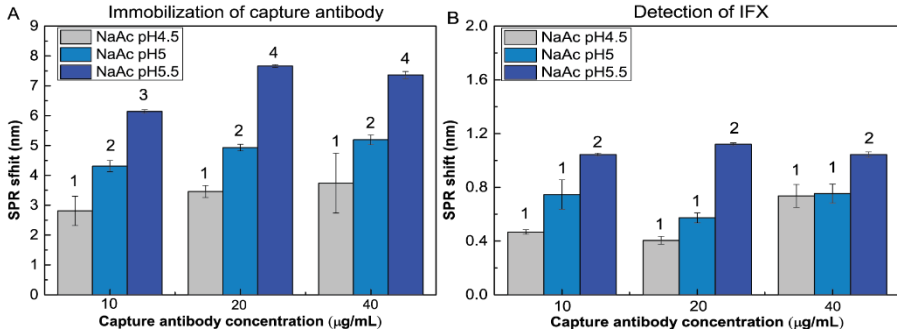


Figure 4.3 Results of immobilization. Summary of immobilization shifts for 10, 20 and 40 µg/mL of the capture antibody diluted in buffer with three different pH values (A), and corresponding SPR shifts for detection of 10 µg/mL of IFX (B). Error bars represent standard deviation ($n = 3$). Threshold numbers (1, 2, 3 and 4) indicate statistically significant different groups from Bonferoni correction.

4.3.2 Controlling the nonspecific binding on the surface of FO probes

Controlling the nonspecific binding of target molecules and other sample components to the sensor surface is critical for the specificity of the assay. Therefore, series of experiments were carried out to test (i) nonspecific binding of target molecules to the sensor surface, (ii) nonspecific interaction of sample matrix components, such as serum, with the capture antibody on the sensor surface and (iii) nonspecific interaction between detection antibodies, immobilized on AuNPs, and capture receptors on the sensor surface. Moreover, the specificity of monoclonal antibodies, employed in this study, has been tested by using another anti-TNF monoclonal antibody, namely adalimumab (ADM).

In order to demonstrate that there is no interaction between IFX and the sensor surface itself, FO probes were immersed in IFX solution in the absence of capture antibodies. Thus, the sensor surface was prepared by activating carboxyl groups of the SAM layer and their subsequent deactivation using blocking buffer. Here, three different blocking buffers were tested, all capable of reacting with unoccupied carboxyl groups on the surface: 50 mM Tris in

PBS, 50 mM ethanolamine in PBS and the commercial blocking solution supplied by Dojindo Laboratories (Kumamoto, Japan). These experiments resulted in no detectable SPR shift (as shown in Section 4.4.2.1 Figure S4.2), irrespective of the type of blocking buffer used, which indicated that all three blocking buffers efficiently prevented undesired interaction between IFX and the sensor surface in the absence of IFX specific receptors.

Next, three blocking buffers were tested for their capacity to prevent the nonspecific binding of the components from the serum matrix. After immobilizing the capture antibody, FO probes were immersed in the blocking buffer, followed by immersion in 50-fold diluted serum or 50-fold diluted serum spiked with 10 $\mu\text{g/mL}$ of IFX. The biggest signal-to-noise ratio was obtained when using 50 mM ethanolamine in PBS (Figure 4.4). The observed differences between Tris and ethanolamine buffers might be due to smaller size of ethanolamine molecules, resulting in easier interaction with unoccupied carboxyl groups among immobilized capture antibodies without blocking the binding sites of the antibodies. However, it is difficult to speculate why the specific signal was lower when using commercial blocking solution since the composition of this commercial reagent is unknown. Finally, because ethanolamine buffer also resulted in the smallest variability over different experiments, this blocking buffer was selected for the further work described in this chapter.

Furthermore, the nonspecific binding between functionalized AuNPs and the capture antibodies on the sensor surface was tested in a sandwich assay in the absence of IFX (0 $\mu\text{g/mL}$). The experiment was performed using AuNPs functionalized with two different detection antibodies, MA-IFX3D5 and MA-IFX6B7. The nonspecific binding was negligible in the buffer (as seen in Figure S4.3), irrespective of the detection antibody used (0.05 ± 0.02 nm and 0.1 ± 0.04 nm for MA-IFX3D5-AuNPs and MA-IFX6B7-AuNPs, respectively) and was very limited in 100-fold diluted serum (0.8 ± 0.04 nm and 0.3 ± 0.2 nm from MA-IFX3D5-AuNPs and MA-IFX6B7-AuNPs respectively (data not shown)), thereby not interfering with detection of the lowest IFX concentration included in the assay (2.5 ng/mL). Therefore, both detection antibodies were utilized further in experiments.

As a final step in testing the specificity of the implemented bioassays, monoclonal antibodies were challenged against ADM, another anti-TNF biological. [24, 25]. Although all three monoclonal antibodies employed here

have been already described as IFX specific in other assays, experiments were performed on the FO-SPR platform as well to test whether the developed bioassay detects other anti-TNF biologicals. The nonspecific signal was first measured in the absence of a target, followed by FO probe surface regeneration and measurement of 75 ng/mL of ADM diluted in buffer or 100-fold diluted serum. In this experiment, MA-IFX3D5 was used as detection antibody conjugated to the AuNPs. The obtained results revealed no significant difference between the blank serum and the one spiked with 75 ng/mL of ADM (Section 4.4.2.3 Figure S4.4), demonstrating the specificity of selected monoclonal antibodies, as also previously shown in other assays [18, 21].

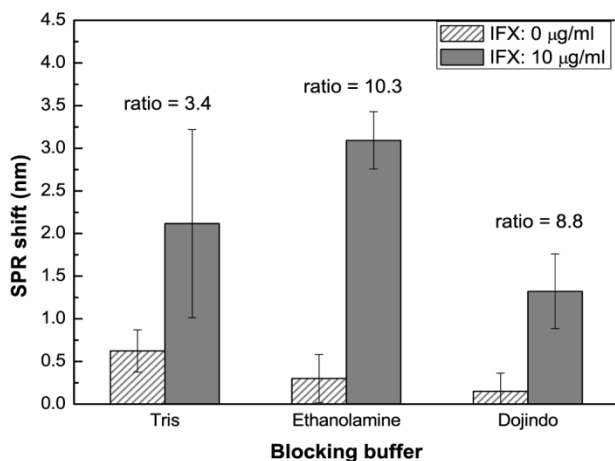


Figure 4.4 Summary of SPR shifts obtained from testing blocking buffers. Nonspecific binding test was performed in 50-fold diluted serum with functionalized FO probes in the absence of IFX. Specific signal was measured with 10 µg/mL of IFX spiked in the same serum dilution. Error bars represent standard deviations ($n = 2$).

4.3.3 Detecting IFX spiked in buffer and serum using FO-SPR platform

Trough levels of IFX in patients' serum are commonly in the range of 0.5 to 10 µg/mL [26]. In order to avoid matrix effect, patients' samples are usually diluted at least 100-fold before testing, resulting in an IFX range of 5 to 100 ng/mL in the diluted serum samples. Because an SPR shift of 1 nm was obtained when measuring 1 µg/mL of IFX diluted in buffer, the sensitivity of

the direct immunoassay was considered as insufficient for detecting clinically relevant IFX concentrations. Moreover, building a sandwich assay with the addition of IFX-specific detection antibody only slightly improved SPR shift for additional 1 nm when using 10 $\mu\text{g/mL}$ of IFX and 20 $\mu\text{g/mL}$ of detection antibody (MA-IFX6B7) (Figure 4.1 dashed line). Therefore, AuNPs were utilized for SPR signal enhancement, as similar successful applications have been previously shown by us and others [10, 27-30].

As expected, SPR signal enhancement was achieved by using AuNPs functionalized with either MA-IFX3D5 or MA-IFX6B7 (Section 4.4.2.2 Figure S4.3). Using such established sandwich bioassay, a series of IFX concentrations, ranging from 0 to 100 ng/mL , were measured in PBS buffer with 0.01% of Tween 20. Measurements were conducted using the same FO probe for the entire range of IFX concentrations, which was attainable due to the removal of AuNPs and IFX in between subsequent steps using 50 mM NaOH/1 M NaCl as the regeneration buffer (Section 4.4.2.2 Figure S4.3). The obtained average SPR shifts ($n = 2$) were plotted as a function of IFX concentrations to generate two calibration curves, one for each of the detection antibodies (Figure 4.5A). Calibration curves were fitted throughout the entire measured concentration range of IFX with nonlinear regression, one-site binding fitting, using Origin 8 (OriginLab, Northampton, US). Equation 4.1, from the one-site binding fitting, was used to calculate the LOD of the established assays:

$$y = x \times A / (x + B) \quad (4.1)$$

where x represents the IFX concentration, y represents SPR shift, and A and B represent fitting parameters. To calculate the LOD, the following equation can be used

$$LOD = \frac{(y(0) + 3\sigma)B}{A - (y(0) + 3\sigma)} \quad (4.2)$$

where $y(0)$ is the average SPR shift of nonspecific binding, σ standard deviation of nonspecific binding ($n = 2$ for buffer and 6 for 100-fold diluted serum). Based on Equation 4.2, the calculated LODs were 0.25 ng/mL (1.7

pM) and 0.51 ng/mL (3.5 pM) in buffer for MA-IFX3D5 and MA-IFX6B7, respectively.

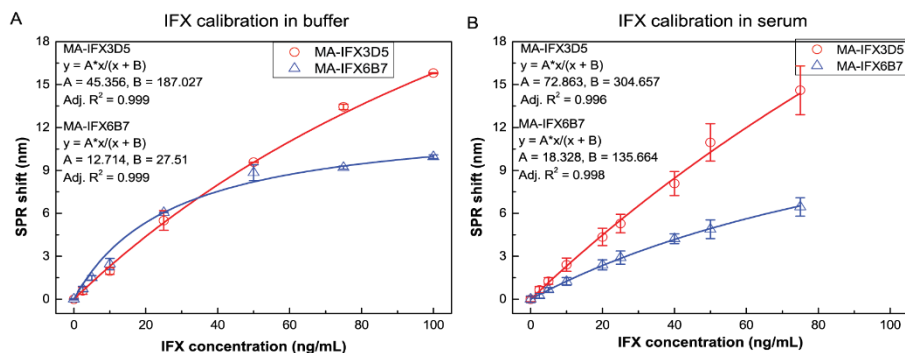


Figure 4.5 Summary of calibration curves. Calibration curves obtained from series of IFX concentrations in buffer (A) and 100-fold diluted serum (B) when using AuNPs conjugated to MA-IFX3D5 and MA-IFX6B7 as labels for signal enhancement. A nonlinear regression (one-site binding) was fitted for both calibration curves. Fitting parameters are indicated on the left of the graph. Error bars represent standard deviations ($n = 2$ for buffer and 6 for serum).

The final assays were performed in 100-fold diluted serum spiked with IFX ranging from 0 to 75 ng/mL. The measurements were done similarly to the experiments performed in buffer with one FO probe used for the entire range of IFX concentrations and implemented regeneration steps in between each concentration. The obtained average SPR shifts ($n = 6$) were plotted as a function of the IFX concentrations spiked in serum (Figure 4.5B). The calculated LODs were 2.2 ng/mL (15 pM) and 5.3 ng/mL (37 pM) in 100-fold diluted serum, which correspond to 0.22 μ g/mL and 0.53 μ g/mL in whole serum for MA-IFX3D5 and MA-IFX6B7, respectively. To evaluate if the concentration of an unknown sample can be accurately determined by interpolating SPR signal into a calibration curve, analysis was carried out with the calibration curve obtained with MA-IFX3D5-AuNPs, as explained in Section 4.4.2.4 Figure S4.5. The difference between the actual and determined IFX concentrations from interpolation in calibration curve was less than 5%.

4.3.4 Validation of established FO-SPR bioassay with sera from IFX treated patients

The developed FO-SPR bioassay for IFX detection was finally evaluated by measuring IFX concentrations in sera of five IFX treated patients. All five serum samples (referred to as S1, S2, S3, S4 and S5) were first diluted 200-fold and then measured with the FO-SPR platform. AuNPs conjugated with MA-IFX3D5 were used for signal amplification in this assay, as this antibody resulted in better LOD compared to MA-IFX6B7 (see Figure 4.5). Four measurements were carried out for each serum sample with two independently prepared batches of fibers and AuNPs, for estimating the inter assay variation. Subsequently, IFX concentrations were calculated from the calibration curve made in 200-fold diluted serum (Section 4.4.2.5 Figure S4.6). Independently, the same serum samples were also tested with the in-house developed IFX ELISA [18]. The obtained IFX concentrations from both assays are summarized in Table 4.1.

From all five tested serum samples from IBD patients, it appeared that the obtained SPR shifts for S2 were indistinguishable from those obtained from 0 ng/ml of IFX. A similar result was confirmed using ELISA. After de-blinding the samples, sample S2 appeared to be obtained from a patient naïve to IFX therapy, corroborating our findings. Because the concentration of IFX in S3 appeared to be out of the dynamic range of the used FO-SPR calibration curve when diluting samples 200-fold, S3 was further diluted to 500-fold. Nevertheless, the interpolation for this sample was obtained from the same calibration curve made in the 200-fold diluted serum, as this had no influence on the final concentration determination (Section 4.4.2.6 Figure S4.7). The IFX concentrations from five serum samples were determined based on 200-fold diluted serum calibration curve as shown in Table 1. The coefficient of variation of the SPR shifts from four measurements of individual samples was less than 10%. Finally, the IFX concentrations measured with the newly developed FO-SPR assay and validated ELISA test had an excellent correlation (Figure 4.6), as demonstrated with a Pearson correlation of 0.998 and an intraclass correlation coefficient (ICC) of 0.983.

Table 4.1 Determined concentrations of 5 serum samples from IBD patients using both ELISA and FO-SPR platform. Errors represent standard error of the mean.

| Clinical sample | S1 ($\mu\text{g/mL}$) | S2 ($\mu\text{g/mL}$) | S3 ($\mu\text{g/mL}$) | S4 ($\mu\text{g/mL}$) | S5 ($\mu\text{g/mL}$) |
|-------------------|----------------------------|----------------------------|----------------------------|----------------------------|----------------------------|
| ELISA (n = 3) | 3.4 ± 0.1 | < 0.2 | 19.2 ± 1.5 | 6.4 ± 0.6 | 4.0 ± 0.5 |
| FO-SPR (n = 4) | 3.8 ± 0.1 | < 0.2 | 23.1 ± 1.7 | 6.2 ± 0.3 | 4.1 ± 0.2 |

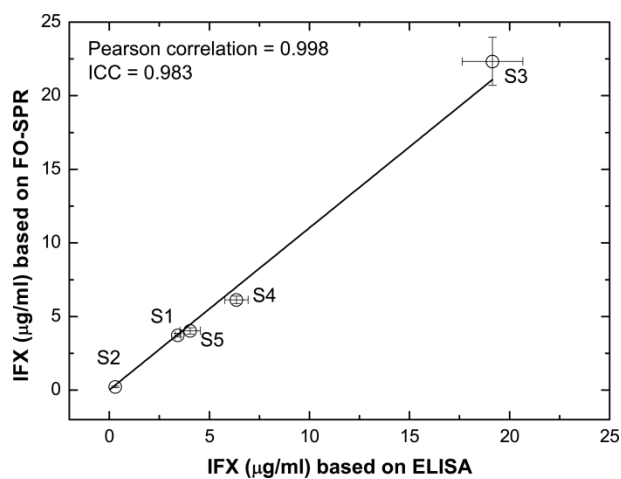


Figure 4.6 Evaluation of the FO-SPR assay with serum samples from IBD patients. The determined IFX concentrations from FO-SPR platform were compared to IFX concentrations measured with the in-house developed ELISA. The Pearson correlation and ICC were determined to be 0.998 and 0.983, respectively. Error bars represent standard errors (n= 4 for FO-SPR and 3 for ELISA).

4.4 Conclusions

In this chapter we described the development of a fast and accurate bioassay for measuring IFX concentration in serum using the FO-SPR biosensor. To achieve this, selection of buffers and range of antibody concentrations was first studied for immobilizing in-house developed IFX specific antibodies on the sensor surface. Among tested conditions, 10 mM sodium acetate buffer with the pH value of 5.5 resulted in the best immobilization of capture antibody, particularly for 20 $\mu\text{g/mL}$ of antibody concentration. Next, a series

of experiments were performed for controlling the nonspecific binding of the target molecules, bioassay components and sample matrix to the sensor surface. These experiments demonstrated that IFX binds specifically to the sensor only in the presence of capture antibodies (MA-IFX20G2) as well as that all three antibodies used in this research have high specificity towards IFX and not towards other anti-TNF biologics. Moreover, among three tested blocking solutions, ethanolamine buffer appeared as the most suitable for detecting IFX in serum due to the maximal obtained signal-to-noise ratio.

Because a direct assay was insufficient for detecting low concentrations of IFX (below 1 $\mu\text{g/mL}$), the SPR signal was amplified using AuNPs conjugated to two different detection antibodies (MA-IFX3D5 and MA-IFX6B7). Using the established sandwich immunoassay, calibration curves were made in buffer and 100-fold diluted serum, with the best obtained LOD of 0.3 ng/ml (1.7 pM) and 2.2 ng/ml (15 pM) respectively, when using MA-IFX3D5 as detection antibody. Final evaluation of the developed FO-SPR bioassay was performed using five serum samples from IFX treated IBD patients, analyzed using ELISA and FO-SPR. These results revealed excellent agreement between the FO-SPR bioassay and the clinically validated ELISA, showing excellent correlation (Pearson correlation of 0.998 and ICC of 0.983) and inter-coefficient of variation being less than 10%.

Although the total time of the presented assay is 2.5 hours (including immobilization of the capture antibody), it is envisioned that fiber probes will be pre-functionalized for future use in a hospital together with kinetic analysis, which will reduce the assay time to less than 20 minutes. Therefore, individual tests on patient samples at point-of-care become feasible. In addition, the FO-SPR biosensor is fully automated and can be run as a single measurement or with 4 parallel FO sensors. Thereby, the developed bioassay combined with characteristics of the FO-SPR platform demonstrates its potential as a POC diagnostic tool that can be used for determining biological drugs in serum samples from patients.

4.4 Supplementary information

4.4.1 FO-SPR platform and preparation of fiber probes

A picture of the in-house developed FO-SPR platform is illustrated in Figure S4.1. Light from a tungsten halogen source (HL-2000, Ocean optics, Dunedin, USA) is delivered to the fiber probe by a bifurcated fiber (Ocean optics, Dunedin, USA) and the reflected SPR signal is collected by the same bifurcated fiber to a spectrometer (USB4000, Ocean Optics, Dunedin, USA). Two fiber probes are integrated onto a computer-controlled robot system using the ColiDrive software (Colinbus, Belgium), which enables fully-automated control of their movements. Data is recorded by a LabVIEW (National Instruments, Zaventem, Belgium) program.

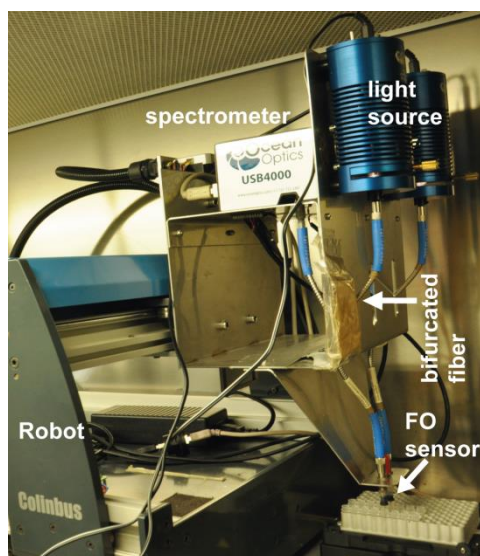


Figure S4.1 The FO-SPR platform.

A multimode optical fiber (TEQS, Thorlabs, Munich, Germany) with a total length of 4.3 cm and a core diameter of 400 μm was used in the experiments. Approximately 0.6 cm of the jacket was removed from one end of the fiber and the cladding was removed with an acetone soaked dust free tissue. The sensing zone was cleaned with ethanol before sputtering with a 50

nm gold layer using a sputter coater (Quorum Q150T ES, Quorum Technologies, East Sussex, UK).

4.4.2 Results

4.4.2.1 Selection of blocking buffer

To ensure the detected signal from IFX is due to the specific interaction with the capture antibodies immobilized on the sensor surface, rather than with the surface itself, FO probes were immersed in IFX solution directly after activation of carboxyl groups and their deactivation using blocking buffer without the presence of the capture antibodies. Three different blocking buffers were tested: 50 mM Tris in PBS, 50 mM ethanolamine in PBS and the commercial blocking solution supplied by Dojindo Laboratories (Kumamoto, Japan) as part of their amine coupling kit, which are all capable of reacting with unoccupied carboxyl groups on the surface. As illustrated in Figure S4.2, there was no detectable SPR signal from 10 $\mu\text{g/mL}$ of IFX. This test demonstrated that all three buffers can efficiently prevent undesired nonspecific binding between IFX and FO surface.

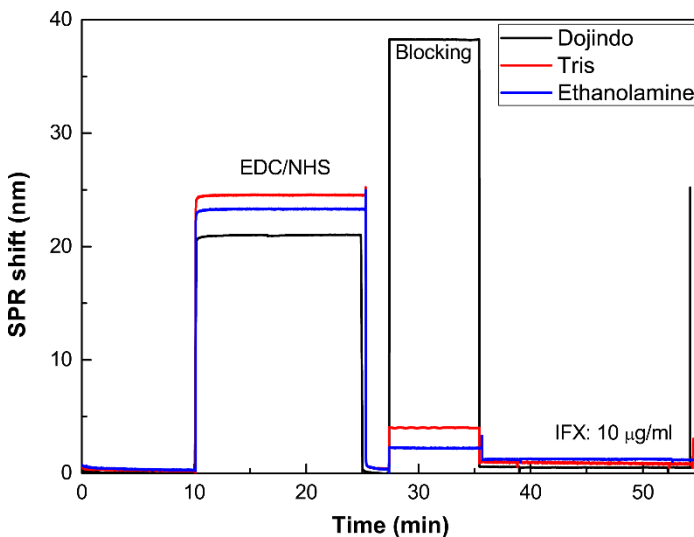


Figure S4.2 SPR sensorgrams of nonspecific binding tests between IFX and FO surface in the absence of capture antibodies. Differences in SPR shifts from different blocking buffers were due to the difference in refractive index.

4.4.2.2 FO-SPR signal amplification with AuNPs

In order to achieve detection of clinically relevant IFX concentrations, SPR signal was amplified by using AuNPs functionalized with IFX specific antibodies, being MA-IFX6B7 or MA-IFX3D5. SPR sensorgrams recorded for series of IFX concentrations (0 – 100 ng/ml) spiked in buffer before and after signal amplification are illustrated in Figure S4.3. As it can be seen from this figure, IFX concentration as low as 2.5 ng/ml becomes feasible to detect when including a signal amplification step with AuNPs. The entire range of IFX concentrations was measured using the same FO probe, which was attainable due to the removal of AuNPs and IFX in between subsequent steps with the regeneration buffer (50 mM NaOH, 1 M NaCl).

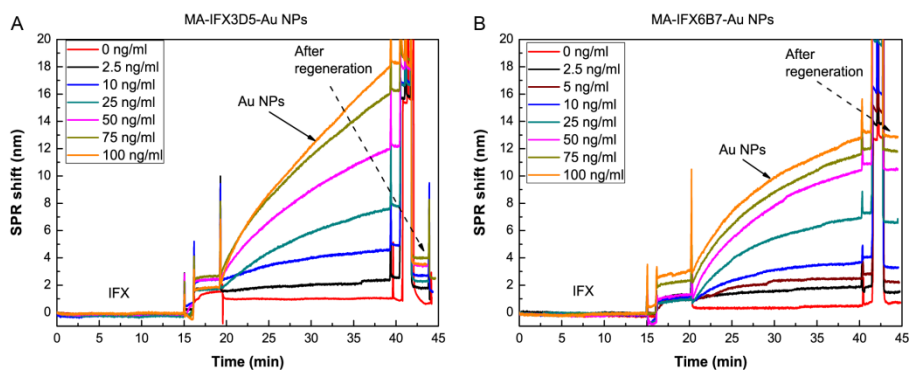


Figure S4.3 SPR sensorgrams for the series of IFX concentrations (0 – 100 ng/ml) spiked in buffer. Signal amplification was achieved by using AuNPs functionalized with detection antibody MA-IFX3D5 (A) and MA-IFX6B7 (B).

4.4.2.3 Controlling nonspecific binding

In order to test the specificity of the developed IFX assay, FO probes functionalized with IFX specific antibodies were used to detect another anti-TNF monoclonal antibody, adalimumab (ADM). Similar to the sandwich assay described in Section 4.2.2.4, functionalized FO probes were immersed in buffer (PBS with 0.01% of Tween 20) or 100-fold diluted serum in the absence of a target, followed by immersion in solution with functionalized AuNPs. After regeneration of the surface, FO probes were immersed in 75 ng/mL of ADM spiked either in buffer or 100-fold diluted serum. The average

SPR shifts obtained from 3 experiments are summarized in Figure S4.4, indicating that insignificant shifts less than 1 nm are obtained in blank buffer or serum as well as in the presence of ADM. Therefore, it can be concluded that ADM did not interact with the capture (MA-IFX20G2) or the detection (MA-IFX3D5) antibody and that the obtained SPR shifts in the developed assays were only due to the specific interactions of these antibodies with their target, namely IFX (e.g. > 12 nm SPR shift was recorded for 75 ng/ml of IFX both in buffer and serum when using MA-IFX3D5 or MA-IFX6B7 as detection antibody, see Figure 4.5).

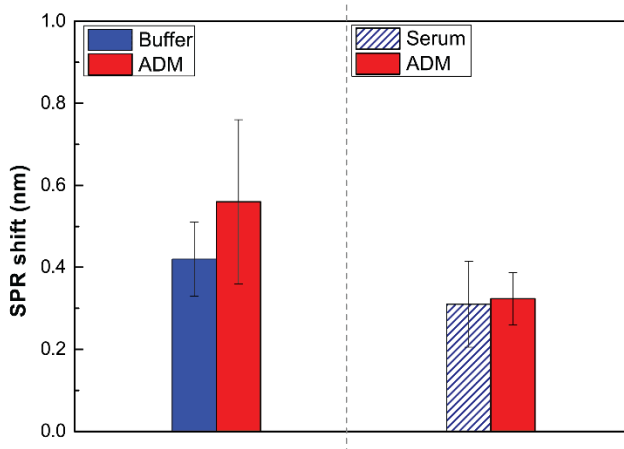


Figure S4.4 Nonspecific binding of ADM to FO probes functionalized with IFX specific antibodies. Error bars represent standard deviations ($n = 3$).

4.4.2.4 Evaluation of the fitting model

The calibration curves generated in buffer and 100-diluted serum were fitted with nonlinear regression, one-site binding model. In order to evaluate the selected fitting, two (out of six) performed measurements of six samples (being six IFX concentrations spiked in serum) were randomly selected for generating calibration curve. The calibration curve was then fitted using the selected model. SPR shifts from four other repetitions were interpolated into this calibration curve and their concentrations were determined using the Equation 4.1 mentioned in Section 4.3.3. The determined concentrations were then compared to the actual concentrations of those six samples and the obtained differences are presented as percentages in Figure S4.5. As it can be

seen from the figure, less than 5% of difference was observed between the actual concentrations of IFX spiked in samples and those determined based on the obtained calibration curve. These experiments have been performed with MA-IFX3D5 as detection antibody.

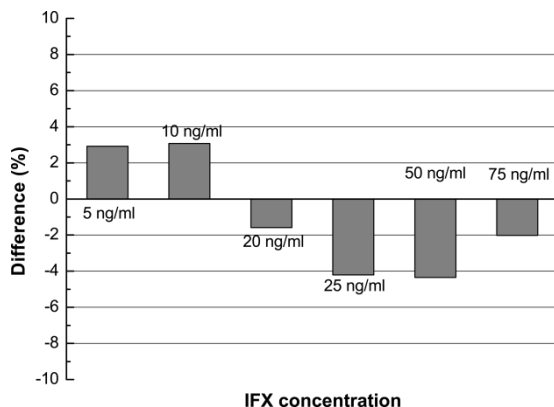


Figure S4.5 Results of evaluation of fitting model. Differences obtained between the determined concentrations and the actual concentrations of six IFX concentrations spiked in serum when using nonlinear regression for fitting the calibration curve.

4.4.2.5 Calibration curve in 200-fold diluted serum

For measuring IFX concentrations in five IFX treated patients' sera using FO-SPR, serum samples were diluted 200-fold. Therefore, calibration curve was generated with series of IFX concentration (0 – 75 ng/mL) spiked in 200-fold diluted serum, similarly as described in Section 4.3.3. Again, one FO probe was used for entire range of IFX concentrations due to the implemented regeneration steps in between each concentration. The calibration curve was made for this experiment using two batches of fibers and AuNPs that were prepared independently on two days. Two repetitions were performed using each batch and final results are indicated in Figure S4.6. The calibration curve was fitted with nonlinear regression and the LOD based on four measurements was 0.7 ng/mL (4.6 pM), corresponding to 0.3 μ g/mL (0.9 nM) in whole serum.

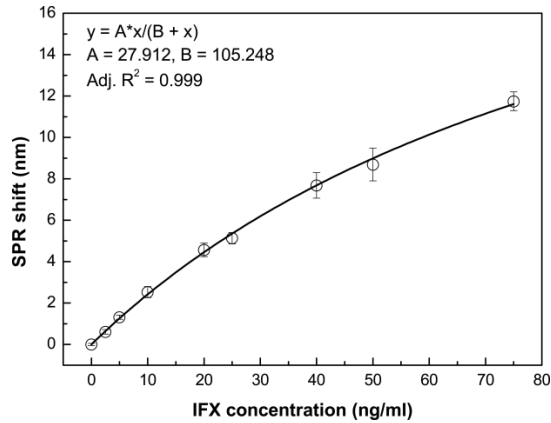


Figure S4.6 Calibration curve with IFX spiked in 200-fold diluted serum and AuNPs functionalized with detection antibody MA-IFX3D5. The represented errors are standard deviations ($n = 4$).

4.4.2.6 Evaluation of established FO-SPR assay with IBD patient samples

Due to the high IFX concentration in S3 sample, which was out of the dynamic range of the used FO-SPR calibration curve when diluting sample 200-fold, S3 was further diluted (500-fold) for the measurement. However, the same calibration curve, made with IFX spiked in 200-fold diluted serum, was used for interpolating IFX concentration of 500-fold diluted S3. To evaluate the influence of this, SPR shifts from other three clinical samples (S1, S4 and S5) were interpolated in calibration curve generated with IFX spiked in 100-fold diluted serum. The differences in determined concentrations from two calibration curves and ELISA can be neglected for all three clinical samples, as shown in Figure S4.7. Therefore, the interpolation of the 500-fold diluted S3 sample from the calibration curve made using 200-fold dilution of serum can be considered as adequate.

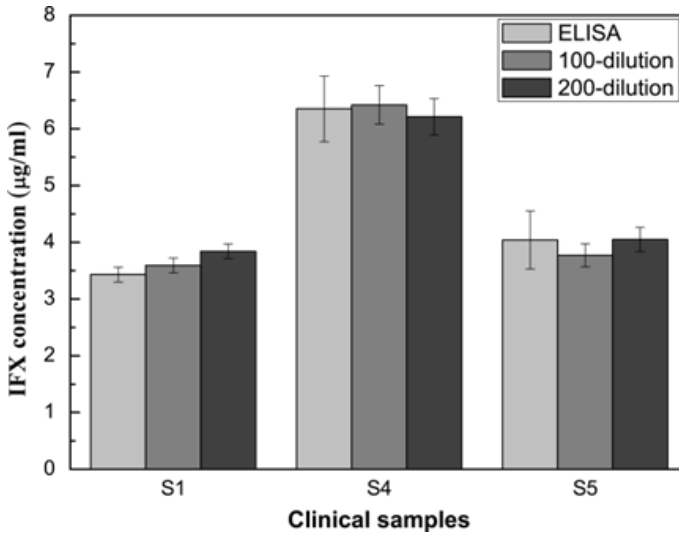


Figure S4.7 Comparison of IFX concentrations of three clinical samples (S1, S4 and S5) determined from FO-SPR calibration curves made with 100-fold and 200-fold diluted serum as well as those concentrations obtained from ELISA tests. The represented errors are standard errors ($n = 4$ for FO-SPR and 3 for ELISA).

4.5 References

1. Bonafede, M.M., *et al.*, *Cost per treated patient for etanercept, adalimumab, and infliximab across adult indications: a claims analysis*. *Advances in therapy*, 2012. **29**(3): p. 234-248.
2. Sandborn, W.J. and S.B. Hanauer, *Infliximab in the treatment of Crohn's disease: a user's guide for clinicians*. *The American journal of gastroenterology*, 2002. **97**(12): p. 2962-2972.
3. Vermeire, S. and A. Gils, *Value of drug level testing and antibody assays in optimising biological therapy*. *Frontline gastroenterology*, 2013. **4**(1): p. 41-43.
4. Ternant, D., *et al.*, *An enzyme-linked immunosorbent assay for therapeutic drug monitoring of infliximab*. *Therapeutic drug monitoring*, 2006. **28**(2): p. 169-174.
5. Vande Casteele, N., *et al.*, *Detection of infliximab levels and anti-infliximab antibodies: a comparison of three different assays*. *Alimentary pharmacology & therapeutics*, 2012. **36**(8): p. 765-771.
6. Van Stappen, T., *et al.*, *Point-of-care assays for rapid quantification of Infliximab*. in *UEG week*. 2015.
7. Situ, C., *et al.*, *Advances in surface plasmon resonance biosensor technology towards high-throughput, food-safety analysis*. *TrAC Trends in Analytical Chemistry*, 2010. **29**(11): p. 1305-1315.
8. Yanase, Y., *et al.*, *Application of SPR imaging sensor for detection of individual living cell reactions and clinical diagnosis of type I allergy*. *Allergy International*, 2013. **62**(2): p. 163-169.
9. Zhang, L. and M. Fang, *Nanomaterials in pollution trace detection and environmental improvement*. *Nano Today*, 2010. **5**(2): p. 128-142.
10. Pollet, J., *et al.*, *Fast and accurate peanut allergen detection with nanobead enhanced optical fiber SPR biosensor*. *Talanta*, 2011. **83**(5): p. 1436-1441.
11. Schasfoort, R.B. and A.J. Tudos, *Handbook of surface plasmon resonance*. 2008: Royal Society of Chemistry.
12. Delport, F., *et al.*, *Real-time monitoring of DNA hybridization and melting processes using a fiber optic sensor*. *Nanotechnology*, 2012. **23**(6): p. 065503.
13. Janssen, K., *et al.*, *Enabling fiber optic serotyping of pathogenic bacteria through improved anti-fouling functional surfaces*. *Nanotechnology*, 2012. **23**(23): p. 235503.

14. Knez, K., *et al.*, *Spherical nucleic acid enhanced FO-SPR DNA melting for detection of mutations in Legionella pneumophila*. *Analytical chemistry*, 2013. **85**(3): p. 1734-1742.
15. Knez, K., *et al.*, *Real-time ligation chain reaction for DNA quantification and identification on the FO-SPR*. *Biosensors and Bioelectronics*, 2014.
16. Pollet, J., *et al.*, *Fiber optic SPR biosensing of DNA hybridization and DNA-protein interactions*. *Biosensors and Bioelectronics*, 2009. **25**(4): p. 864-869.
17. Tran, D.T., *et al.*, *Nanocrystalline diamond impedimetric aptasensor for the label-free detection of human IgE*. *Biosensors and Bioelectronics*, 2011. **26**(6): p. 2987-2993.
18. Van Stappen, T., *et al.*, *Generation of a highly specific monoclonal anti-infliximab antibody for harmonization of TNF-coated infliximab assays*. *Therapeutic drug monitoring*, 2014.
19. Arghir, I., *et al.*, *Improved surface plasmon resonance biosensing using silanized optical fibers*. *Sensors and Actuators B: Chemical*, 2015.
20. Jans, H., *et al.*, *Dynamic light scattering as a powerful tool for gold nanoparticle bioconjugation and biomolecular binding studies*. *Analytical chemistry*, 2009. **81**(22): p. 9425-9432.
21. Van Stappen, T., *et al.*, *Transferability of antibody pairs from ELISA to fiber optic-surface plasmon resonance for infliximab detection*. in *SPIE BiOS*. 2015. International Society for Optics and Photonics.
22. Pillet, L., *et al.*, *Immunoglobulin immobilization by the Langmuir-Blodgett method*. *Thin solid films*, 1994. **244**(1): p. 857-859.
23. Pei, Z., *et al.*, *Optimizing immobilization on two-dimensional carboxyl surface: pH dependence of antibody orientation and antigen binding capacity*. *Analytical biochemistry*, 2010. **398**(2): p. 161-168.
24. Malottki, K., *et al.*, *Adalimumab, etanercept, infliximab, rituximab and abatacept for the treatment of rheumatoid arthritis after the failure of a tumour necrosis factor inhibitor: a systematic review and economic evaluation*. 2011.
25. Billioud, V., W.J. Sandborn, and L. Peyrin-Biroulet, *Loss of response and need for adalimumab dose intensification in Crohn's disease: a systematic review*. *The American journal of gastroenterology*, 2011. **106**(4): p. 674-684.
26. Steenholdt, C., *et al.*, *Cut-off levels and diagnostic accuracy of infliximab trough levels and anti-infliximab antibodies in Crohn's disease*. *Scandinavian journal of gastroenterology*, 2011. **46**(3): p. 310-318.
27. Lyon, L.A., M.D. Musick, and M.J. Natan, *Colloidal Au-enhanced surface plasmon resonance immunosensing*. *Analytical Chemistry*, 1998. **70**(24): p. 5177-5183.

28. Wang, L., *et al.*, *Water-soluble ZnO–Au nanocomposite-based probe for enhanced protein detection in a SPR biosensor system*. *Journal of colloid and interface science*, 2010. **351**(2): p. 392-397.
29. Law, W.-C., *et al.*, *Sensitivity improved surface plasmon resonance biosensor for cancer biomarker detection based on plasmonic enhancement*. *Acs Nano*, 2011. **5**(6): p. 4858-4864.
30. Tran, D.T., *et al.*, *Selection of aptamers against Ara h 1 protein for FO-SPR biosensing of peanut allergens in food matrices*. *Biosensors and Bioelectronics*, 2013. **43**: p. 245-251.

Chapter 5

Immunoassay for detection of infliximab in whole blood using a fiber-optic surface plasmon resonance biosensor

The work presented in this chapter is adapted from:

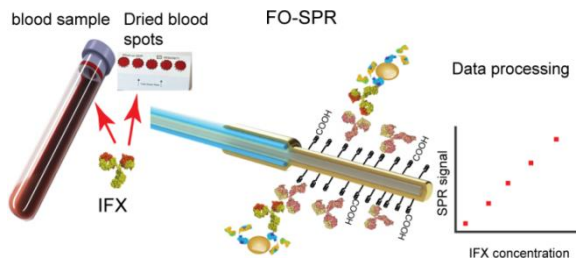
**analytical
chemistry**

Lu J., Spasic D., Delpont F., Van Stappen T., Detrez I., Daems D., Vermeire S., Gils A. and Lammertyn J. (2017).

Immunoassay for Detection of Infliximab in Whole Blood Using a Fiber-Optic Surface Plasmon Resonance Biosensor.

Analytical Chemistry, 89 (6), pp 3664–3671

Contribution of Lu J. to the manuscript: Planning and performing the experiments, analyzing data, writing and editing the manuscript.



Abstract

Monitoring the concentration of a therapeutic drug antibody, infliximab (IFX), is recommended for enhancing its efficacy in patients with inflammatory bowel disease (IBD). However, IFX concentrations are currently determined in patients' serum/plasma, which requires sample preparation from blood, hence hampering the turnaround time. In this chapter, we present a short immunoassay (10 min) using a fiber-optic surface plasmon resonance (FO-SPR) biosensor for detection of IFX spiked in 100-fold diluted serum, plasma, and whole blood. The calculated limits of detection (LOD) based on calibration curves were 1.42, 1.00, and 1.34 ng/mL, respectively, which coincides with expected IFX concentrations in diluted samples from IBD patients. A linear correlation was established among different matrices, indicating that the matrix effect was insignificant. The established point-of-care (POC) FO-SPR bioassay was also used to measure IFX in 100-fold diluted extracts of dried blood spots (DBS), and LOD achieved was below 2 ng/mL. Although DBS might be ideal for POC, this is the first report of using an SPR biosensor for measuring DBS samples. Finally, the POC FO-SPR immunoassay was validated by using matching serum and plasma samples from five IBD patients. A Pearson correlation of 0.968 was obtained between serum and plasma samples. IFX concentrations determined with FO-SPR were compared to a clinically validated enzyme-linked immunosorbent assay (ELISA), resulting in excellent Pearson correlation and intraclass correlation coefficient, both being 0.99 for serum and plasma samples. In conclusion, this chapter demonstrates that our FO-SPR biosensor can be used as a true POC diagnostic tool for determining IFX concentrations in a variety of matrices.

Keywords: point-of-care, surface plasma resonance, fiber-optic, infliximab, whole blood, dried blood spots

5.1 Introduction

Infliximab (IFX) is a chimeric monoclonal antibody used in treatment of patients with moderate-to-severe inflammatory bowel diseases (IBD). Monitoring the IFX trough concentration (defined as the lowest IFX concentration in patient's blood immediately prior to the next infusion) is recommended for enhancing the therapeutic outcome of IBD patients, which is mostly done using an enzyme-linked immunosorbent assay (ELISA). However, several significant disadvantages make ELISA unsuitable as a point-of-care (POC) technique: (i) requirement for well-trained staff to run the tests, (ii) relatively long time to result (approximately 2 h), and (iii) the need for multiple patient samples to be collected in a central laboratory before the test can be executed. Thus, immediate dose adaptation with ELISA tests is impossible. A recently reported lateral flow-based immunoassay has important advantages such as fast detection time (less than 20 min) and single sample testing [1, 2]. However, either serum or plasma samples are still required for applying this technique. Therefore, an inexpensive platform that allows for single sample testing with a short detection time, good accuracy and minimum sample preparation is desirable to facilitate POC testing.

A sandwich immunoassay has recently been developed for IFX detection in serum using an in-house developed fiber-optic surface plasmon resonance (FO-SPR) biosensor, which is a fully automated multichannel platform with inexpensive and disposable FO-SPR sensors [3]. However, despite all these advantages, the described method still required preparation of serum samples by centrifugation. Establishing direct IFX measurements in whole blood, such as blood from finger prick, while using the same FO-SPR platform, would eliminate the need for sample preparation, thereby making this a true simple-to-use POC with reduced turnaround time. Furthermore, direct measurements in blood could potentially allow patients to collect blood samples at home through dried blood spot (DBS) sampling. In recent years, there has been growing interest in DBS sampling for therapeutic drug monitoring [4-6], as it is a simple, convenient and flexible sampling method for patients. Importantly, the DBS samples can be easily transported to a laboratory for further testing. In this way, regular monitoring of the drug level could be arranged without patients visiting the hospital.

In this chapter, we present the development of an advanced FO-SPR immunoassay with three distinct features: (i) fast assay time, (ii) clinically relevant sensitivity and (iii) capacity for detecting IFX in serum, plasma, citrated whole blood (used in place of the finger prick blood) and DBS. Starting from the previously established bioassay [3], several aspects have been improved for maximizing signal-to-noise ratio in different matrices and establishing a true POC testing concept. The developed immunoassay was validated using clinical samples (both serum and plasma) from five IFX treated IBD patients. This paper demonstrates the versatility and robustness of the FO-SPR biosensor that can be used as a POC diagnostic tool in various types of patient samples.

5.2 Materials and methods

5.2.1 Buffers and reagents

All buffer reagents were obtained from Sigma-Aldrich (Diegem, Belgium), unless stated otherwise. All solutions were prepared with deionized water purified by a Milli-Q Plus system (Millipore, Marlborough, MA, USA). Acetone and acetic acid were purchased from Chemlab (Zedelgem, Belgium). Tween 20 and Tween 80 was provided by AppliChem GmbH (Darmstadt, Germany). Carboxylic acid-SAM formation reagent was produced by Dojindo Laboratories (Kumamoto, Japan). 1-Ethyl-3-[3-(dimethylamino)propyl] carbodiimide (EDC), N-hydroxysuccinimide (NHS) and Superblock™ (PBS) Blocking Buffer were obtained from Thermo Fisher Scientific (Erembodegem, Belgium). AuNPs EMGC20 with an average diameter of 20 nm were provided by BBI Solutions (Cardiff, U.K.). Bovin serum albumin (BSA) was supplied by Sigma-Aldrich (Diegem, Belgium). Infliximab (Remicade®) was obtained from Janssen Biologics B.V. (Leiden, The Netherlands). Anti-IFX monoclonal antibodies MA-IFX20G2 and MA-IFX3D5 [7] were generated in the Laboratory of Therapeutic and Diagnostic Antibodies (KU Leuven, Belgium). Human sodium citrate-treated whole blood (will be referred to as whole blood in the paper), plasma and pooled serum from healthy donors were purchased from Valley Biomedical (Winchester, USA). Human whole blood was collected in sodium citrate coated tubes and plasma was processed from this whole blood. Filter paper

(903 Protein saver card) was purchased from Sigma-Aldrich (Diegem, Belgium). De-identified serum and plasma samples from five IFX-treated IBD patients were taken in the framework of the Vlaams Erfelijkheidsonderzoek crohn en colitis ulcerosa (VLECC) study (B322201213950/S53684) after obtaining informed consent from the patients. High binding 96-well plates were provided by Costar (Corning Inc., Corning, NY, USA). Phosphate buffer saline (PBS), 2-(N-morpholino)ethanesulfonic acid (MES) and sodium acetate buffers were 10 mM at pH 7.4, 50 mM at pH 6.0 and 10 mM at pH 5.5, respectively unless otherwise specified.

5.2.2 FO-SPR platform and preparation of FO-SPR sensors

A detailed description of the FO-SPR biosensor and preparation of FO-SPR sensors can be found in Section 5.5.1.1 Figure S5.1A and Chapter 4. Although all the results in this chapter were obtained using the platform illustrated in Figure S5.1 A, a more compact and user-friendly FO-SPR platform, has been developed in the group for the POC use, as shown in Figure S5.1B. When the IFX-specific bioassay described in Chapter 4 was implemented on this platform, excellent agreement was achieved with the published results (data not shown), revealing the great potential of this fully integrated FO-SPR device.

5.2.3 Detection of IFX spiked in 10-fold diluted whole blood

A calibration curve in 10-fold diluted whole blood was established using the previously developed FO-SPR sandwich bioassay in Chapter 4 for detection of IFX [3]. In brief, gold-coated FO-SPR sensors were functionalized overnight with a carboxyl self-assembling monolayer (SAM). Carboxyl groups were activated by EDC/NHS (0.4 M/0.1 M) chemistry for covalently binding the MA-IFX20G2 capture antibodies, supplied in a final concentration of 20 $\mu\text{g}/\text{mL}$. After removing noncovalently bound capture antibodies with regeneration buffer (10 mM glycine/HCl pH 2), the unoccupied carboxyl groups were deactivated using a blocking buffer (Superblock PBS). To obtain a calibration curve, the FO-SPR sensor was immersed for 15 min in the range of IFX concentrations (0, 2.5, 5, 10, 20, 40, 80 and 100 ng/mL) prepared in 10-fold diluted whole blood, followed by 20 min of signal amplification using AuNPs conjugated with detection antibody.

In this chapter, IFX and blood were diluted using PBS with 0.01% of Tween 20. Storage buffer of AuNPs was PBS with 0.5% of BSA, unless otherwise stated. An overview of the bioassay is indicated in Section 5.5.1.2 Table S5.1A. The process of functionalization of the AuNPs with the detection antibody, MA-IFX3D5, was the same as described in our previous publication [3]. In contrast to the previous publication, in this chapter each IFX concentration was measured with an individual FO-SPR sensor.

5.2.4 Preparation and extraction of DBS samples

For preparation of 100-fold diluted DBS samples, IFX was first 10-fold diluted from the stock solution in whole blood (by adding 10 μL of IFX into 90 μL of whole blood), resulting in the range of IFX concentrations (0, 0.25, 0.5, 1, 2, 4, 8, 10 $\mu\text{g}/\text{mL}$). An amount of 45 μL of this dilution was applied onto a disc of a filter paper (903 protein saver card, Whatman). The DBS samples were allowed to dry overnight at room temperature. Subsequently, diameter of 6 mm disks were punched out from the filter paper and placed into an Eppendorf tube containing 240 μL of extraction buffer (PBS with 0.1% of Tween 80). This was placed on a shaker (Thermomixer comfort, Eppendorf) for 1 h set at 300 rpm and 21 $^{\circ}\text{C}$. The samples were centrifuged (Microstar 17R, VWR) for 5 min at 13 000 rpm (16 249 g) and used immediately after preparation. The blood volume from 6 mm disk was approximately 10 μL , which led to the first 25-fold dilution in the 240 μL of extraction buffer. To reach final concentrations of IFX in DBS, being 0, 2.5, 5, 10, 20, 40, 80, and 100 ng/mL , the DBS samples were additionally diluted 4-fold using the detection buffer (PBS with 0.01% of Tween 20). In this chapter, we refer to this type of DBS sample as a spiked DBS sample.

To estimate the extraction efficiency, DBS samples without IFX were also prepared. For this, 10 μL of detection buffer was added into 90 μL of whole blood instead of IFX. The extraction procedure was the same as described above resulting in 25-fold diluted whole blood. The extracted blood was additionally diluted 4-fold with the detection buffer and spiked with IFX in order to obtain the same series of final concentrations as above (0, 2.5, 5, 10, 20, 40, 80, and 100 ng/mL). In the context of this paper, we refer to this type of DBS sample as a reference DBS sample.

5.2.5 Establishing a POC FO-SPR bioassay for IFX detection

A POC FO-SPR bioassay was established following the protocol for functionalization with the capture antibodies as described in the previous section. Functionalized FO-SPR sensors were subsequently immersed in IFX solution (i.e., samples spiked with IFX) for 5 min, AuNP storage buffer (PBS with 0.5% of BSA) for 3 min and AuNP solution for 5 min, reducing the total detection time to 13 min (as seen in Section 5.5.1.2 Table S5.1B). This shortened detection assay was used to obtain calibration curves in 10-fold diluted whole blood, 100-fold diluted whole blood, serum, plasma, and DBS extracts, spiked with final IFX concentrations ranging from 0 to 100 ng/mL. For each calibration curve, four repetitions were included, which were generated with two batches of independently prepared FO-SPR sensors and AuNPs.

5.2.6 Validation of the POC FO-SPR bioassay using serum and plasma samples from IFX-treated patients

The POC FO-SPR bioassay was validated using five IFX-treated patient samples, with matching serum and plasma samples from each patient. Three samples were 100-fold diluted. Due to higher IFX concentrations in the other two samples, one of them was 150-fold diluted and the other one was 300-fold diluted. Three repetitions were measured for each sample.

5.2.7 IFX quantification in serum and plasma samples from IFX-treated patients using ELISA

IFX in serum samples from IFX-treated IBD patients was quantified using ELISA as previously described [8]. Each sample was measured three times on different days.

5.2.8 Data analysis

To assess the influence of FO-SPR sensors and AuNPs that were generated on different days, results were analyzed using a randomized block design in JMP Pro12 (SAS Institute Inc., Cary, USA). For investigation of the sample matrix effect, correlations were made between calibration curves prepared in

different matrices. A 95% confidence interval (95% CI) for slope was calculated using linear fitting in Origin® 8 (OriginLab, Northampton, USA).

5.3 Results and discussion

5.3.1 FO-SPR bioassay for detection of IFX in 10-fold diluted whole blood

Detection of IFX trough levels is usually conducted in serum or plasma, which requires blood sample processing, leading to a longer time to result. Therefore, performing bioassays directly in whole blood, such as from a finger prick, would create a significant improvement in the disease management of IBD patients. In order to establish such bioassay in this chapter, venous citrated whole blood was used as a matrix as obtaining blood from a finger prick was not feasible. Whole blood was diluted 10-fold and spiked with a series of IFX concentrations, ranging from 0 to 100 ng/mL. Starting from the previously established FO-SPR bioassay for IFX detection in serum [3], two major modifications were introduced to minimize the matrix effect from whole blood: (i) calibration curves were generated by using an individual FO-SPR sensor for each concentration, in contrast to one FO-SPR sensor used previously for a series of IFX concentrations and (ii) Superblock PBS was introduced as a blocking buffer, resulting in less than 0.5 nm shift for the nonspecific binding ($n = 4$, measured by immersing the FO-SPR sensor functionalized with capture antibody in 10-fold diluted whole blood in the absence of the target, followed by a AuNP amplification step). A considerable decrease in the SPR-shift due to nonspecific binding is observed when using Superblock (red) compared to ethanolamine (black) as blocking agent. (see Figure 5.1A). To generate a calibration curve, the obtained average SPR shifts ($n = 2$) were plotted as a function of the IFX concentrations (Figure 5.1) and fitted with nonlinear regression (one-site binding fitting) using Origin 8 (OriginLab, Northampton, USA). The limit of detection (LOD) was determined as explained in Section 5.5.1.3, and equaled 1.12 ng/mL with a coefficient of variation (CV) below 10%.

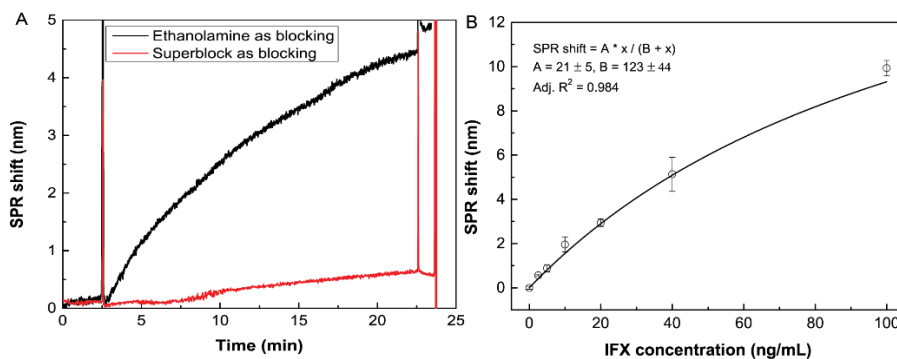


Figure 5.1 (A) Nonspecific binding from 10-fold diluted whole blood using ethanolamine and Superblock as blocking buffer, (B) IFX calibration curve in 10-fold diluted whole blood measured with the FO-SPR bioassay. Unless otherwise stated, the equations displayed in all the graphs refer to the one-site binding fitting equation; x stands for IFX concentration in nanograms per milliliter. The errors are standard deviations based on two repetitions.

5.3.2 Accelerated POC FO-SPR bioassay for detection of IFX in 10-fold diluted whole blood

Although the obtained results demonstrated for the first time measurements of IFX directly in whole blood, the total detection time was approximately 40 min (as seen in Table S5.1A), which is not fully compatible with a POC testing concept. In order to further shorten the FO-SPR bioassay, the IFX incubation time and AuNP amplification step were reduced from 15 and 20 min, respectively, to 5 min each, resulting in total detection time of 13 min (time of the assay corresponds to the time from the moment that the FO-SPR probe was immersed in IFX solution, as seen in Table S5.1B). Using the established POC bioassay, a series of IFX concentrations (ranging from 0 to 100 ng/mL) was spiked in 10-fold diluted whole blood and measured. The SPR shifts obtained from AuNP binding were plotted as a function of IFX concentrations to generate a calibration curve (will be referred to as method 1 in this thesis, Figure 5.2A). On the basis of four repetitions, the calculated LOD was 0.75 ng/mL with an average CV value below 12%. All the measurements were performed in a random manner, meaning that IFX concentrations were not measured in ascending or descending order.

Since binding curves of the AuNPs showed a linear behavior within the first 2 min (Section 5.5.2.1 Figure S5.2), this part of the curve was used to perform a slope analysis. The obtained values of the slope were further plotted as a function of IFX concentrations to generate a calibration curve (will be referred to as method 2 in this thesis, Figure 5.2B), which resulted in an LOD value of 0.9 ng/mL with an average CV below 18%. Although the CV value for method 2 was slightly higher compared to method 1, it is still acceptable as it lies below 20% [9]. Moreover, the obtained LODs from the two methods were comparable, suggesting that the detection time of the bioassay can be further reduced by 3 min, toward a total detection time of 10 min.

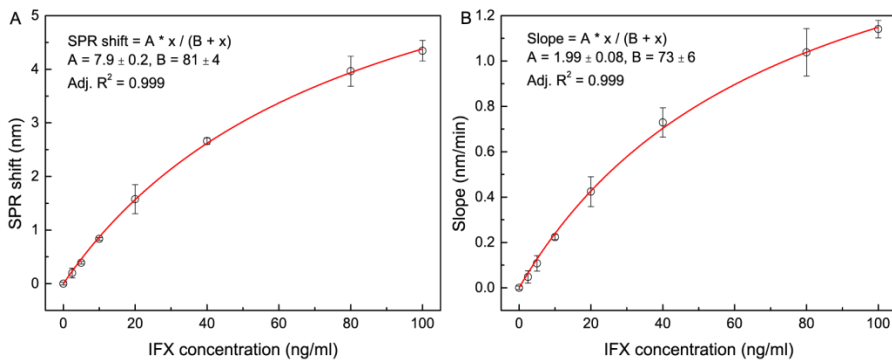


Figure 5.2 Calibration curves in 10-fold diluted whole blood with the POC FO-SPR immunoassay, using method 1 (A) and method 2 (B). The error bars are standard deviations based on four repetitions.

Measurements of IFX concentrations in whole blood have never been previously reported in the literature, mainly for two reasons. First, red blood cells and platelets typically rupture when handling blood samples, causing clotting and an increase in nonspecific absorption to the sensor surface, making it more challenging to detect target molecules. The nonspecific absorption from blood on the sensor surface was minimized by using Superblock PBS [10, 11]. Second, IFX trough concentrations in whole blood are expected to be lower than in serum or plasma. In general, the serum/blood ratio is approximately 45%. Therefore, IFX trough concentrations in whole blood are approximately 45% of those in serum, which is in the range of 0.23–4.5 $\mu\text{g/mL}$ (based on trough concentrations in serum samples, ranging from 0.5 to 10 $\mu\text{g/mL}$). This suggests that detection of IFX in whole blood

requires a more sensitive assay than in serum. Here, the concentrations encompassed by the calibration curve were 2.5–100 ng/mL in 10-fold diluted blood, which corresponds to 0.025–1 µg/mL in whole undiluted blood. Therefore, in order to achieve detection of IFX in the clinically relevant range, the dilution factor was further adjusted as discussed in the next section of this chapter.

5.3.3 POC FO-SPR bioassay for detection of IFX in 100-fold diluted serum, plasma and whole blood

To measure IFX concentrations in the clinically relevant range (i.e. 0.5–10 µg/mL in serum samples and 0.23–4.5 µg/mL in whole blood), samples need to be diluted 100-fold in order to fall in the dynamic range of the POC FO-SPR bioassay (0 and 100 ng/mL). Therefore, IFX concentrations, ranging from 0 to 100 ng/mL, were spiked in 100-fold diluted serum, plasma, and whole blood and quantified with the POC FO-SPR bioassay. All the concentrations were measured in a random manner. By using methods 1 and 2, calibration curves were generated for all three matrices (Figure 5.3, part A and B). The data were fitted using a ‘one-site binding’ model [12] with the model parameters as indicated in Figure 5.3. The LOD values in 100-fold diluted serum, plasma and whole blood were respectively 1.05, 1.00 and 1.05 ng/mL obtained with method 1 and 1.42, 1.00 and 1.34 ng/mL for method 2. Based on these results, it is evident that the obtained LODs were comparable for all three matrices irrespective of the used method. The CVs were below 15% for both methods.

To investigate whether the FO-SPR sensors and AuNPs prepared on different days had an impact, all the results were analyzed with a randomized block design in JMPPro12 (SAS Institute Inc., Cary, USA). For all the calibration curves, the difference between the results measured on two independent days was statistically insignificant, implying that there was no statistical difference between two batches of FO-SPR sensors and AuNPs (data not shown). This further suggested that the FO-SPR biosensor does not require a new calibration curve to be generated for each new batch of FO-SPR sensors or AuNPs that is being produced. Therefore, it is sufficient to perform only one control measurement (i.e. no target) and one concentration of IFX and compare the obtained values to the established calibration curve.

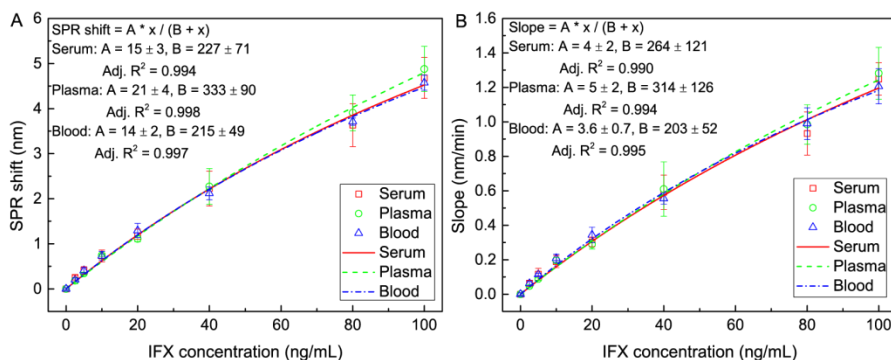


Figure 5.3 Summary of calibration curves. Calibration curves obtained from series of IFX concentrations using method 1 (A) and method 2 (B). A nonlinear regression (one-site binding) was fitted for both calibration curves. Fitting parameters are indicated on the left of the graph. Error bars represent standard deviations ($n = 6$ for all matrices).

5.3.4 POC FO-SPR bioassay for detection of IFX in 100-fold diluted DBS

Capillary blood collected by finger-prick in the form of DBS might be ideal for POC as patients can perform sample collection by themselves at home and requirements for transportation of the DBS samples are minimal. However, mainly two concerns have made this practice difficult so far: (i) bursting of red blood cells after whole blood is dried, which can result in higher nonspecific interaction between the ruptured cell fragments and the sensor surface, and (ii) altered structure of analytes due to the drying process, which can influence the efficiency of the analytes entering the extraction buffer and induce increased variation of the extraction efficiency. The most frequently reported technologies for detection of DBS samples include ELISA [13], high-pressure liquid chromatography (HPLC) [14] and liquid chromatography–tandem mass spectrometry (LC–MS/MS) [15]. This is the first time that an SPR biosensor has been deployed for measuring DBS samples.

To develop a consistent and reproducible method for DBS sample preparation, a protocol was optimized as explained above. In order to determine the extraction efficiency of the developed protocol and assess the potential of using the FO-SPR platform in combination with DBS samples, IFX concentrations were measured in 100-fold diluted reference and spiked

DBS samples. Here, a reference DBS sample refers to whole blood spiked with IFX after extraction through the filter paper, while a spiked DBS sample refers to whole blood spiked with IFX prior to extraction through the filter paper (see Section 5.2.4 for more details). On the basis of the obtained calibration curves when using the POC FO-SPR bioassay (Figure 5.4), the LOD values were 1.17 (spiked DBS) with a CV of 18% and 1.39 (reference DBS) ng/mL with a CV of 20% for method 1 and 1.83 (spiked DBS) with a CV of 17% and 1.59 (reference DBS) ng/mL with a CV of 20% for method 2 (n = 4).

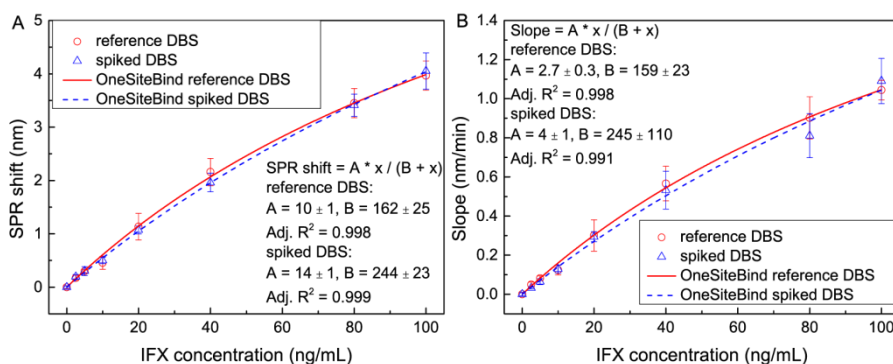


Figure 5.4 Calibration curves generated in 100-fold diluted reference DBS and spiked DBS samples based on method 1 (A) and method 2 (B). The error bars are standard deviations based on four repetitions.

The extraction efficiency is usually estimated by calculating the ratio of the analyte concentration from DBS samples and serum/plasma. However, in this chapter, it was calculated as ratio of the analyte concentration (i.e., obtained SPR shifts for each IFX concentration) between spiked and reference DBS samples. The ratio was first individually calculated for each of the seven IFX concentrations (ranging from 2.5 to 100 ng/mL). The individual ratio values were subsequently used for calculating the average value, resulting in 0.98 when using method 1 and 0.97 for method 2. These results demonstrated that (i) the drying process of blood did not affect the extraction of IFX or its interaction with the antibodies used in the FO-SPR bioassay and (ii) the distribution of IFX on the DBS paper was uniform since blood with and without IFX was spread out on the paper and only part of it was taken for extraction process. Similar values for extraction efficiency were also obtained

when performing a correlation analysis between calibration curves from the reference and spiked DBS samples (Section 5.5.2.2 Figure S5.3, parts A and B). This resulted in the slopes of 0.99 (95% CI slope: 0.99 ± 0.02) for method 1 and 0.98 (95% CI slope: 0.99 ± 0.04) for method 2, with the Pearson correlation of 0.998 and 0.995, respectively.

5.3.4 Comparison of the POC FO-SPR bioassay performance in different matrices

Next, to investigate the impact that different matrices might have on measuring IFX concentrations with the POC FO-SPR bioassay, correlations were calculated between calibration curves obtained for 100-fold diluted whole blood, serum, plasma and DBS. The results are presented in Table 5.1 when using method 1 and in Section 5.5 Table S5.2 for method 2. For a given cell shown in the table, a correlation was obtained by using the matrix from the column as the x axis and the matrix from the row as the y axis. The linear equation of the fitted curve, 95% CI of the slopes and Pearson correlation are included in the tables.

When comparing all the results from 100-fold diluted serum, plasma and whole blood (indicated as bold in tables), the slope values were approximately 1 for both method 1 and 2. This suggested that for a given dilution factor, the SPR signal was almost identical regardless of the matrix, i.e. that the matrix effect from 100-fold diluted serum, plasma and whole blood was insignificant. A summary of linear regression analysis can be seen in Section 5.5.2.3 Figure S5.4.

When the SPR signals from 100-fold diluted whole blood/serum/plasma were compared to those from spiked DBS samples, slope values of approximately 1.1 were obtained, suggesting a nearly 10% higher signal for 100-fold diluted blood/serum/plasma (Table 5.1 and Section 5.5.2.3 Figure S5.5). This difference could be attributed to two different factors: (i) a matrix effect of DBS samples due to bursting of the blood cells during the drying process, which may interfere with the interactions between IFX and capture antibody/AuNP, thereby reducing the SPR signal and (ii) the calculation of dilution factor during DBS sample preparation: although the volume of blood from the 6 mm DBS disk was assumed to be 10 μ L, in practice, however, this

could be less, suggesting that the final dilution factor in DBS sample preparation can be potentially greater than 100-fold.

5.3.5 Validation of the POC FO-SPR bioassay with plasma and serum samples from IFX treated patients

The developed POC FO-SPR bioassay was validated using matching serum and plasma samples from five IFX-treated IBD patients. The same serum and plasma samples were also tested using a clinically validated ELISA, based on the assay described in ref [8]. Taking 150-fold diluted serum/plasma into account, the ELISA cutoff and lower limit of quantification were 0.2 and 0.5 $\mu\text{g/mL}$ of IFX, respectively.

Measurements were first conducted with five serum samples (referred to as S1, S2, S3, S4 and S5) diluted 100-fold. Due to the high SPR shifts from S1 and S5, these two samples were further diluted 150- and 300-fold, respectively. IFX concentrations from serum samples were calculated by interpolating the obtained SPR signals into the calibration curve, which was made using the series of IFX concentrations spiked in 100-fold diluted serum. Although dilution factors of S1 and S5 were different from the calibration curve, it was demonstrated in our previous publication [3] that this has no influence on determining IFX concentrations. Next to this, IFX was quantified in the five plasma samples (referred to as P1, P2, P3, P4, and P5) from the same patients. Because the difference between serum and plasma is only in the presence of clotting factors in plasma but not in serum, similar IFX concentrations are expected in both matrices from the same patient. Therefore, the dilution factors of the plasma samples were kept the same as for the serum samples and the calibration curve was made using 100-fold diluted plasma spiked with series of IFX concentrations.

The measured IFX concentrations in serum and plasma samples were used for establishing the correlation between these two matrices (Section 5.5.2.4 Figure S5.6). As seen from the figure, good Pearson correlations of 0.959 and 0.968 were obtained for method 1 and method 2, respectively. Slopes in the correlations were smaller than 1 for both methods, which indicated that IFX concentrations in the plasma samples were slightly lower than those in the corresponding serum samples. This can be due to the clotting factors in plasma

that make these samples less stable compared to serum concerning handling and storage.

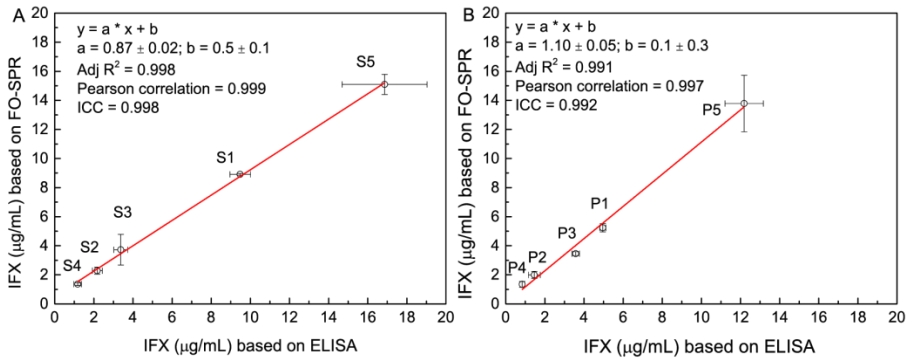


Figure 5.5 Evaluation of the POC FO-SPR immunoassay with serum (A) and plasma (B) samples from IBD patients. The IFX concentrations from FO-SPR platform were compared to the clinically validated ELISA. The equations displayed in the graphs represent the correlation of IFX concentrations ($\mu\text{g/mL}$) obtained based on FO-SPR and ELISA. Error bars represent standard deviation ($n= 3$ for both FO-SPR and ELISA).

Table 5.1. Correlations between Calibration Curves Based on Method 1 in Various Matrices. Linear regressions were fitted using calibration curves in the column as x-axis and calibration curves in the row as y-axis.

| x-axis | y-axis | | | |
|------------------------------|--|--|--|--|
| | 100-fold diluted whole blood | 100-fold diluted serum | 100-fold diluted plasma | 100-fold diluted spiked DBS |
| 100-fold diluted whole blood | | $y = 1.01x - 0.02$ 95% CI: 0.04 Pearson: 0.999 | $y = 1.08x - 0.09$ 95% CI: 0.04 Pearson: 0.998 | $y = 0.91x - 0.05$ 95% CI: 0.02 Pearson: 0.999 |
| 100-fold diluted serum | $y = 0.99x + 0.01$ 95% CI: 0.04 Pearson: 0.999 | | $y = 1.07x - 0.07$ 95% CI: 0.04 Pearson: 0.999 | $y = 0.93x - 0.07$ 95% CI: 0.02 Pearson: 0.999 |
| 100-fold diluted plasma | $y = 0.93x + 0.07$ 95% CI: 0.04 Pearson: 0.999 | $y = 1.00x + 0.01$ 95% CI: 0.1 Pearson: 0.996 | | $y = 0.88x - 0.01$ 95% CI: 0.02 Pearson: 0.999 |
| 100-fold diluted spiked DBS | $y = 1.10x + 0.01$ 95% CI: 0.04 Pearson: 0.999 | $y = 1.10x + 0.06$ 95% CI: 0.06 Pearson: 0.998 | $y = 1.18x - 0.02$ 95% CI: 0.06 Pearson: 0.998 | |

Finally, IFX concentrations measured with the POC FO-SPR bioassay were compared to those measured with ELISA, as seen in Figure 5.5. FO-SPR method 2 was selected for validating the POC FO-SPR bioassay with the ELISA since it gave very similar IFX concentrations for both serum and plasma patients' samples as method 1 (demonstrated with the excellent correlations between the results in SI Figure S5.7), but with a shorter detection time. Similar to the FO-SPR, a lower IFX concentration was also obtained for P1 sample compared to S1 when using ELISA. The POC FO-SPR bioassay and ELISA had an excellent correlation as demonstrated with the Pearson correlation and intraclass correlation coefficient (ICC) of 0.999 and 0.998, respectively, for serum samples, and 0.997 and 0.992, respectively, for plasma samples. The average CV of the FO-SPR from both serum and plasma samples was approximately 10%.

5.4 Conclusions

This chapter describes the development and validation of a FO-SPR based immunoassay for the detection of IFX in a variety of matrices including serum, plasma, whole blood, and DBS extracts. Starting from the previously published concept [3], two types of bioassays were first established for detecting IFX in 10-fold diluted blood: (i) 40-minutes bioassay and (ii) POC bioassay, with a total detection time of 13 or 10 minutes. The difference in detection time was based on whether the SPR shift (method 1) or the curve slope (method 2) from the AuNP binding step was used for generating calibration curves. The obtained LOD values were 1.12 ng/mL for the 40-minutes bioassay and 0.75 or 0.9 ng/mL for POC bioassay based on method 1 or method 2, respectively. This demonstrated for the first time measurements of IFX directly in whole blood, thereby surpassing difficulties often linked to measurements in whole blood, such as high nonspecific binding on the sensor surface and almost 2 times lower levels of IFX trough levels in blood compared to serum.

Next, in order to measure IFX concentrations in the clinically relevant range with the developed POC FO-SPR bioassay (i.e., 0.5–10 $\mu\text{g/mL}$ in serum samples and 0.23–4.5 $\mu\text{g/mL}$ in whole blood), new calibration curves were generated in 100-fold diluted serum, plasma, and whole blood. The LOD values for all three matrices were below 1.5 ng/mL for both method 1 and

method 2. Moreover, excellent correlations between different calibration curves indicated that the matrix effect was insignificant for the given dilution factor. Importantly, all the calibration curves were analyzed with a randomized block design. There was no statistical significance between measurements generated on two different days using two batches of independently prepared FO-SPR sensors and AuNPs. These results demonstrated that a new calibration curve is unnecessary for each batch of FO-SPR sensors and AuNPs.

The capacity of developed POC FO-SPR bioassay was further assessed using DBS samples. Following the optimized protocol for DBS sample preparation, it was calculated that the extraction efficiency of IFX was 99 %, suggesting that (i) the drying process of blood did not affect the extraction of IFX or its interaction with the antibodies used in the FO-SPR bioassay, (ii) the distribution of IFX on the DBS paper was uniform given that only part of the paper was used for extraction process, and (iii) nonspecific binding (due to the bursting of blood cells caused by drying of whole blood) was not interfering with the FO-SPR bioassay. The obtained LOD values were below 2 ng/mL, irrespective of whether IFX was spiked in the whole blood prior to or after the extraction. This demonstrated the potential of the POC FO-SPR bioassay to be used for testing DBS samples that are collected by finger prick, as patients can perform sample collection by themselves at home and requirements for transportation of the DBS samples are minimal.

The final validation of the POC FO-SPR immunoassay was performed with 10 clinical samples from IFX-treated IBD patients, being five matching serum and plasma samples from the same five patients. The measured IFX concentrations were compared to the values obtained using clinically validated ELISA, revealing excellent agreement between two methods, with the Pearson correlation and ICC of 0.999 and 0.998, respectively for serum samples, and 0.997 and 0.992, respectively, for plasma samples.

By comparison to the previous work, the POC FO-SPR bioassay presented in this chapter has the advantages of shorter detection time (10 min compared to 40 min), lower LOD (1.05 compared to 2.2 ng/mL in 100-fold diluted serum), and comparable accuracy when testing patient samples. Importantly, it was also demonstrated that not only SPR shift but the slope of the obtained binding curves can be used for generating calibration curves. This so called method 2 in this chapter allowed us to establish bioassay in complex

sample matrices of only 10 min without compromising on the sensitivity or reproducibility of the detection as both LOD and CV values were comparable to method 1 (i.e., method based on the SPR shift measurements). In conclusion, the FO-SPR biosensor offers advantages including fully automated setup, single-sample access, and rapid detection. The fact that the same platform can detect IFX in a variety of matrices, such as serum, plasma, whole blood, and DBS extracts, with clinically relevant sensitivities in 10 min demonstrated that the FO-SPR biosensor can be used as a versatile POC diagnostic tool.

5.5 Supplementary information

5.5.1 Materials and Methods

5.5.1.1 FO-SPR platform and preparation of FO-SPR sensors

A picture of the in-house developed FO-SPR platform is illustrated in Figure S5.1A. To suit the point-of-care applications, the FO-SPR platform was integrated to a more compact and user-friendly system (FOx Biosystems) as shown in Figure S5.1 B. This system has the option of operation with either single FO-SPR sensor or four FO-SPR sensors measuring simultaneously.

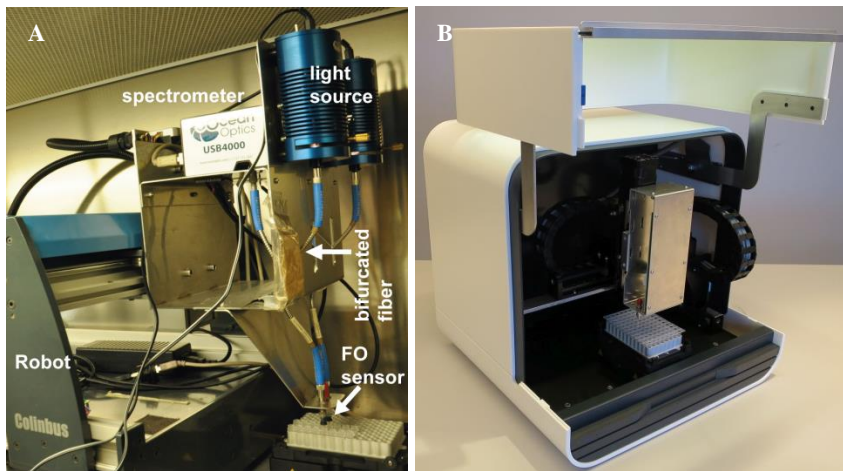


Figure S5.1 The FO-SPR platform (A) and a compact FO-SPR platform (B).

5.5.1.2 FO-SPR bioassay and POC FO-SPR bioassay steps

The complete protocol of the FO-SPR bioassay is illustrated in Table S1. In Table S5.1A, both antibody immobilization and target detection steps are shown. FO-SPR sensors were attached to the fully automated system as described in S5.5.1.1. The protocol started with antibody immobilization by immersing FO-SPR sensors in MES buffer (step 1) to achieve stable baseline, followed by activation of carboxyl groups of the SAM (step 2), using EDC/NHS (0.4 M /0.1 M), for covalently binding capture antibodies, MA-IFX20G2, supplied in a final concentration of 20 $\mu\text{g}/\text{mL}$ (step 4). Non-

covalently bound capture antibodies were removed by a regeneration buffer (10 mM glycine/HCl pH 2) (step 6 and 7), and the unoccupied carboxyl groups were deactivated (step 9), using a blocking buffer (Superblock PBS). The immobilization of capture antibody on FO-SPR sensors was completed with the step 9. Afterwards, functionalized FO-SPR sensors were immersed in samples containing IFX diluted in matrices, including serum, plasma, blood and DBS or patient samples (step 11). Signal amplification (step 14) was achieved by using AuNPs conjugated to detection antibodies (MA-IFX3D5).

For the POC FO-SPR bioassay, immobilization steps were identical, whereas both step 11 and 14 were shortened and step 12 in Table S5.1A was skipped, as seen in Table S5.1B.

Table S5.1 A. Full protocol of the FO-SPR bioassay including both immobilization and detection steps.

| | Step | Time (min) | Sample* | Action |
|--------------------------------|------|------------|----------------|---|
| Antibody immobilization | 1 | 10 | MES | Obtaining stable baseline |
| | 2 | 15 | EDC/NHS | Activation carboxyl groups |
| | 3 | 3 | NaAc | Obtaining stable baseline |
| | 4 | 30 | MA-IFX20G2 | Immobilization of capture antibodies |
| | 5 | 2 | NaAc | Washing |
| | 6 | 0.5 | Glycine/HCl | Remove non-covalently bond capture antibodies |
| | 7 | 0.5 | Glycine/HCl | Remove non-covalently bond capture antibodies |
| | 8 | 1 | NaAc | Washing |
| | 9 | 8 | Superblock PBS | Blocking |

| | | | | | |
|------------------|-------------------------|----|----|-----------------|---------------------------|
| Target detection | Interaction with sample | 10 | 3 | PBS/Tween | Obtaining stable baseline |
| | | 11 | 15 | Sample | Interaction with IFX |
| | | 12 | 1 | PBS/Tween | Washing |
| | Signal amplification | 13 | 3 | PBS/BSA | Obtaining stable baseline |
| | | 14 | 20 | AuNPs/MA-IFX3D5 | Signal amplification |
| | | 15 | 1 | PBS/BSA | Washing |

Table S5.1 B Detection steps of the POC FO-SPR bioassay.

| | | Step | Time (min) | Sample* | Action |
|------------------|-------------------------|------|------------|-----------------|---------------------------|
| Target detection | Interaction with sample | 10 | 3 | PBS/Tween | Obtaining stable baseline |
| | | 11 | 5 | Sample | Interaction with IFX |
| | Signal amplification | 12 | 3 | PBS/BSA | Obtaining stable baseline |
| | | 13 | 5 | AuNPs/MA-IFX3D5 | Signal amplification |

Used labels for the samples: MES, 50 mM MES-buffer pH 6.0; EDC/NHS, 0.4 M EDC and 0.1 M NHS in MES; NaAc, 10 mM sodium acetate buffer pH 5.5; MA-IFX20G2, 20 µg/mL in 10 mM sodium acetate buffer pH5.5; Glycine/HCl, 10 mM glycine pH 2; PBS, 10 mM PBS pH 7.4; PBS/Tween: PBS with 0.01% of Tween 20; Sample, IFX in serum, plasma, whole blood, DBS and patient samples; PBS/BSA, PBS with 0.5% of BSA; AuNPs/MA-IFX3D5, AuNPs conjugated with MA-IFX3D5 stored in PBS with 0.5% of BSA.

5.5.1.3 Determining limit of detection

All the calibration curves were fitted with on-site binding, using Origin 8 (OriginLab, Northampton, US). To calculate the limit of detection (LOD), Equation S5.1, from the one-site binding fitting, was used:

$$y = x * A / (x + B) \quad (S5.1)$$

where, y is the SPR shift, x represents the IFX concentration, and A and B are fitting parameters. The LOD can be calculated with Equation S5.2:

$$\text{LOD} = \frac{(y(0) + 3\sigma)B}{A - (y(0) + 3\sigma)} \quad (\text{S5.2})$$

where $y(0)$ is the average SPR shift of nonspecific binding and σ is the standard deviation of nonspecific binding.

5.5.2 Results

5.5.2.1 Binding kinetics of AuNPs in the POC FO-SPR bioassay

Binding curves of the AuNPs in the POC FO-SPR bioassay showed linear behavior within the first 2 minutes (Figure S5.2). Therefore, this part of the curve was used to perform the slope analysis. Calculated slope values were used for generating calibration curves (referred to as method 2 in the chapter), leading to a total detection time of 10 minutes.

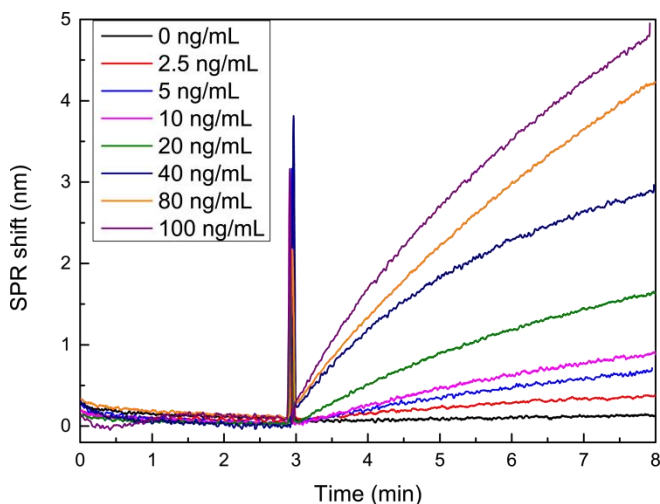


Figure S5.2 Binding curves of AuNPs for a series of IFX concentrations (0 – 100 ng/mL).

5.5.2.2 Correlation between spiked and reference DBS samples

To assess the extraction efficiency of IFX when using developed protocol for DBS sample preparation, two calibration curves were compared: calibration curve obtained with POC FO-SPR bioassay for IFX-spiked DBS sample and calibration curve obtained using the same bioassay for reference DBS samples. Results are illustrated in Figure S5.3. The slopes of spiked DBS samples were approximately 1% lower compared to reference DBS samples for both method 1 as seen in Figure S5.3 A (slope = 0.99) and method 2 in Figure S5.3 B (slope = 0.99). This indicated that IFX function was not affected during the drying process and that the extraction efficiency was approximately 99%.

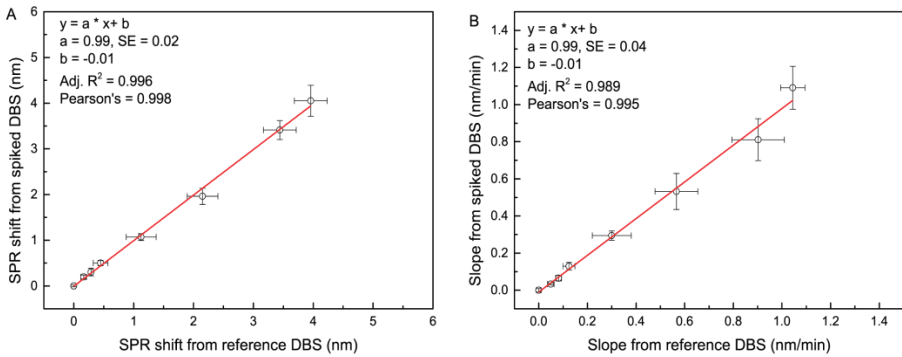


Figure S5.3 Correlations between calibration curves in spiked DBS and reference DBS based on method 1 (A) and method 2 (B).

5.5.2.3 Studying the impact of different sample matrices on the POC FO-SPR bioassay

To investigate the matrix effect, correlations were made between calibration curves generated in 100-fold diluted blood, serum and plasma when using method 1 (Figure S5.4 A, C and E) and method 2 (Figure S5.4 B, D and F). All the slopes were approximately 1, meaning that SPR signals or slopes from all 100-fold diluted matrices were similar. Moreover, Pearson correlations were all above 0.995. These results indicated that when the dilution factor was identical, there was no matrix effect observed. A summary of correlations based on method 2 can be found in Table S5.2.

Table S5.2 Correlations between calibration curves based on method 2 in various matrices. Linear regressions were fitted using calibration curves in the column as x axis and calibration curves in the row as y axis.

| x-axis | y-axis | | | |
|------------------------------|--|--|--|--|
| | 100-fold diluted whole blood | 100-fold diluted serum | 100-fold diluted plasma | 100-fold diluted spiked DBS |
| 100-fold diluted whole blood | | y = 1.01x - 0.01 95% CI: 0.06 Pearson: 0.997 | y = 1.07x - 0.02 95% CI: 0.06 Pearson: 0.998 | y = 0.90x - 0.02 95% CI: 0.06 Pearson: 0.996 |
| 100-fold diluted serum | y = 0.98x + 0.02 95% CI: 0.06 Pearson: 0.997 | | y = 1.07x - 0.02 95% CI: 0.06 Pearson: 0.998 | y = 0.91x - 0.02 95% CI: 0.04 Pearson: 0.998 |
| 100-fold diluted plasma | y = 0.92x + 0.04 95% CI: 0.04 Pearson: 0.998 | y = 0.94x + 0.01 95% CI: 0.02 Pearson: 0.998 | | y = 0.84 - 0.01 95% CI: 0.04 Pearson: 0.997 |
| 100-fold diluted spiked DBS | y = 1.10x + 0.03 95% CI: 0.08 Pearson: 0.996 | y = 1.12x + 0.02 95% CI: 0.04 Pearson: 0.999 | y = 1.19x + 0.01 95% CI: 0.08 Pearson: 0.997 | |

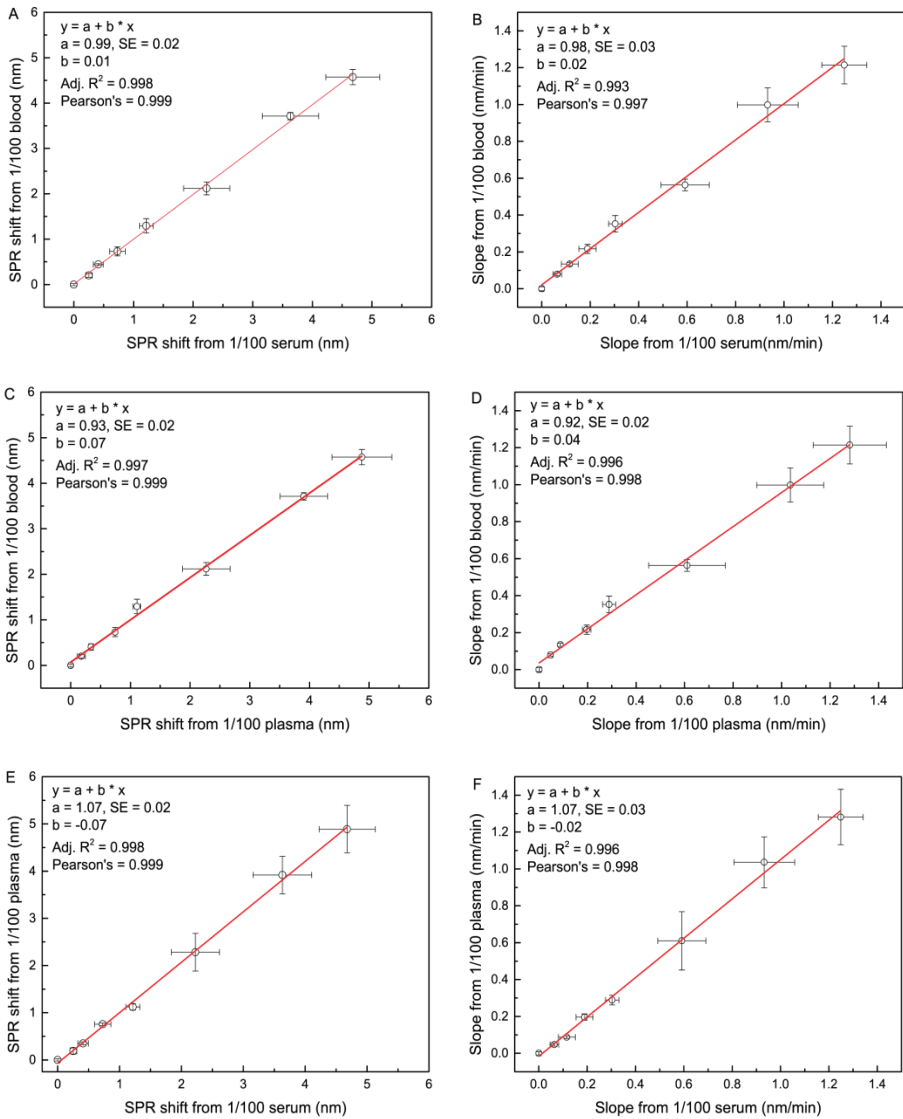


Figure S5.4 Correlations between calibration curves in 100-fold diluted blood and serum (A) and (B), blood and plasma (C) and (D), plasma and serum (E) and (F) based on method 1 and 2.

To investigate matrix effect of DBS samples, correlations were made between calibration curves in 100-fold diluted whole blood/serum/plasma and spiked DBS samples, as indicated in Figure S5.5.

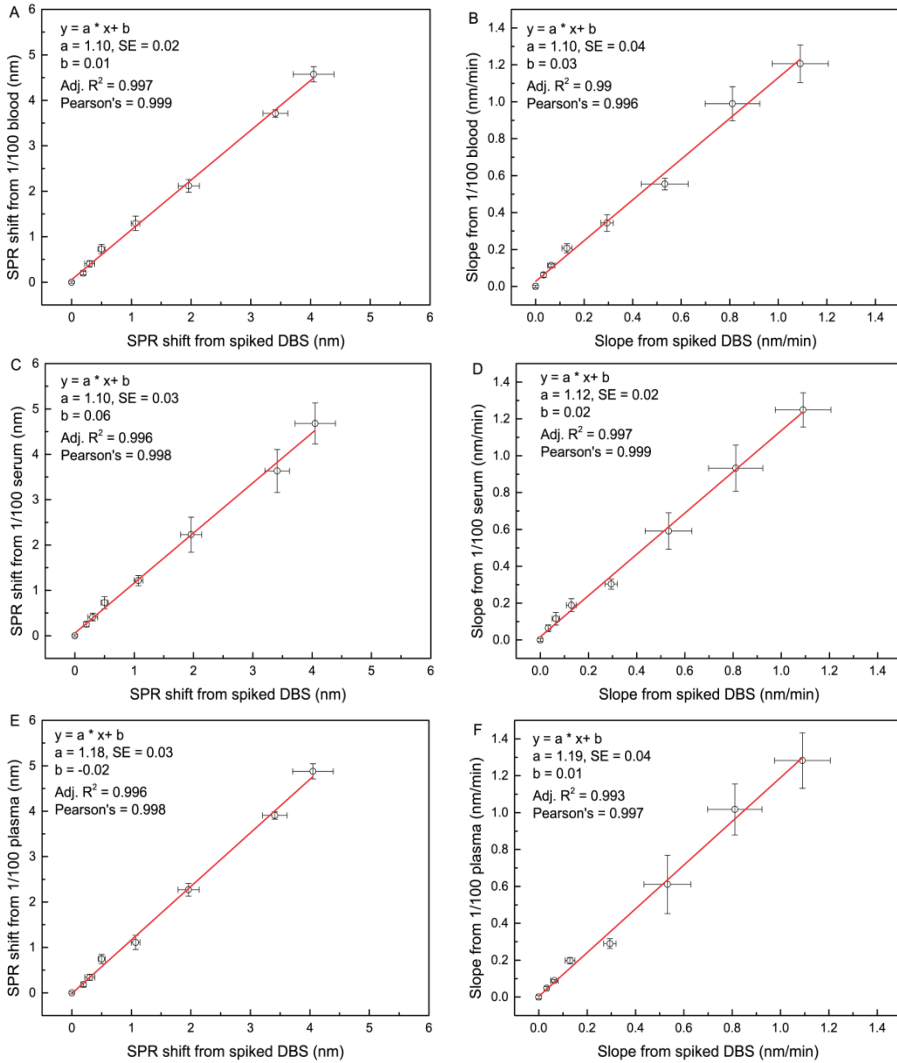


Figure S5.5 Correlations between calibration curves in 100-fold diluted blood and spiked DBS (A) and (B), 100-fold diluted serum and spiked DBS (C) and (D) and 100-fold diluted plasma and spiked DBS (E) and (F), when using method 1 and 2.

5.5.2.4 Validation of the POC FO-SPR bioassay with plasma and serum samples from IFX treated patients

Validation of the POC FO-SPR immunoassay was performed with clinical samples from five IFX-treated IBD patients. The measured IFX concentrations in serum and plasma samples were used for establishing the correlation between these two matrices. Good Pearson correlations of 0.959 and 0.968 were obtained for method 1 Figure S5.6A and method 2 Figure S5.6B.

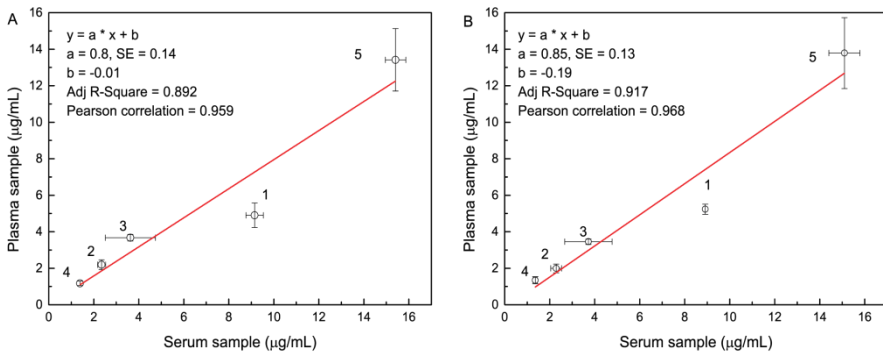


Figure S5.6 Correlations between estimated IFX concentration in plasma and serum samples based on method 1 (A) and method 2 (B) ($n = 3$, error bars represent standard deviation).

IFX concentrations measured with the POC FO-SPR bioassay in patients' serum and plasma samples were compared for method 1 and method 2, as depicted in Figure S5.7. Excellent correlations were found with both Pearson correlations and ICC of 0.999 for both serum and plasma samples. These results demonstrated that method 2 did not influence the accuracy of determining IFX concentrations in patient samples. Therefore, further comparison with ELISA was performed with these results, as indicated in the manuscript.

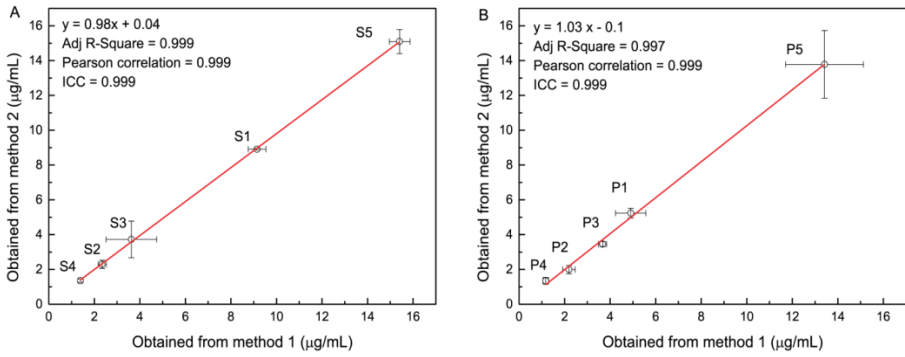


Figure S5.7 Correlations between estimated IFX concentration when using method 1 and 2 in serum (A) and plasma samples (B) ($n = 3$, error bars represent standard deviation).

5.6 References

1. Corstjens, P.L., *et al.*, *A rapid assay for on-site monitoring of infliximab trough levels: a feasibility study*. Analytical and bioanalytical chemistry, 2013. **405**(23): p. 7367-7375.
2. Van Stappen, T., *et al.*, *Rapid Test for Infliximab Drug Concentration Allows Immediate Dose Adaptation*. Clinical and Translational Gastroenterology, 2016. **7**(12): p. e206.
3. Lu, J., *et al.*, *Fiber optic-SPR platform for fast and sensitive infliximab detection in serum of inflammatory bowel disease patients*. Biosensors and Bioelectronics, 2016. **79**: p. 173-179.
4. Hofman, S., *et al.*, *Role of therapeutic drug monitoring in pulmonary infections: use and potential for expanded use of dried blood spot samples*. Bioanalysis, 2015. **7**(4): p. 481-495.
5. de Wit, D., *et al.*, *Dried blood spot analysis for therapeutic drug monitoring of pazopanib*. The Journal of Clinical Pharmacology, 2015. **55**(12): p. 1344-1350.
6. McDade, T.W., S. Williams, and J.J. Snodgrass, *What a drop can do: dried blood spots as a minimally invasive method for integrating biomarkers into population-based research*. Demography, 2007. **44**(4): p. 899-925.
7. Van Stappen, T., *et al.*, *Transferability of antibody pairs from ELISA to fiber optic surface plasmon resonance for infliximab detection*. in *SPIE BiOS*. 2015. International Society for Optics and Photonics.
8. Van Stappen, T., *et al.*, *Generation of a highly specific monoclonal anti-infliximab antibody for harmonization of TNF-coated infliximab assays*. Therapeutic drug monitoring, 2014.
9. UNODC, *Guidance for the Validation of Analytical Methodology and Calibration of Equipment Used for Testing of Illicit Drugs in Seized Materials and Biological Specimens*. United Nations, New York. 2009: United Nations Office on Drugs and Crime.
10. Barbosa, A.I., *et al.*, *A lab-in-a-briefcase for rapid prostate specific antigen (PSA) screening from whole blood*. Lab on a Chip, 2014. **14**(16): p. 2918-2928.
11. Stelter, L., *et al.*, *Imaging of tumor vascularization using fluorescence molecular tomography to monitor arginine deiminase treatment in melanoma*. Molecular imaging, 2013. **12**(1): p. 7290.2012. 00009.
12. Ferreon, A.C.M., *et al.*, *Modulation of allostery by protein intrinsic disorder*. Nature, 2013. **498**(7454): p. 390-394.

13. Tuailon, E., *et al.*, *Dried blood spot for hepatitis C virus serology and molecular testing*. *Hepatology*, 2010. **51**(3): p. 752-758.
14. Suyagh, M.F., *et al.*, *Development and validation of a dried blood spot–HPLC assay for the determination of metronidazole in neonatal whole blood samples*. *Analytical and Bioanalytical Chemistry*, 2010. **397**(2): p. 687-693.
15. Vu, D.H., *et al.*, *Determination of moxifloxacin in dried blood spots using LC–MS/MS and the impact of the hematocrit and blood volume*. *Journal of Chromatography B*, 2011. **879**(15–16): p. 1063-1070.

Chapter 6

General conclusions and future perspectives

6.1 General conclusions

In the last century biosensors have been attracting increasing attention as tools for a wide variety of applications ranging from food safety and production to healthcare and environmental monitoring. Biosensors that can provide sensitive, accurate, fast and robust detection are highly desirable in all these fields. A major challenge, however, in biosensor design is to make it work in complex matrices like waste water, soil, food, and human fluids. Complex matrices induce undesirable nonspecific binding to the sensor surface, making it more challenging to conduct a sensitive detection of the target molecule. Moreover, some target analytes are present in the sample matrix in very low concentrations. Therefore, the biosensors need to be specifically designed to both minimize the nonspecific binding from the matrix and achieve the desired sensitivity. Although conventional bioanalytical techniques such as ELISA, RIA and HMSA meet many of the requirements for different applications, they are labor-intensive, time consuming and bulky. In past decades, extensive research has been conducted on biosensors, to provide solutions to many of the disadvantages of the conventional bioanalytical techniques. In this thesis,

we proposed a fiber optic SPR based biosensor which exploits the advantages of the SPR phenomenon to achieve sensitive and reliable detection. To demonstrate the versatility of the FO-SPR platform for detecting various target analytes in different types of matrices, this thesis was directed towards the sensitive detection of progesterone (small molecule) in milk for applications in the agriculture industry and IFX (antibody) in blood for TDM applications in the health sector.

To provide a better understanding of the FO-SPR biosensor, the physics of the SPR phenomenon and important characteristics of SPR sensors were explained in **Chapter 2**. Three optical measurement concepts including GC-SPR, PC-SPR, and FO-SPR sensors were introduced in this chapter. The state-of-the-art SPR sensors were discussed and surface modification of the sensor surface for implementation of immunoassays was reviewed.

In the agricultural sector, maximum yields are crucial to allow farmers to remain competitive. In the case of milk production, it is critically important to detect cows that are in heat allowing herd owners to conduct artificial insemination to attain an optimal successful pregnancy rate. Monitoring the level of P4 is commonly used for detection of estrus but the search continues for a sensitive, accurate, cost-effective device for on-farm use. Since direct detection of small molecules is challenging, a competitive assay is often used for detection of progesterone. In **Chapter 3**, the development of a competitive inhibition immunoassay using the FO-SPR biosensor for sensitive detection of P4 in milk was presented. To achieve the maximum binding capacity, optimizations were made in three steps. Firstly, the concentration of BSA-P4 complex that was immobilized on the sensor surface was optimized to reach the maximum immobilization capacity. Following, the concentration of GAM-AuNPs was increased for a better signal amplification for the detection of the desired concentrations (1 to 10 ng/mL) in milk. Lastly, the concentration of anti-P4 antibody was optimized to reach the maximum binding capacity. The ciFO-SPR immunoassay was utilized for the generation of calibration curves ranging from 1 to 10 ng/mL in both buffer and milk standards, resulting in LODs of 0.6 ng/mL (1.9 nM) and 0.5 ng/mL (1.6 nM) of P4 and CV values of 8% and 16%, respectively. Validation of the ciFO-SPR immunoassay was conducted on 6 bovine milk samples and benchmarked to the reference cELISA, where a good correlation was obtained (ICC = 0.97). This chapter proved that the FO-SPR biosensor is capable of

detecting small molecules in the low nanomolar range in a complex milk matrix.

IFX is highly effective for reducing the symptoms of inflammation in moderate to severe IBD patients. For improving therapeutic outcomes, TDM is required, where the IFX concentration in a patient's blood is monitored. Since conventional methods such as ELISA, RIA and HMSA are performed in a central laboratory and have long detection times (2 hours), they are unsuitable for POC diagnostics. In this thesis, the development of a biosensor to monitor the IFX level in blood in a sensitive, accurate, and reliable way was described. In **Chapter 4**, a AuNP based sandwich immunoassay was implemented on the FO-SPR setup for detecting IFX in clinically relevant concentrations (5 to 10 $\mu\text{g/mL}$) in serum. Firstly, a selection of buffers and antibody concentrations were tested for optimal immobilization of the capture antibody onto the sensor surface. Secondly, to optimize the specificity of the immunoassay, three blocking buffers were studied. These experiments proved that the detection signal of IFX was solely induced by the specific binding of the capture antibody/IFX/detection antibody-AuNP. Thirdly, the established immunoassay was employed for generating calibration curves in buffer and 100-fold serum with LODs of 0.3 ng/mL (1.7 pM) and 2.2 ng/mL (15 pM), respectively. Finally, the biosensor was tested with 5 serum samples from IFX-treated IBD patients. The results showed an excellent agreement between the FO-SPR biosensor and the clinically validated ELISA (Pearson correlation of 0.998 and ICC of 0.983 with inter-CV being less than 10%). When the FO-SPR sensors were pre-functionalized with capture antibody, the total detection time was approximately 40 min. Next steps include the further reduction of the assay time and to miniaturize the technology.

The biosensor that was developed in Chapter 4 was further advanced in **Chapter 5**, to allow detection of IFX in serum, plasma, citrate-treated whole blood and dried blood spot extracts with a shortened detection time. Direct detection of IFX in whole blood instead of serum eliminated the sample preparation step, but introduced a few extra challenges including (i) the rupture of red blood cells and platelets causing an increase in the nonspecific binding, and (ii) almost two times lower IFX trough levels in blood compared to serum. The nonspecific binding was minimized by using a commercially available blocking reagent. Once the nonspecific binding was under control, both the IFX and AuNP binding times were decreased. A new method of data

analysis was deployed by calculating the slopes of the first 2 minutes of the AuNP binding curves. This resulted in a total detection time of 10 min (including both IFX detection and AuNP binding steps). A calibration curve ranging from 2.5 to 100 ng/mL was generated using this shortened FO-SPR immunoassay in 10-fold diluted citrate-treated whole blood and gave an LOD of 0.9 ng/mL (5 pM). For detection in the clinically relevant range, calibration curves were made in 100-fold diluted serum, plasma and whole blood and an LOD below 1.5 ng/mL (7.5 pM) was obtained for all three matrices. Excellent correlations between different calibration curves indicated there was an insignificant matrix effect for the 100-fold dilution.

The performance of the FO-SPR biosensor was evaluated using DBS samples, where an LOD below 2 ng/mL (10 pM) was achieved. All of the calibration curves were performed on two independent days with two batches of independently prepared FO-SPR sensor and AuNPs in a random manner. The statistical analysis indicated insignificant difference between these results, which demonstrated that a new calibration was unnecessary for each batch of FO-SPR sensors and AuNPs. The final validation of the immunoassay was performed with 10 clinical samples from IFX-treated IBD patients and benchmarked with the clinically validated ELISA. Excellent agreements (Pearson correlation and ICC of 0.999 and 0.998 for serum samples, and 0.997 and 0.992 for plasma samples) were obtained between the two systems. Since good sensitivity was achieved with an LOD below 1.5 ng/mL (7.5 pM) in various matrices using the FO-SPR biosensor within 10 min, it can be concluded that the biosensor has great potential to be deployed as a POC tool for this application.

6.2 Future perspectives

In this thesis, the development of immunoassays for the detection of small molecules (progesterone) and antibodies (IFX) has been successfully achieved using the FO-SPR platform. However, with the current set-up it is challenging to detect large biological entities due to the relatively short penetration depth of the surface plasmon waves. To further explore the potential of the FO-SPR platform, so-called long-range SPR can be implemented (Figure 6.1 grey box) for detecting whole prokaryotic and eukaryotic cells. Moreover, to further improve the performance of the sensor, the concept of a self-referenced sensor

is introduced (Figure 6.1 green box). This type of sensor can effectively eliminate the signal variations caused by external parameters, and as a consequence , improve the signal-to-noise ratio and the sensitivity.

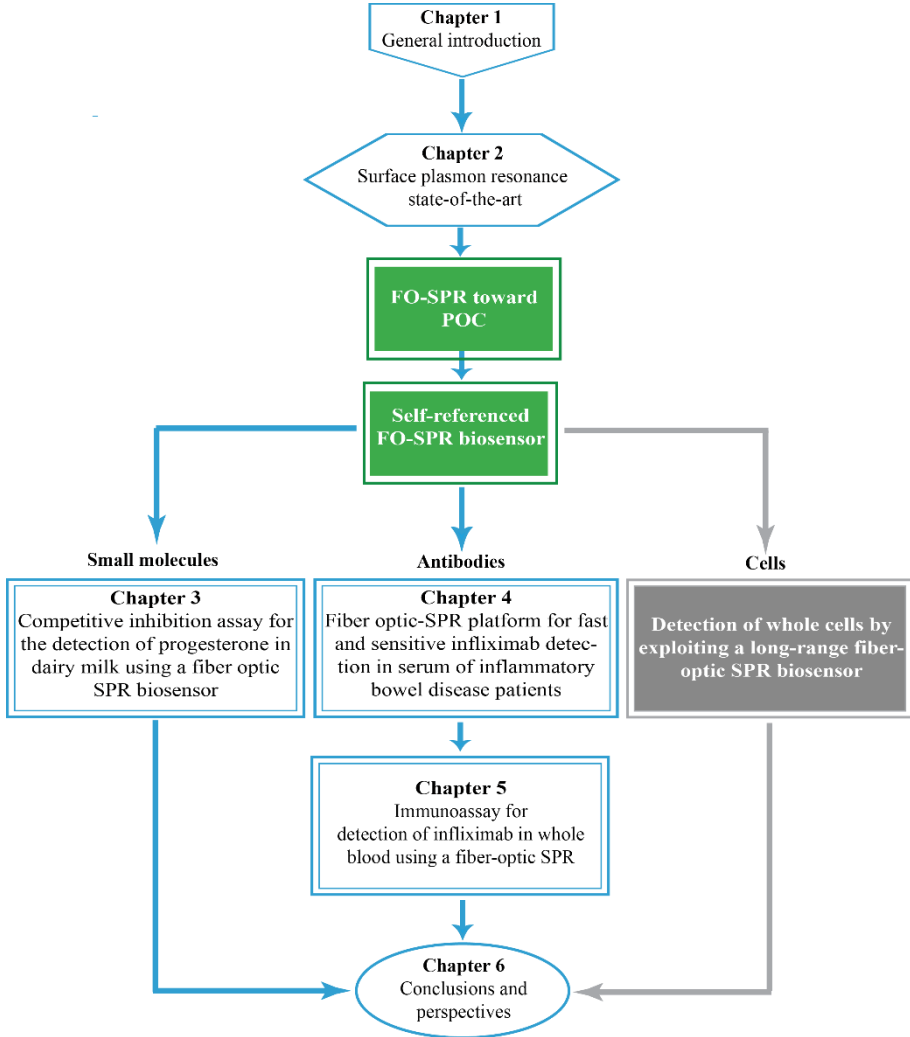


Figure 6.1 Schematic overview of the achievement in this thesis (blue) and opportunities for future research: LRSPR sensing (grey), self-referenced sensing and FO-SPR toward POC (green).

6.2.1 Long-range SPR for detection of whole cells

The concept of long-range SPR (LRSPR) was first proposed by Sarid in 1981. The paper described a new geometry of SPR, where a thick metal film was sandwiched between two identical dielectric media. At the two metal/dielectric interfaces, there were two identical SP waves extending both into the metal film and the dielectric medium. When the thickness of the metal film was decreased, the SP waves on the opposite sides of the metal film began to overlap, resulting in symmetric and asymmetric electric field distributions, which were referred to as long-range SPR (LRSPR) and short-range SPR (SRSPR), respectively, as seen in Figure 6.2A. The attenuation of the LRSP mode was much lower than the SRSP mode, resulting in a larger penetration depth of the SP waves. The paper modeled a PC-SPR configuration and demonstrated that (i) the LRSP dip showed a narrower FWHM, (ii) no LRSP mode existed with Au thickness below 200 nm, and, (iii) if the dielectric layer was too thick, the evanescent waves were not able to penetrate through the dielectric layer to excite LRSP, whereas if the dielectric layer was too thin, it caused the prism to load and wipe out the LRSP waves [1]. An example of the SRSP and LRSP dips is illustrated in Figure 6.2B, where the resonant wavelength for the LRSP and SRSP modes are present at shorter and longer wavelength ranges, respectively. Craig *et al.* experimentally demonstrated that the penetration depth of the LRSP mode was 64 times greater than that of the conventional single-interface SP by using 10 nm of silver bounded by glass and index matching oil [2]. As discussed above, the penetration depth of SP waves in the sample is relatively short (within 200 nm) and therefore not efficient for detecting whole cells. Due to the greater penetration depth of the LRSP mode, it is favored in biosensing for detecting large biological entities such as viruses, spores and bacteria. A large number of publications have been reported on fundamental studies of the LRSP mode, which were covered in a comprehensive review on LRSP [3].

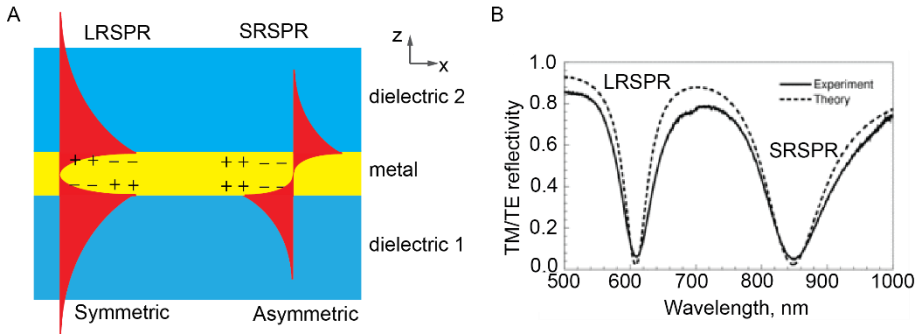


Figure 6.2 (A) Schematic drawing of SP field distribution from SRSP and LRSP mode, (B) an example of the SPR dip from SRSP and LRSP mode reprinted with permission from ref. [4]. Copyright (2006) IOP publishing.

When selecting the intermediate dielectric material between metal and glass, two fluoropolymers that have an RI close to water are frequently used, namely Teflon AF (RI = 1.31) and Cytop (RI = 1.34). The reason that these two materials are chosen is because most target analytes in biosensing applications are usually in buffer or bodily fluids with a similar RI to water.

For PC-SPR sensors, deposition of Teflon AF or Cytop on the prism can be easily achieved by spin-coating. As discussed above, the thicknesses of Teflon AF or Cytop and gold should be carefully adjusted to excite LRSPR. It has been reported that Teflon AF with a thickness of 1200 nm which was spin-coated on a glass substrate and subsequently coated with 24 nm of Au was able to achieve LRSPR sensing. The bulk sensitivity of the LRSPR sensor was tested using water and salt dilutions, which showed a significantly greater resonant wavelength shift compared to the conventional SPR (cSPR) sensor. The sensitivity of the LRSPR sensor was 5.7×10^4 nm/RIU, compared to 6×10^3 nm/RIU from the cSPR sensor [5]. For detecting large entities, the LRSPR sensor was tested with a diameter of 1 μm biotinylated-latex beads and showed 2.5-fold higher signal than that of the cSPR sensor. Furthermore, the LRSPR sensor was implemented in biosensing, where detection of bacterium *Escherichia coli* (*E. coli*) HB101P was achieved and indicated a 5.5-fold higher signal compared to the cSPR sensor [6]. These results demonstrated the advantage of LRSPR regarding detection of large biological entities.

Due to the geometric structure of optical fibers, it is more challenging to deposit Teflon or Cytop on the FO-SPR sensors. Therefore, to date, most of

the work on FO-LRSPR has mainly focused on theoretical and fundamental studies. Numerical simulations have been presented using Teflon AF thickness ranging from 300 to 500 nm and Au thickness ranging from 30 to 50 nm using MMF. By contrast with the PC-LRSPR, the paper demonstrated that the dip from the LRSP mode has larger FWHM and was at a higher wavelength range compared to the SRSP mode. The LRSP mode showed a 40% increase in sensitivity compared to the cSPR sensor [7].

The FO-SPR platform in this thesis employs an automated robot system to manipulate the movements of the FO-SPR sensors. This feature is advantageous for fabrication of the FO-LRSPR sensors. The deposition of Teflon AF on the FO-SPR sensors can be achieved by dip-coating. Based on Landau-Levich equation, when the concentration of Teflon AF was fixed, the thickness of Teflon AF was determined by the pull-up speed [8]. In preliminary experiments in this thesis, Teflon AF-1600 with a concentration of 6% was used and silanization treatment was applied to the sensor surface to enhance the adhesion between glass and Teflon AF. The protocol was obtained from Arghir *et al* [9]. After silanization, the FO-SPR sensors were dip-coated with Teflon AF and followed with drying steps [10]. Once Teflon AF was dry, the FO-LRSPR were coated with Au.

FO-LRSPR sensors were fabricated using a range of pull-up speeds. The Au thicknesses were in the range of 12 to 25 nm. Combinations of different Teflon AF and Au thicknesses were tested and the final condition was chosen based on the wavelength shift between water and ethanol (data now shown). The estimated thicknesses of Teflon AF and Au were 1000 and 38 nm, respectively. Due to the geometry of the optical fibers, it was challenging to accurately measure the thicknesses of both materials. Nonetheless, it was possible to carry out thickness measurements with an atomic force microscope (AFM). An example of the LRSPR dips from these conditions in water and ethanol is illustrated in Figure 6.3 A. Sensitivity measurements were carried out using water, ethanol, isopropanol and butanol, with the RI ranging from 1.333 to 1.393. The results obtained from four FO-LRSPR sensors and four FO-SPR sensors are indicated in Figure 6.3 B. Linear regressions were fitted through both data sets and the slopes were regarded as the bulk sensitivity. The sensitivities from FO-LRSPR sensors and FO-SPR sensors were 6431 and 1560 nm/RIU, respectively.

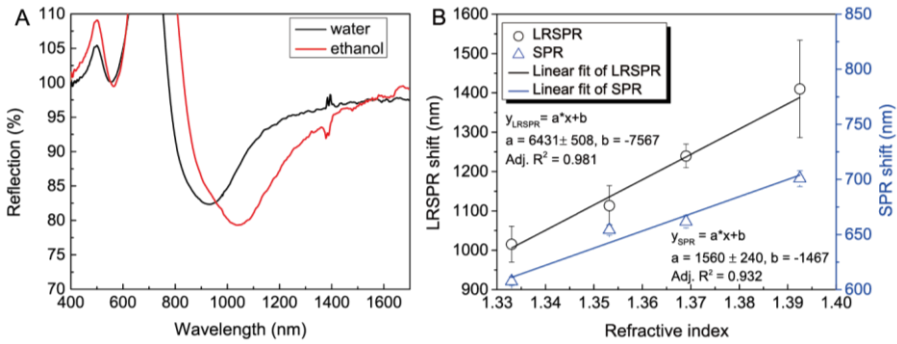


Figure 6.3 (A) LRSRP dips obtained from water and ethanol and (B) sensitivity measurements in the RI range between 1.333 and 1.393 from FO-LRSRP and FO-SPR sensors ($n = 4$).

A proof-of-concept bioassay for detecting *Salmonella* was implemented using these FO-LRSRP sensors as seen in Figure 6.4. Due to a restricted timeframe, only one repetition was obtained for each concentration. The results showed a 2-fold increase in the intensity of the sensor signals was obtained for the LRSRP compared to the regular FO-SPR sensors.

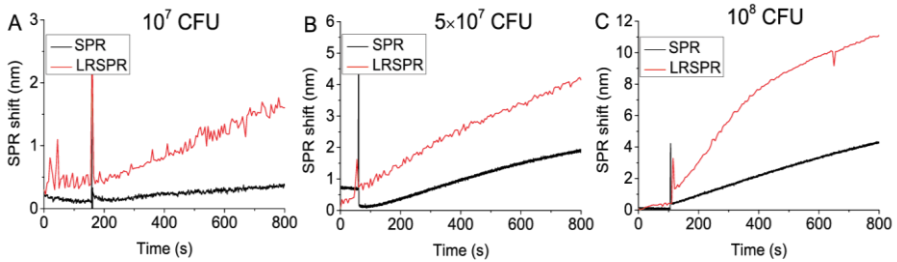


Figure 6.4 SPR sensorgram obtained from FO-LRSRP and FO-SPR sensors measuring *Salmonella* concentrations of 1.0×10^7 (A), 0.5×10^7 (B) and 1.0×10^8 CFU (C).

In conclusion, the literature introduced in this section demonstrated that by adding an intermediate polymer layer with the right thickness, the LRSP mode can be excited, which will enable sensitive detection for large biological entities. The preliminary experiments demonstrated the potential of the FO-SPR platform for detecting whole cells. However, there is a great deal of remaining work in this area. To begin with, the thicknesses of Teflon AF and Au should be accurately determined, which will be carried out with AFM.

Moreover, a calibration curve with a higher resolution should be established. This can be achieved by varying the mixtures of water/sodium chloride or water/ethanol. For the bioassay, measurements with lower concentrations of *Salmonella* and more repetitions should be performed to fully characterize the device.

6.2.2 Self-referenced sensor

As described in Chapter 2, SPR sensors are sensitive to any RI changes in the surrounding medium close to the Au surface, which is advantageous for sensitive detection of target analytes. However, apart from the specific binding between target analytes and bioreceptors on the sensor surface, RI changes can be also caused by external factors such as temperature, fluctuation of light source and nonspecific binding. Self-referenced sensors have been described in the literature as a solution to this problem.

There are several methods to achieve self-referencing. For instance, multi-channel SPR sensors use a control/referencing channel, which contains buffer/matrix with the same RI as the sample but without targets [11]. This way, any changes to the external environment which lead to bulk RI changes are monitored. When calculating the SPR response from the measuring channel, the SPR signal from the referencing channel is deducted, hence, the SPR response is solely induced by the specific binding between the target and the bioreceptor. For the FO-SPR biosensor in this thesis, one of the FO-SPR sensor probes can be used as the referencing channel since up to 4-channels can be measured simultaneously. For the transmission mode (Figure 2.5A), two fiber probes can be spliced together and one of them can be used as the referencing channel. However, as each FO-SPR sensor probe may have a different sensitivity, this can lead to different results depending on which sensor probe was used as the referencing channel.

Exciting both SRSP and LRSP modes simultaneously is another way of creating referencing signals. It has been demonstrated that the SPR wavelength shifts caused by bulk RI change and the presence of a thin film on the surface due to specific binding events are similar in the shorter wavelength region (LRSP mode), whereas the change due to bulk RI change is more pronounced in the longer wavelength region (SRSP mode) [12]. Therefore, by using the SRSP mode as the reference and LRSP mode as the sensing element,

subtracting the reference signal from the sensing signal, this type of sensor can distinguish between surface layer thickness changes due to specific binding events from the background bulk RI fluctuations [4].

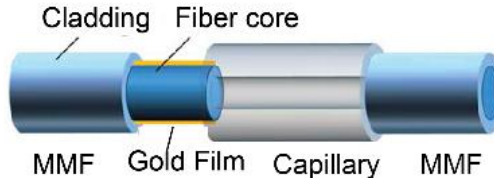


Figure 6.5 An idea of creating self-referenced FO-SPR sensor, by introducing a capillary structure, reproduced from ref. [13]. Copyright (2016) IEEE.

For the FO-SPR biosensor, a novel way to obtain a referencing signal is to exploit the approach of the hetero-core structure discussed in Section 2.3.3 [13]. As shown in Figure 6.5, a silica-fused capillary is spliced in between two identical sections of MMF, where one end is coated with Au. Since the core of the MMF ($62.5\ \mu\text{m}$) is larger than that of the capillary ($50\ \mu\text{m}$), when light propagates from the MMF to the capillary, part of the light escapes to the cladding of the capillary, resulting in interference from multiple beams. Due to the material properties of the capillary, it is insensitive to the temperature change so the interference signal caused by the capillary acts as a referencing channel. Therefore, by slightly modifying the structure of the FO-SPR sensor probe, a self-referenced FO-SPR sensor can be achieved. The signal-to-noise ratio can be enhanced with this type of sensor, which can potentially improve the sensitivity of the sensor.

6.2.3 FO-SPR biosensor toward POC

Preliminary tests have demonstrated that the results from the bench-top system were transferable to the FOx Biosystems device. To meet the criteria of POC devices for low-resource countries, the device requires further reduction in size. One approach to achieve this is to exploit smartphones. In recent years, smartphones have been integrated with biosensors, as they provide integrated light sources, sensitive cameras, powerful CPUs, touchscreen displays, advanced connectivity features and high pixel-count. By exploiting these features of the smartphones, the cost of the biosensors can be drastically reduced. An example of the FO-SPR integrated with smartphone

utilizing the transmission mode is illustrated in Figure 6.6 A: a built-in LED flash from the phone emits light into an optical fiber, which is connected to the sensing fiber, and the signal is collected by the CMOS camera on the phone. The sensor has been tested for detecting IgG, where a lowest detectable concentration of 0.2 mg/mL was achieved [14, 15]. Another example with all the components enclosed in a case has been introduced in Section 2.4, where an LOD of 4.5 nM for direct detection of IgG was achieved. By comparison with a commercially available portable PC-SPR biosensor, the cost was 1000-fold lower [16]. Based on the two references, integration of the FO-SPR biosensor and smartphones can be easily achieved. This approach enables the FO-SPR biosensor to be employed as a POC diagnostic tool.

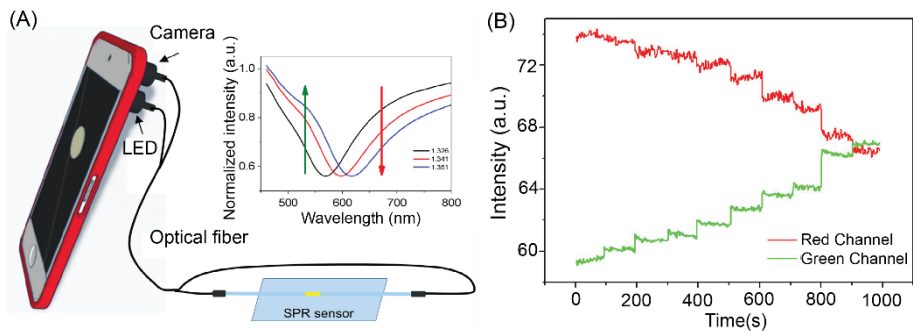


Figure 6.6 (A) Schematic diagram of smartphone-based dual-color fiber optic SPR sensor. (Inset) Normalized spectrums of the sensor in different RIs obtained by spectrometer, (B) Real time responses from two channels, reprinted with permission from Liu et al [14, 15].

6.2.4 DBS sample collection using a glass capillary

When calculating the concentrations of the DBS samples in Section 5.2.4, it was assumed that the volume of blood from the 6 mm DBS disc was 10 μ L. As discussed in Section 5.3.4, this volume might not be accurate. When pipetting blood onto the DBS disc, the spread area can differ depending on the hematocrit level of the blood. As seen in Figure 6.7, when the hematocrit level was low, the blood spread area was larger. Therefore, when a 6 mm DBS disc was cut, a lower volume of blood sample was collected from blood with a low level of hematocrit, potentially leading to a lower concentration of IFX. The experiments in this thesis were less affected because the blood was pooled

from multiple healthy donors, whose hematocrit level is in the range of 37% to 54%. Therefore, by pooling blood samples from healthy donors, the difference in the hematocrit level between each batch of blood is minimal. However, for individual patients, the hematocrit level between one sample and another can vary, which can lead to an inaccurate determination of IFX concentration in an individual patient sample. To overcome this problem, DBS sample collection using a glass capillary has been proposed by Neto *et al.* [17].

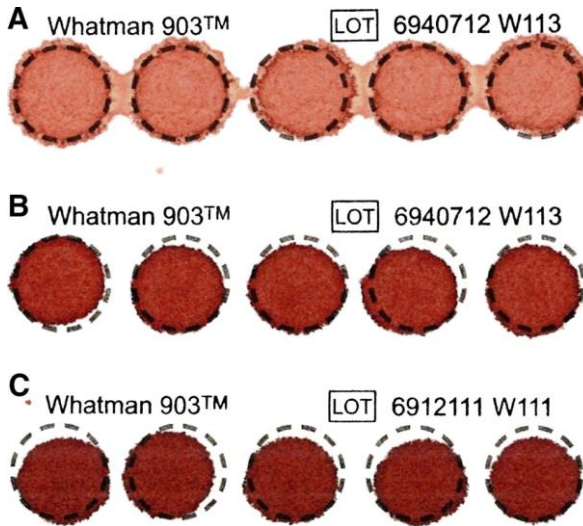


Figure 6.7 Appearance of DBS with different hematocrit levels when 50 μL of blood was applied to the paper. Hematocrit levels were 0.18 (A), 0.35 (B) and 0.5 (C), respectively. Reprinted with permission from [18], copyright (2014) Springer Link.

To do so, a 3.2-mm-diameter disk of DBS paper was pre-cut and placed in a plastic DBS cartridge as illustrated in Figure 6.8A. Each glass capillary was placed in a vertical position under the DBS cartridge (Figure 6.8B) with the paper facing down. One end of the glass capillary was filled by placing the inlet orifice in contact with the blood via capillary force. Once the other end of the glass capillary made contact with the DBS paper, the collected blood transferred to the paper via capillary force. The volume of collected blood was determined by its inner diameter and length. In the case of ref [17], the volume was 3 μL . The paper demonstrated this method was effective to prevent any

human errors during operation and the performance was identical to standard pipette or digital syringe dispensing methods.

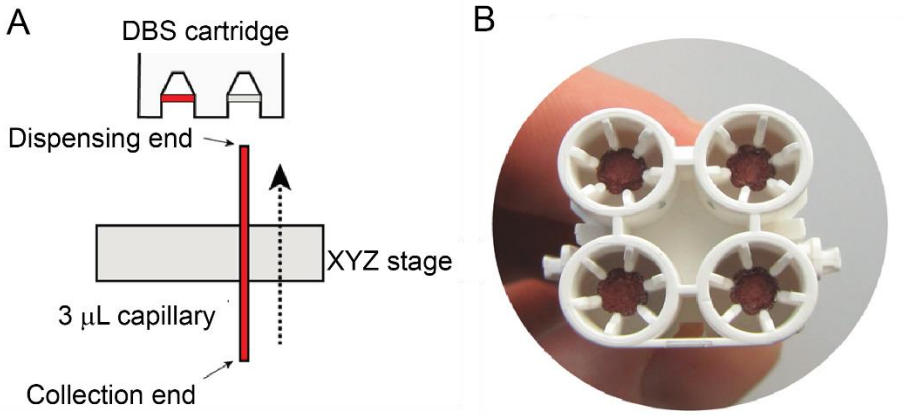


Figure 6.8 (A) Schematic drawing of the setting for collecting an accurate volume of blood using a glass capillary, (B) A picture of the DBS cartridge loaded with pre-cut DBS papers after dispensing of blood. Reprinted with permission from [17], copyright (2018) Springer Nature.

In conclusion, when the ideas mentioned above are implemented on the FO-SPR biosensor, the performance can be further improved. It can be employed in a wider range of biosensing applications, ranging from small molecules to whole cells, which require specific, sensitive, rapid and robust detection with an affordable and portable device for POC diagnostics.

6.3 Reference

1. Sarid, D., *Long-range surface-plasma waves on very thin metal films*. Physical Review Letters, 1981. **47**(26): p. 1927.
2. Craig, A.E., G.A. Olson, and D. Sarid, *Experimental observation of the long-range surface-plasmon polariton*. Optics letters, 1983. **8**(7): p. 380-382.
3. Berini, P., *Long-range surface plasmon polaritons*. Advances in optics and photonics, 2009. **1**(3): p. 484-588.
4. Slavík, R., J. Homola, and H. Vaisocherová, *Advanced biosensing using simultaneous excitation of short and long range surface plasmons*. Measurement Science and Technology, 2006. **17**(4): p. 932.
5. Slavík, R. and J. Homola, *Ultrahigh resolution long range surface plasmon-based sensor*. Sensors and Actuators B: Chemical, 2007. **123**(1): p. 10-12.
6. Vala, M., et al., *Long-range surface plasmons for sensitive detection of bacterial analytes*. Sensors and Actuators B: Chemical, 2009. **139**(1): p. 59-63.
7. Sharma, A.K. and B. Gupta, *Fibre optic sensor based on long-range surface plasmon resonance: a theoretical analysis*. Journal of Optics A: Pure and Applied Optics, 2007. **9**(7): p. 682.
8. Puetz, J. and M.A. Aegerter, *Dip Coating Technique*, in *Sol-Gel Technologies for Glass Producers and Users*, M.A. Aegerter and M. Mennig, Editors. 2004, Springer US: Boston, MA. p. 37-48.
9. Arghir, I., et al., *Improved surface plasmon resonance biosensing using silanized optical fibers*. Sensors and Actuators B: Chemical, 2015. **216**: p. 518-526.
10. Belz, M. and G. Guan, *High temperature coating techniques for amorphous fluoropolymers*. 2011, Google Patents.
11. Naimushin, A.N., et al., *Detection of Staphylococcus aureus enterotoxin B at femtomolar levels with a miniature integrated two-channel surface plasmon resonance (SPR) sensor*. Biosensors and Bioelectronics, 2002. **17**(6): p. 573-584.
12. Dostálek, J., H. Vaisocherová, and J. Homola, *Multichannel surface plasmon resonance biosensor with wavelength division multiplexing*. Sensors and Actuators B: Chemical, 2005. **108**(1-2): p. 758-764.
13. Chen, S., et al., *Self-Reference Surface Plasmon Resonance Biosensor Based on Multiple-Beam Interference*. IEEE Sensors Journal, 2016. **16**(21): p. 7568-7571.
14. Liu, Q., et al., *A smartphone based red-green dual color fiber optic surface plasmon resonance sensor*. IEEE Photonics Technology Letters, 2018.

15. Liu, Q., *et al.*, *Real-time biodetection using a smartphone-based dual-color surface plasmon resonance sensor*. Journal of biomedical optics, 2018. **23**(4): p. 047003.
16. Liu, Y., *et al.*, *Surface Plasmon Resonance Biosensor Based on Smart Phone Platforms*. Scientific Reports, 2015. **5**: p. 12864.
17. Neto, R., *et al.*, *Precise, accurate and user-independent blood collection system for dried blood spot sample preparation*. Analytical and bioanalytical chemistry, 2018. **410**(14): p. 3315-3323.
18. Wilhelm, A.J., J.C. den Burger, and E.L. Swart, *Therapeutic drug monitoring by dried blood spot: progress to date and future directions*. Clinical pharmacokinetics, 2014. **53**(11): p. 961-973.

Publications

Articles in internationally review academic journals

Bian S., **Lu J.**, Delpoort F., Vermeire S., Spasic D., Lammertyn J., Gils A. (2018). Development and validation of an optical biosensor for rapid monitoring of adalimumab in serum of patients with Crohn's disease. *Drug Testing and Analysis*, 10 (3), art.nr. 10.1002/dta.2250, 592-596.

Lu J., Spasic D., Delpoort F., Van Stappen T., Detrez I., Daems D., Vermeire S., Gils A., Lammertyn J. (2017). Immunoassay for detection of infliximab in whole blood using a fiber-optic SPR biosensor. *Analytical Chemistry*, 89 (6), 3664-3671.

Daems D., **Lu J.**, Delpoort F., Mariën N., Orbie L., Aernouts B., Adriaens I., Huybrechts T., Saeys W., Spasic D., Lammertyn J. (2017). Competitive inhibition assay for the detection of progesterone in dairy milk using a fiber optic SPR biosensor. *Analytica Chimica Acta*, 950, art.nr. doi.org/10.1016/j.aca.2016.11.005, 1-6.

Decrop D., Toon B., Gijzenbergh P., **Lu J.**, Spasic D., Kokalj T., Beunis F., Goos P., Puers B., Lammertyn J. (2016). Optical Manipulation of Single Magnetic Beads in a Microwell Array on a Digital Microfluidic Chip. *Analytical Chemistry*, 88, 8596-8603.

Lu J., Van Stappen T., Spasic D., Delpoort F., Vermeire S., Gils A., Lammertyn J. (2016). Fiber optic-SPR platform for fast and sensitive infliximab detection in serum of inflammatory bowel disease patients. *Biosensors & Bioelectronics* (79), 173-179.

Papers at international scientific conferences and symposia, published in full in proceedings

Van Stappen T., **Lu J.**, Bloemen M., Geukens N., Spasic D., Delpoort F., Verbiest T., Lammertyn J., Gils A. (2015). Transferability of antibody pairs from ELISA to fiber optic-surface plasmon resonance for infliximab detection. *Proc. of SPIE: Vol. 9317*. SPIE Photonics West. San Francisco, 7-12 February 2015 (art.nr. 931705).

Meeting abstracts, presented at international scientific conferences and symposia, published or not published in proceedings or journals

Daems D., Delpoort F., **Lu J.**, Van Stappen T., Gils A., Spasic D., Lammertyn J. (2016). Using Fiber Optic SPR technology to combine immunoassays, DNA biosensing and kinetic analysis in one universal point-of-care platform. Biosensors 2016. Gothenburg, Sweden, 25 - 27 May 2016, Abstract No. BIOS2016_0479.

Daems D., **Lu J.**, Delpoort F., Aernouts B., Adriaens I., Huybrechts T., Saeys W., Spasic D., Lammertyn J. (2016). Progesterone detection in milk using a fiber optic SPR biosensor. Precision Dairy Farming 2016. Leeuwarden, Netherlands, 21-23 June 2016.

Van Stappen T., **Lu J.**, Geukens N., Spasic D., Delpoort F., Zali N., Kölmel Y., Rameil S., Vermeire S., Lammertyn J., Vande Castelee N., Gils A. (2015). Point-of-care assays for rapid quantification of infliximab. United European Gastroenterology Week. Barcelona, Spain, 24-28 October 2015, Abstract No. P1572.

Lu J., Van Stappen T., Spasic D., Delpoort F., Gils A., Lammertyn J. (2015). A Fast Assay to Determine Infliximab Trough Level using Fiber-Optic Surface Plasmon Resonance Sensor. Surface Plasmon Photonics. Jerusalem, Israel, 31 May - 5 June 2015.

Van Stappen T., **Lu J.**, Geukens N., Spasic D., Delpoort F., Lammertyn J., Gils A. (2014). Transferability of ELISA to novel biosensor platforms for quantitative detection of infliximab. Diatech2014. Leuven, Belgium, 6-8 October 2014.

Delpoort F., Knez K., Janssen K., Arghir I., **Lu J.**, Mariën N., Spasic D., Lammertyn J. (2014). Fiber optic biosensing for multiplex DNA and protein quantification. Diatech. Leuven, 6-8 October 2014.

Lu J., Van Stappen T., Spasic D., Delpoort F., Gils A., Lammertyn J. (2014). A Fast Assay for Infliximab Detection using Fiber-Optic Surface Plasmon Resonance Sensor. Diatech. Leuven, 06-08 October 2014.

Meeting abstracts, presented at other scientific conferences and symposia, published or not published in proceedings or journals

Daems D., **Lu J.**, Delpoort F., Van Stappen T., Geukens N., Gils A., Saeys W., Spasic D., Lammertyn J. (2015). FOx diagnostics: Integration of DNA and protein quantification technologies in one innovative FO-SPR biosensing platform for in vitro diagnostics. Next-Generation Antibodies and Protein Analysis: Tools and Technologies. Gent, Belgium, 15 - 16 June 2015.